Characterization of Gemini Nanoparticle Assembly by Fluorescence Correlation Spectroscopy

by

Chilbert Dong

A thesis
presented to the University of Waterloo
in fulfillment of the
thesis requirement for the degree of
Master of Science
in
Pharmacy

Waterloo, Ontario, Canada, 2013

Author's declaration

I hereby declare that I am the sole author of this thesis. This is a true copy of the thesis, including any required final revisions, as accepted by my examiners.

I understand that my thesis may be made electronically available to the public.

Abstract

Research in the field of non-viral gene delivery has demonstrated that a deeper understanding of the fundamental processes of nanoparticle assembly is required in order to improve their efficacy. While gemini nanoparticles (gemini NPs) and other non-viral delivery systems have been vigorously characterized using several techniques, our knowledge is still incomplete. The first objective of this study was the development of new methodology using fluorescence correlation spectroscopy (FCS) to investigate the stages of gemini NPs assembly. It was demonstrated that by labeling the plasmid, different stages of gemini NP assembly from the gemini-plasmid pre-complex (GP) to the final gemini nanoparticle (or gemini-plasmid-lipid complex; GPL), could be studied. Based on diffusion coefficients and particle numbers extrapolated from the autocorrelation function (ACF), FCS was able to determine that each phase of assembly had distinct characteristics. The FCS study using 12-3-12 gemini surfactant showed that both the diffusion coefficient and particle number of GPs ($0.98\pm0.31 \times 10^{-12}$ m^2/s) was significantly lower than the final GPL ($3.11\pm0.41 \times 10^{-12}$ m^2/s). Based on the Stokes-Einstein equation the particle size was calculated to be 300-500 nm for GP and 200-300 nm for GPLs. The raw intensity histograms showed that both GPs and GPLs are composed of multiple plasmids. Furthermore the study showed that the final GPLs contain fewer plasmids compared to the intermediate GP. FCS results were validated by using existing characterization methods including dynamic light scattering (DLS), zeta potential and dye exclusion assays. The second objective involved the detailed characterization of gemini NP. Nine different gemini surfactants and two different phospholipids were used in a systematic study to assess the effect of gemini surfactant and lipid structure on the final morphology of gemini NP. The study revealed that gemini surfactant structure had a strong effect on structure of GP intermediates, but addition of phospholipids resulted in the formation of uniform gemini NPs. Based on the results of this study a new model for GP and GPL assembly is proposed based on the formation of supramolecular aggregates of gemini-plasmids, governed by gemini surfactant chemical structure, and dispersed by phospholipids to form GPLs.

Keywords: Gene delivery, gemini surfactants, non-viral, fluorescence correlation spectroscopy

Acknowledgements

I would like to start by thanking my supervisor and mentor Dr. Marianna Foldvari for her professional and support over the years. Your tireless work ethic and passion for your work has been contagious. The many years working as part of your group has truly been an opportunity for personal and professional growth. Again, thank you.

I would also like to thank my committee members Dr. Jamie Joseph and Dr. Zoya Leonenko. Thank you both for your time and expertise in critically reviewing my thesis. Your insight has given me a deeper understanding of my work and thought process in reviewing.

A big thanks also goes out to past and present members of the Foldvari group for their support. It has been a pleasure to get to meet so many wonderful people. You all helped create a professional, yet fun work environment. A special call out goes to Samih for both his professional help and friendship (and construction of "the fort") throughout this program.

I would like to thank my family, especially my parents Ken and Sui-yi and my sister Veanne for their patience and always believing I could do anything (and not asking too many times when I'm going to graduate). I would finally like to thank my best friend and better half Jen. You continue to stand by me thick and thin and without your endless support and love, none of this, and many other things, would never have been possible.

"*Nature uses only the longest threads to weave her patterns, so that each small piece of her fabric reveals the organization of the entire tapestry"*

Richard P. Feynman

Table of Contents

List of Figures

List of Tables

List of Abbreviations

ACF ..... Auto correlation function
ADA ..... Adenosine deaminase deficiency
AFM ..... Atomic force microscopy
CD ..... Circular dichroism
CCD ..... Charged-coupled device
CLSM ..... Confocal laser scanning microscopy
cmc ..... Critical micellar concentration
Cy3 and Cy5 ..... Non-systematic name for cyanine dyes
Cy5-gWiz GFP ..... Cyanine 5 labeled gWiz GFP plasmid
D ..... Diffusion coefficient
D_H ..... Hydrodynamic diameter
DLS ..... Dynamic Light Scattering
DNA ..... Deoxyribonucleic acid
dsDNA ..... Double-stranded DNA
ssDNA ..... Single-stranded DNA
DPPC 1,2-dipalmitoyl-sn-glycero-3-phosphocholine
DOPE 1,2-dioleoyl-sn-glycero-3-phosphoethanolamine
DOTAP 1,2-dioleoyl-3-trimethylammonium-propane
DOTMA ..... 1,2-di-O-octadecenyl-3-trimethylammonium propane
DSC ..... Differential scanning calorimetry
ECM ..... Extracellular matrix
EM ..... Electron microscopy
EtBr ..... Ethidium bromide
FCS ..... Fluorescence correlation spectroscopy
FFF ..... Field flow fractionation
FRAP ..... Fluorescence recovery after photobleaching
FRET ..... Fluorescence resonance energy transfer
FTIR ..... Fourier transform infrared spectroscopy
GAG ..... Glycosaminoglycan
GFP ..... Green fluorescent protein

GP .....Gemini plasmid (Gemini plasmid pre-complex)

GPL .....Gemini plasmid lipid complex (Gemini nanoparticle)

ITC .....Isothermal titration calorimetry

LDME .....Laser Doppler micro-electrophoresis

MEM .....Minimal essential medium

NP .....Nanoparticle

N/P ratio.....Charge ratio (amine to phosphate ratio)

PCH .....Photon counting histogram

PDI .....Polydispersity index

PEG .....Polyethylene glycol

PEI .....Polyethyleneimine

PLL .....Poly-L-lysine

PO .....Poly-L-ornithine

pDNA ..... Plasmid DNA

R6G ..... Rhodamine 6G

RNA .....Ribonucleic acid

TEM .....Transmission electron microscopy

ζ .....Zeta potential

Gemini Abbreviations

m-s-m ..... Gemini surfactant abbreviation: m= alkyl tail length; s =spacer length

12-3-12 ..... 1,3-propanediyl-bis(dimethyldodecylammonium) dibromide

12-6-12 .....1,6-hexanediyl-bis(dimethyldodecylammonium) dibromide

12-7-12 .....1,7-heptanediyl-bis(dimethyldodecylammonium) dibromide

12-10-12 ..... 1,3-decanediyl-bis(dimethyldodecylammonium) dibromide

12-16-12 ..... 1,3-hexadecanediyl-bis(dimethyldodecylammonium) dibromide

12-7NH-12..... 1,9-bis(dodecyl)-1,1,9,9-tetramethyl-5-imino-1,9-nonanediammonium dibromide

Py-3-12..... N^1-dodecyl,N^1,N^1,N^3,N^3-tetramethyl-N^3-(5-(pyren-6-yl)pentyl)propane-1,3-diammonium dibromide

16-3-16.....1,3-propanediyl-bis(dimethylhexadecylammonium) dibromide

18-3-18..... 1,3-propanediyl-bis(dimethyl-octadecylammonium) dibromide

1.0 Introduction

This section will introduce the current status of gene delivery in terms of human gene therapy. It will lead into a brief outline of the tools used to characterize delivery systems and the significance of their insight in increasing our understanding and improving efficacy of these therapeutics. Finally, the role of new fluorescence techniques, with a focus on FCS, and why it is being investigated as a new tool to further our understanding of gene delivery systems using gemini nanoparticles (NPs) as a model.

1.1 Introduction to gene therapy

Human gene therapy is the treatment of disease by introducing therapeutic nucleic acids into the cell to change the course of a disease. This concept of treating hereditary diseases was first proposed in 1947 by Clyde E. Keeler. As a geneticist, he saw the limitations of traditional medicines in treating such diseases as it only provided temporary relief of the symptoms. He realized the problems were "rooted deep within the germplasm" and "fated always to re-appear generation after generation forever". He went on to propose that "what is in effect a therapeutic technique [gene therapy] actually is widely in use in applied genetics, and presumably in nature in the evolution of gene systems. This has the effect of achieving a permanent correction of hereditary diseases or dyscrasias occurring in strains of organisms, by a homozygous modification of the genetic formula" [1]. In description, Keeler imagined modern gene therapy. Although the concept appeared simple to him, Keeler realized the limitation of the technology of his time, and therefore, could only describe the principles. These theories would not be placed into practice until 1980s, when advancements in the field of molecular biology allowed for the transfer of exogenous genes into host cells [2].

The goal of gene therapy depends on the application. For example, for genetic diseases (e.g. cystic fibrosis and cancer) the goal is to override the influence of malfunctioning gene in order to restore normal physiological function [3-5]. Gene therapy can also be applied to prevention of diseases. By introducing genes that would code for the production of an antigen gene therapy can be used for vaccination against cancer, bacterial infection and allergies [6, 7]. For the context of this discussion, the term gene therapy will be directed towards the treatment of somatic cells versus germline cells [8]. Since the first human gene therapy trial in 1989 by Rosenberg and colleagues, the number of gene therapies approved for clinical trials has exceeded 1800 in over 32 different countries, with 63% of the trials taking place in the United States. A majority of the trials (over 63%) are focused towards treating a spectrum of

cancers, but monogenic disorders such as cystic fibrosis, neurological, ocular diseases, bone fractures and erectile dysfunction are being tested in clinical trials of gene therapy [9].

Even with our current understanding the human genome (with the completion of the human genome project and the completion of the first stage of the 1000 genome project) and the identification of genetic markers of certain diseases (e.g. BRCA1 for breast cancer), that gene therapy still has a long way before it can be seen as a routine application tool in the medical world [10]. In the past two decades, various hurdles, both ethical and technical, have hampered the development of clinical gene therapy treatments. One of the major technical barriers lies with the delivery of the therapeutic gene of interest. Early gene therapy studies have shown low levels of gene expression after localized injection of a therapeutic gene in diseased tissue [11-13]. This example shows that the limiting factor of successful gene therapy is not in the lack of therapeutic genes, but in its delivery [14].

1.2 Gene delivery systems

1.2.1 The "ideal" delivery system

The need for an effective delivery system for gene therapy has sparked intense research in the field of gene delivery. To understand why there is such a wide selection of delivery systems one must first consider what makes an ideal delivery system. A delivery system would have several characteristics optimized for clinical gene therapy applications. The ideal delivery system would have no immunogenic effect; it would not be cytotoxic once disassociated in its target cell. It would have high transfection with controllability over its expression, and the effects would be long lasting without the risk of mutagenic insertions or generating unwanted dosing effects. The delivery system should also be tunable; meaning it can be rationally modified to meet specific needs and increase specificity to target tissues [15-18]. This would avoid unwanted interaction with other biological materials (e.g. unwanted interaction with other blood components and healthy tissues) [19-22]. From an economical standpoint, the ideal delivery system would also be manufactured from commercially available materials (to streamline approval), low costing with a long shelf life to aid in storage and distribution. Currently, there are no delivery systems that have all of these characteristics (yet). Delving into the field of nanomedicine, there is a prominent effort to develop novel delivery systems with enhanced properties for clinical uses. The following section will briefly introduce various delivery systems that are been studied.

1.2.2 Physical delivery methods

Since the beginning of gene therapy, the use of naked DNA has been readily investigated. Studies with animals in the past have demonstrated that even the direct introduction of naked plasmid to target tissues have minimal efficacy due to short half life and uptake of therapeutic DNA by the liver [23, 24]. To aid the delivery of naked plasmids, various physical methods have been explored to enhance gene transfer both *in vitro* and *in vivo*. These methods include electroporation, gene gun, hydrodynamic gene transfer (Table 1). All these methods enhance gene delivery by bringing the transgene closer to the cell, and causing reversible disruptions to the plasma membrane, which increase the intake of the transgene. These methods make up approximately 18% of the clinical gene therapy. Although these methods work *in vitro* and have been applied *in vivo*, their usefulness is limited by invasiveness, tissues damage or poor penetration of deep tissues [25].

Table 1: Summary of physical gene delivery systems. Adapted from [25-27]

System	***Mechanism***	***Route***	***Advantages***	***Disadvantages***
Direct Injection	Direct injection of DNA into target tissue	Intramuscular	• Simplicity • low toxicity	• Low efficacy
Gene gun	Bombardment of tissue/cells with gold particles coated with DNA	Topical	• Good efficacy • Good for skin, mucosa areas	• Tissue damage • Unsuitable for deep tissue
Electroporation	Electric field is generated to disrupt plasma membrane to facilitate entry of DNA	• Topical • Intratissue	• High efficacy • Introduce multiple plasmid • Localized dose	• Tissue damage (high voltage) • Invasive: Require incision to reach deeper tissue, require injection prior to electroporation • Requires large quantity of plasmid
Ultrasound	Ultrasound creates membrane pores. Can also rupture delivery systems loaded with DNA	• Topical • Systemic	• Non invasive	• Low efficacy *in vivo* • Accessibility • Large volume of plasmid needed
Hydrodynamic delivery	In mice, large volume of saline is injected through tail to infuse tissues with DNA solution	Intravenous	• Simplicity • High effectiveness for highly perfused organs	• Require large volume of dose, hard to translate to humans • Tissue damage

1.2.3 Viral vectors

Viral vectors have made significant landmarks in the history of gene therapy. In 1989 Rosenberg and his group utilized a viral vector and were in the first human clinical trials for the treatment of metastatic melanoma [28, 29]. This pioneering work sparked great interest in gene therapy in the 90s. In 2004 China became the first country to approve a gene therapy for commercial use, with the release of adenovirus-based Gendicine, used to treat head and neck tumors. Then in the summer of 2012, European drug regulators gave approval for Glybera a gene therapy to treat lipoprotein lipase (LDL) deficiency [30].

Currently, several classes of viruses are used for gene therapy - the majority being adenoviruses and retroviruses, each with their own unique properties and characteristic (see Table 2) [9]. The success of viral vectors is due to the nature of viruses to gain access to their hosts in order to replicate as part of their life cycles and therefore make good candidates for gene delivery system. This is achieved by re-engineering the wild virus by removing large fragments of the genome, generally sections related to life cycle and pathogenesis, with the therapeutic gene of our interest, while leaving viral genome elements responsible for packaging of DNA and DNA integration in the host chromosome intact. [31, 32]. However several concerns about viral vectors have arisen and have been the cause of many clinical trials to fail. One major disadvantage is capsid coat which limits the size of therapeutic DNA that can be packaged inside. Furthermore the risk of immunogenicity, due to the capsid coat, limits the dose that be administered and its re-administration for long-term treatment [33, 34]. Another disadvantage is production costs for bioreactors required to culture viral vectors and also poses a risk of contamination [35]. Some undesirable results from these trials have manifested as symptoms of leukemia-like diseases, and even death. Needless to say, these outcomes raise key safety concerns about the use of viral vectors [36, 37]. There is active research into making viral vectors safer; however there are other groups that make for a safer alternative [31].

Table 2: Main groups of viral vectors. Table modified from [31, 32]

Vector	*Genetic Material*	*Particle Size*	*Packing Capacity*	*Coat*	*Tropism*	*Inflammatory Potential*	*Host Genome Interaction*
Retrovirus	RNA	100 nm	8 kb	Enveloped	Dividing Cells	Low	Integrated
Lentivirus	RNA	100 nm	8 kb	Enveloped	Broad	Low	Integrated
Herpes Simplex Virus-1	dsDNA	150-200 nm	40 kb	Enveloped	Favors Neurons	High	Episomal
Adeno-associated Virus	ssDNA	20-25 nm	<5 kb	Naked	Broad	Low	Episomal (90%) Integrated (10%)
Adenovirus	dsDNA	70-100 nm	8 kb	Naked	Broad	High	Episomal

1.2.4 Non-viral delivery systems

An emerging alternative to the mainstream viral vectors is the use of synthetic or non-viral delivery systems. Although the term "non-viral" has been used with physical methods of naked DNA delivery, for the context of this study, the term non-viral delivery systems will be used to describe pre-encapsulated methods of gene delivery. Since the first non-viral transfection by Felgner and colleagues in 1987, decades of research in the field of non-viral delivery has resulted in development of several delivery systems [38, 39]. Non-viral delivery systems, an extensive class of man-made complexes or NPs, are composed of nucleic acid cargo, typically a plasmid, with one or more soft matters used as the carrier [39]. Generally non-viral delivery systems are composed of cationic material that will electrostatically bind nucleic acids and condense genetic material at a size of a few tens or hundreds of nanometer in diameter (see Figure 1 below).

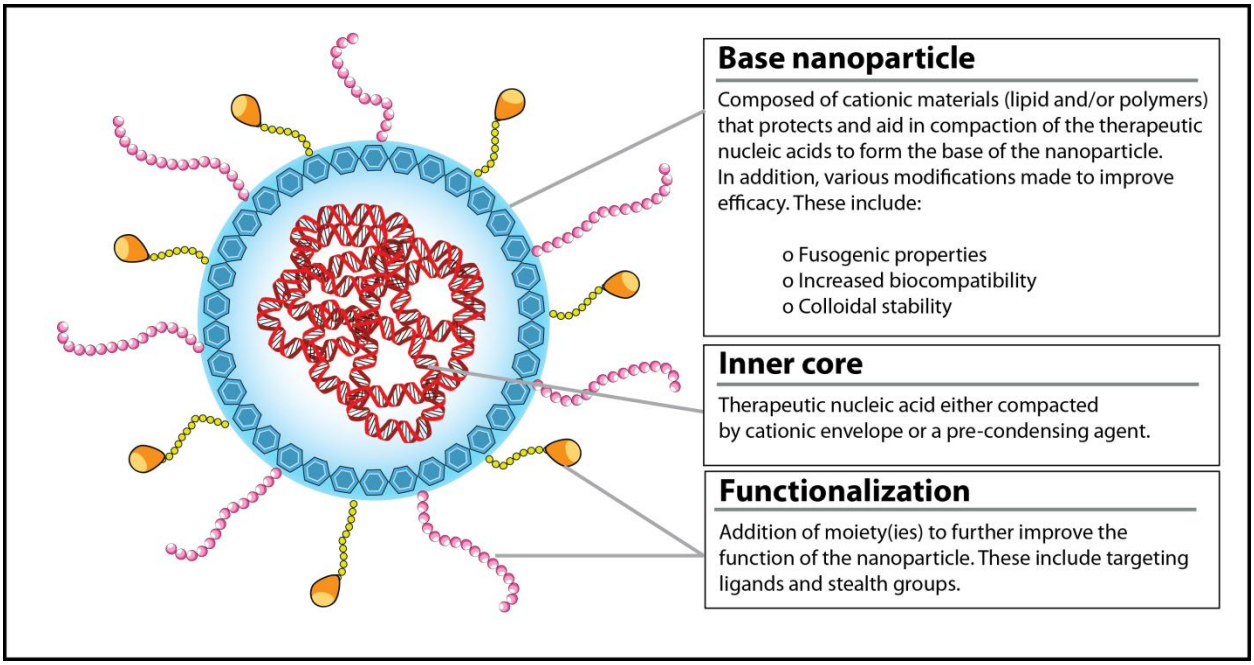

Figure 1: Basic anatomy of a non-viral gene delivery system: Non-viral delivery systems are composed of three fundamental elements. The first is the nucleic acid that forms core of the NP. Second, is the soft material that forms the basic element of the NP and encapsulate the DNA into a NP. Finally additional functional groups can be added to the base NP to augment the system and improve overall efficacy.

This mechanism occurs due to the neutralization of the negative charge on the phosphate backbone of nucleic acid by the polycations. This results in the relief of the repulsive forces and the loss of volume or compaction of the nucleic acids [40]. The resulting NPs have a positive surface charge to facilitate binding to the negatively charged plasma membrane of the cell. Compaction of the genetic material also provides protection against degradation [41-45]. These NPs are defined by their composition and exist as two major classes: lipoplexes and polyplexes as outlined in Table 3.

Table 3: Main classes of non-viral delivery systems [46-50].

Delivery System	***Composition***	***Examples***
Lipoplexes	Cationic and neutral* lipids	• DOGS • DOTMA • DOTAP • DC-Chol* • DOSPA and DOPE* (Lipofectamine)
Polyplexes	Polymers	• Polyethylenimine (PEI) • Poly-L-lysine (PLL) • Poly-L-ornithine(PO) • Chitosan • Cyclodextrin • Dendrimers
Lipopolyplexes	Hybrid of lipids and polymers	• PEI-DOTAP-Dc-Chol • DOTAP-Chol-protamine sulfate (LPD) • PLL-DOTOP

The first class of non-viral delivery systems is composed of cationic lipids that spontaneously assemble into liposomes. Liposomes are closed micro-nano vesicles, of uni- or multilamellar forms composed from the self-assembly of one or more phospholipids. Their biological origin makes liposomes a good candidate for clinical applications due to their biocompatibility [51]. Most literature on lipoplex analysis is *in vitro* studies performed in solution. [26, 52-54]. There are many variables that are considered in these solution studies which include: chemical structure of the lipid(s), the ratio of lipids or charge ratio, the physical structure of the lipoplex, and of course, the intended target. To consider the chemical structure of a lipid, its structure can be modified at three major areas, at the head group, linker and hydrophobic tail. Although there are a variety of lipid formations used in lipoplex formulations, generally, the composition of the lipoplex utilizes cationic lipids. The positive charge on the lipid head facilitates the spontaneous interactions with DNA where upon it aids in the binding the r lipoplex with the negatively-charged plasma membrane. The amount of cationic lipid also plays a role in determining the charge-ratio of the final lipoplex, which has been shown to have profound effects on transfection efficiency [55, 56]. Lipoplex can also incorporate zwitterionic lipids, known as helper lipids, to enhance the cationic lipoplex. These phospholipids enhance the effectiveness of cationic lipoplexes by increasing stability and bestowing fusogenic properties to aid in endosomal release [57-59].

A second class of non-viral delivery systems is polyplexes. They utilize a wide range of synthetic and biological polymers to form complexes with DNA. Although polymers also condense DNA (through electrostatic interactions to aid in endosomal uptake), there are key differences compared to lipoplexes that were previously discussed. The key difference between a lipoplex and a polyplex is the chemical nature of monomers. Although there are a wide range of polymers used, generally all cationic polymers lack a hydrophobic domain. This means that polyplexes generally form more compact (smaller) and uniform particles (relative to lipids) due to higher number of amine and positive charges. For example, polyethyleneimine (PEI), one third of its molecular structure is composed of nitrogen with one sixth carrying a positive charge at physiological pH [60]. One drawback with the absence of the hydrophobic domain is that polymers do not readily interact with lipid membranes [61]. The problem with early polyplexes such as poly-L-lysine (PLL) is they lack an effective mechanism to escape the endosome Therefore these polyplexes suffered from low transfection efficiencies without the addition of endosomal lytic agents or additional modifications [62]. Nonetheless, commonly used polymers are not biodegradable (PEI, PLL), which can result in increased cytotoxicity. Other biodegradable polymers such as chitosan have been investigated as a solution to decrease cytotoxicity [63].

Non-viral delivery systems show promise *in vitro*, however there are problems that are exhibited *in vivo*. Early studies with lipoplexes showed that systemic distribution of NP was quite poor in biological systems [64]. Unlike viral vectors which developed mechanisms to reach their targeted cells, non-viral carriers are impeded by intracellular trafficking [39, 65-67]. Nevertheless, research has also demonstrated flexibility of the NP in allowing for modifications to improve its systemic distribution [68].

1.3 Nanoparticle design

As described previously (Section 1.2.1) the ideal delivery system would have various characteristics to achieve high degree of transfection in target cells. Although neither lipid nor polymer based delivery systems have all of these characteristics, modifications can be made to impart new functions to optimize the amount of transfection. This rational design of NPs takes into consideration the applications of the delivery system in order to overcome hurdles, increase efficacy and develop a profile to match a particular therapeutic strategy. One important modification is the introduction of targeting ligands to NPs that are specific for certain receptor expressed on certain cells. The field of targeting ligands is popular in the field of cancer research where several ligands are added to increase NP-specificity to cancer cells [69]. This important modification not only increases the effectiveness of the NP, but also reduces side effect by decreasing toxicity to non-targeted cells. Once the NPs are taken into

the cells, the next barrier escapes the endosome to avoid lysomal degradation. Modifications such as fusogenic lipids, pH sensitive chemical structures (respond to shift in pH of the late endosome) or addition of endolytic agents can be added to aid the release of the NP and its contents [70, 71]. Recently new ligand have been used to exploit new pathways to the nucleic via the Golgi body, therefore bypassing the lysosome, as a new mechanism of entry into the cell [72]. A final consideration for building NPs is to increase their stability. This factor is particularly important for *in vivo* applications of these delivery systems**,** where non-specific biological interactions such as serum proteins and the immune system can result in the clearance of the NPs [73]. A common solution in preventing this unwanted uptake is the application of polyethylene glycol (PEG). PEG is functionalized to the outer coat of NPs and decreases steric interactions and provides stealth capabilities against cells of the immune system. In a study it was shown that addition of a PEG coat significantly increased the systemic circulation of NPs from hours to days [74, 75]. Other novel functions that have been evaluated include environment stimuli such as light and magnetic fields, adding an additional degree of control to NPs [70, 76, 77].

This flexibility of engineering non-viral delivery systems provides several key advantages over their viral counter-parts. These advantages include reduced immunogenicity based on their construction from biologically inert materials and at reduced costs of production. Furthermore, many of these materials are previously FDA-approved for implants and injection, aiding with regulations [78, 79]. Overall, the "bottom-up" design allows for customization in composition and incorporation of specific moieties to suit a wide range of applications. [54, 80, 81]. Although the number of non-viral delivery systems currently in clinical trials has increased to 18%, , they are still the dark horse in the world of gene therapy compared to viral counterparts [28]. Although there is active research in this field, there are many unknown factors about the intracellular fate of non-viral delivery systems [67, 82-84]. To further develop non-viral delivery systems, critical information must be obtained on how the carriers interact in the extra- and intracellular environments. To truly appreciate the extensive research, one must also investigate the various barriers they were designed to overcome to develop more effective therapeutic options.

1.4 Barriers to gene transfer

The site of action of somatic gene therapy is the nucleus of the target cell. The barriers to gene delivery vary and depend on the location of targeted cells and the route of administration. These barriers can be classified as either intracellular or extracellular that will be discussed below. Intracellular barriers will be discussed first due to the extensive use of tissue culture to evaluate and development of new gene delivery systems.

1.4.1 Intracellular barriers

At the molecular level of a single cell, there are numerous obstacles that hinder transfection of exogenous DNA. Upon contact with the cell, the DNA must adhere to the plasma membrane, overcoming columbic interactions on the surface of the cell to make contact with plasma membrane, a lipid bilayer of various phospholipids embedded with proteins that governs the entry and exit of molecules into cell. Upon binding this outer membrane, the gene must be internalized by some form endocytosis or other uptake mechanism [85-89]. Even entering the cell, the gene is separated from the cytoplasm by a lipid vesicle or endosome. The DNA must then escape the endosomal pathway or risk degradation within the lysosome. After leaving the internalization pathway, the gene must navigate through the cytoplasm, which contains networks of cytoskeleton and endonuclease and macromolecules that hinder the gene to its final barrier [90, 91]. The nuclear membrane consists of a double membrane that is fenestrated with thousands of nuclear pore complexes. Although numerous, the nuclear pore complexes are very narrow (9 nm closed, to 39 nm dilated), are highly selective, and without a specific tag sequence for facilitated transport the DNA cannot reach the host genome within [92]. Only then can the therapeutic DNA access the host genome to express its therapeutic effect [65, 66, 93, 94]. This tortuous path to the nucleus demonstrates the need for a carefully orchestrated delivery method to ensure sufficient quantity of the gene reaches the nucleus to achieve a therapeutic dose. Even after leaving the endosome, the DNA must continue to overcome various physical and biochemical barriers within the cytosol and cross the final barrier, the nuclear membrane. In the field of gene delivery, these delivery systems are divided into two broad categories: viral and non-viral delivery systems. A large body of work investigating the mechanism of gene delivery has focused on the intracellular barriers that the delivery system must overcoming to transfer genes into the host cell's nucleus. Although this is vital step in study of gene delivery systems, another important consideration for *in vivo* applications are the extracellular barriers.

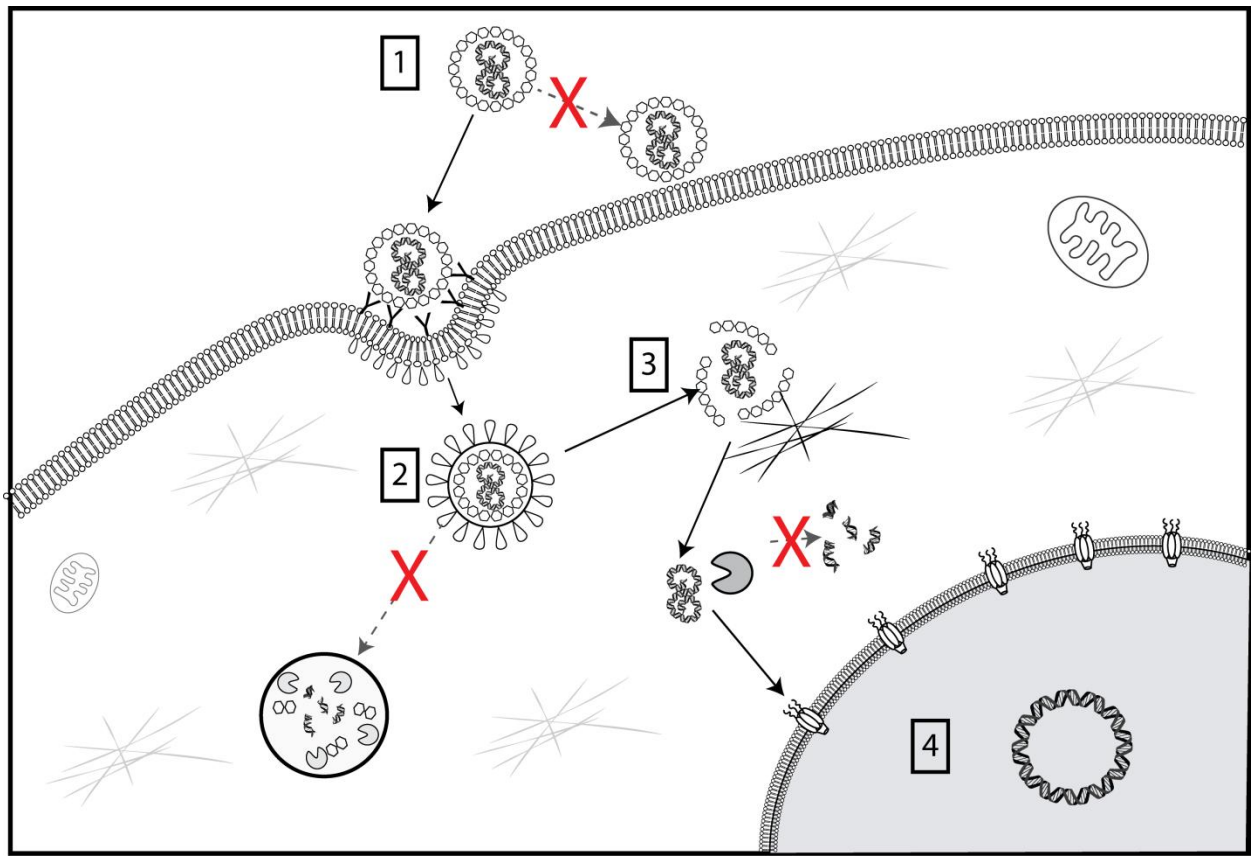

Figure 2: Overcoming cellular barriers to gene delivery. The plasma membrane is the first cellular barrier that must be overcome. This is achieved through adherence and triggering internalization (1). Upon entering the cell the delivery system must escape the endosome to reach the cytosol or risk lysosomal degradation (2). The cargo must also be released from the carrier and transit through the highly structured and dense cytoplasm and avoid degradation by various nucleases (3). Depending on the cargo (e.g. anti-sense oligonucleotide, journey ends at the cytosol), but plasmids for instance must also pass the nuclear membrane in order to be expressed (4).

1.4.2 Extracellular barriers: Challenges to clinical use

Although a great deal of research has been done to study the intracellular barrier role in transfection efficiency, it has been established that *in vitro* results are poor prediction for *in vivo* applications [95-98]. The main reason for this discrepancy is the presence of extracellular barriers, obstacles that hinder delivery system from the point of entry to surface of the target cell. Approaching the cell, therapeutic genes must bypass the extracellular environment; a maze of physical and biochemical hurdle that either adhere or degrade free DNA. These barriers can be classified as anatomical barriers, interactions with biological fluids, extracellular matrix and non-specific cell interactions.

One of the key anatomical barriers to gene therapy is epithelial cells that line the various surfaces in the host body. This broad class of cells, vary in composition depend on it location in the body, but is

generally made of closely arranged cells in one or more layers and plays a key role in the protection of the host [99]. Specific epithelium such the one found in the eyes, airways, gastrointestinal tract and colon have an additional layer of mucus, a robust, semi-permeable gel that exchange nutrient with the epithelial cells below and block bacteria and pathogens[100]. However, these barriers also limit the uptake of therapeutic genes to the targeted tissues resulting in lower efficacy [101-104].

Additional barriers depend on the route of administration. Oral delivery is the simplest and most ideal route of drug administration, but it is challenging due additional physiological barriers such as the acidic environment of the stomach, and the digestive enzymes of the intestines [105]. Even with systemic administration, the therapeutic gene faces several barriers before efficient transfection can occur. In the circulation genes are traveling through the blood, a specialized fluid, containing a suspension of cells and macromolecules. The gene must make it through various hurdles such as immune system, avoid unspecific interaction with serum protein (albumin) and lipoprotein (HDL and LDL [106, 107]. Depending on the target site, the gene must escape the vasculature through fenestrate and find the target cell or risk degradation by various nucleases and scavenging by hepatocytes in the liver [23, 108-110]. While in circulation, or upon entering the target tissue, the nucleic acids must avoid being scavenged by immune systems components [111, 112]. Even upon avoiding these obstacles, unless guided, the gene still have to find the target cells or risk uptake by unspecific cells, which can reduce the efficacy of the therapeutic drug and increase the risk of side effects. Even with topical gene delivery; whether through direct injection into tissue or application to surrounding tissues, the nucleic acid still must bypass the extracellular matrix (ECM) upon approaching the target cells. The ECM is composed of a meshwork of proteins and polysaccharides that are extruded locally by the cells within the matrix. Within this matrix key units are the polyanionic molecules such as glycosaminoglycans (GAGs) that form the structural unit of protoglycans that cover the surface of all mammalian cells. This matrix not only plays a structural function, but also plays role in governing cell growth and behavior and is even the unique marker for specific viruses. Due to their anionic nature and abundance, GAGs pose a barrier and inhibit gene transfer [113-115]. To overcome these numerous hurdles, extensive research has been done to development method to increase the stability and expression of the therapeutic gene.

1.5 Nanoparticle design and transfection efficiency

In general non-viral delivery systems assemble through electrostatic interaction between the highly anionic nucleic acids and a polycation (cationic lipids, dendrimers, PEI etc). The bottom-up engineering of NPs allow for the production of multi-functional particles in a modular fashion to meet a variety of therapeutic strategies. It is difficult to correlate all factors to ultimate delivery system efficiency amongst various physiochemical properties that govern the efficacy of the NPs. However, there are several factors that are routinely monitored in delivery system design.

1.5.1 Size

One of the most studied factors in gene delivery is particle size. Although on average most particles range between 100-300 nm, in the literature there is no ideal size for a delivery system. A number of groups have reported that either smaller or larger particles are more effective [54]. One of the key reasons for this discrepancy is due to the factors that govern the particle size of delivery systems. The factors that govern the size and size-distribution of NPs are efficiency of compaction (in turn controlled by the N/P), preparation method and the environment (pH and ionic strength). In addition, due to spontaneous self-assembly of non-viral delivery systems, even in the simplest NPs, composed of two elements (DNA and single polycation material) will generate a population of particles [54, 116-123]. Generally, since numerous groups have various formulations of their own NPs, and without a standardized method to monitor particle size, it is easy to see why there is little agreement on the issue of size. Furthermore characterization studies performed by single groups have begun to demonstrate that size does not always correlate with transfection efficiency [122]. Nevertheless, particle size still defines the route to the target and determines which obstacles it will face. For instance it has been reported that particles within a specific size range are favored by certain endocytosis pathways compared to others. A control study using labeled beads of increasing size range (50, 100, 200, 500 nm) showed that smaller particles (<200nm) were rapidly taken up, via the clathrin-mediated pathway, but resulted in lysosomal clearance. On the other hand larger particles (>200 nm) were taken up slower by an alternative pathway, the caveolae pathway, but showed prolonged circulation within the cell, and more importantly, avoided lysosome degradation [124].

On the contrary to *in vitro* results, *in vivo* studies have shown that smaller particles have better results. Smaller particles (<100nm) showed reduced adsorption to plasma proteins, reduced hepatic filtration, and opsonization and clearance by the immune system. Along with the increased circulation

time in the blood, smaller sizes aid in the permeation of NPs into target tissues [125, 126]. On the whole, size still remains a fundamental characteristic to consider in terms of the mechanism of uptake available to specific cell lines [16, 17]. Size can be used as a measure of the physical properties which play a key role in quality control and assurance. Especially in terms of manufacturing gene delivery system it does not always correlated to final efficacy, in which other factors must also be considered [53, 61, 127, 128].

1.5.2 Surface charge

Surface charge of the delivery system, like size, is determined by the composition of the particle. *In vitro*, the charge ratio (ratio of cationic material to nucleic acid) may vary based on the chemical structure of the delivery systems. Typically, an overall positive surface charge provides increases transfection efficiency. This is widely accepted due to the ability of the cationic delivery system to electrostatically interact with the negatively-charged plasma membrane of the cell and improve adhesion (the first step in cellular uptake process). The effect of charge ratio on transfection efficiency is also material (e.g. PEI, cationic lipids and dendrimers) and cell-line dependent, generally a 1:1 ratio is the minimal, which is the amount required to neutralize the negative charge on nucleic acids. The charge ratio also needs to be optimized for each case because an excess of charge ratio generally results in reduced transfection efficiency. This is widely believed to be due to cytotoxicity related to the presence of free or unbound cationic material [129-131].

Although the effect of surface charge *in vitro* is well defined, its role *in vivo* is not as clear. Several groups have reported that cationic delivery systems suitable for *in vitro* applications show reduced efficiency *in vivo*. This is because simple electrostatic interactions that help delivery systems bind to cells *in vitro*, result in non specific interactions with other molecules in the body such as serum proteins and immune cells. This reduces the number of particles reaching the target cell and resulting in reduced efficacy. It has been shown that anionic or weakly cationic delivery systems provided increase transfection efficiency *in vivo* [125, 126]. In a study using mouse lungs by He and colleagues, showed that higher charges, either positive or negative, resulted in increased opsonization and interaction with macrophages and clearance of the NPs [126]. The paper demonstrated that for *in vivo* applications, mixtures that were stable after extend periods of storage resulted in high expression in mouse lungs [98].

1.5.3 Nanoparticle structure

Another parameter that is assessed is the overall structure of the delivery system that can be divided into external and internal features. The external structure, or shape of particle and its internal structure are evaluated based on the interaction of DNA with the delivery system. As with other physiochemical properties, the composition of the delivery system will have profound effects on its shape. In terms of external structure, the majority of particles are believed to be spherical, although other shapes such as rods, globules and toriods have also been reported [132-134]. Studies have also demonstrated that the shape of the delivery system affects transfection efficiency, but why that is has yet to be understood [135]. One main explanation for this discrepancy is the methods of visualizing the delivery systems. Techniques such as electron microscopy (EM) and atomic force microscopy (AFM) have been traditionally utilized but are prone to artifacts (to be discussed later in Section 1.6.1).

As well as looking at external structures of delivery systems, there are internal structures to be considered and believed to be more significant. Internal structure refers to the long-range order or internal arrangement molecules within the delivery system. In lipoplex delivery systems, various polymorphic phases such as lamellar, hexagonal and cubic occur [136, 137]. Studies have indicated that hexagonal phases provide higher levels of transfection compared to lamellar structures. This is due to lamellar phases being more stable within cells, while hexagonal phases encounter fusogenic properties aid in the release of the delivery system's cargo. New research has demonstrated lamellar phase mechanism to be charge-density dependent in contrast to hexagonal phase being independent [138]. Furthermore research by our group has also demonstrated that other polymorphic phases exist and aids in increasing the efficacy of the delivery systems [139].

To build an ideal delivery system, a multi-faceted approach must be taken to optimize a delivery system for delivery. One of the key issues lies in the condition in which these test are performed. Despite pure delivery system populations and well-controlled environments, *in vitro* studies and *in vivo* studies are not well-correlated. Therefore new techniques must be used to extend our current understanding in the cellular world.

1.6 Physicochemical characterization of nanoparticles: Current methods

Numerous physicochemical parameters have been shown to affect NPs making the relationship between NP assembly and transfection efficiency difficult to describe. To advance the field of non-viral gene delivery for *in vivo* applications, additional information is required on the effects of different materials of NP composition. Therefore, a method of monitoring the influence of different compositions is required to show the true relationship between structure and function. This section will review commonly used techniques in studying these physiochemical parameters and their limitations. Figure 3 highlights the most important NP properties assessed by non-viral research groups. It is beyond the scope of this thesis to discuss the theory for each technique, though some key concepts will be touched upon.

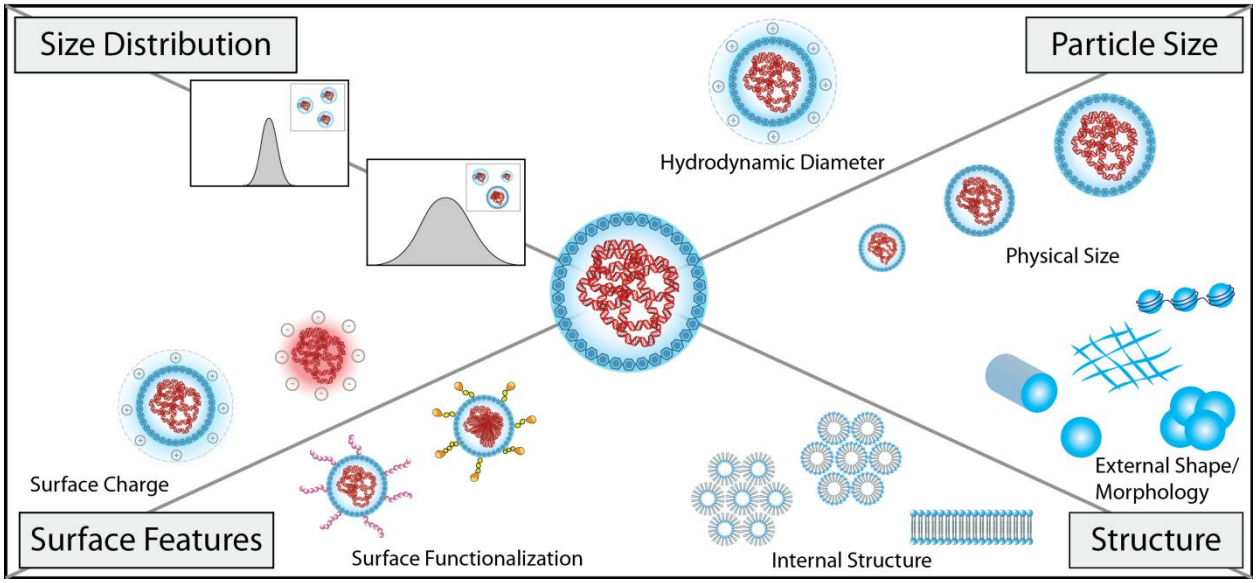

Figure 3: Summary of NP characterization. Various biophysical properties of NPs are evaluated using several techniques each with their own unique advantages and disadvantages. Size distribution and hydrodynamic diameter can be determined by DLS. External morphology and direct measure of physical size can be done with EM and AFM. Surface charge can be studied using zeta potential measurements. Internal structures can be evaluated using SAXS, WAXS, and XRD.

1.6.1 Particle size and size distribution

The two key parameters of delivery systems that are monitored by researchers are particle size and size distribution. As described previously, the key to performance of NP is their small size. Therefore it is crucial to monitor the size and stability of the particle to ensure optimal activity. Additionally, these parameters can also give insight into the stability of the systems, encapsulation efficiency which are crucial for pharmaceutical quality control [140]. Due to its importance it is not surprising that several techniques have been employed to screen particle size - each technique having their own advantages and disadvantages (Table 4).

Table 4: Summary of particle sizing techniques used to characterize NPs

Technique	***Mechanism***	***Advantage***	***Disadvantage***
EM (TEM)	Microscopy: Electrons	• High Resolution • Direct size, shape and distribution measurement	• Low throughput • Extensive sample prep • Artifact due to sample preparation • Extensive user training
AFM	Microscopy: Atomic probe	• High Resolution • Direct size, shape and distribution measurement	• Artifact due to mounting • Extensive user training
DLS	Light scattering	• Minimal sample preparation • Fast measurement • Simple operation	• Measure hydrodynamic diameter not physical size • Affect by large particle in solution • Poor sensitivity at low concentration
NTA	Light scattering and particle tracking	• Fast measurement • Simple operation	• Measure hydrodynamic diameter, not physical size • Affect by large particle in solution • Requires sample labeling
FFF	Chromatographic	• Analysis of large size range • Molecule specific detection • Minimal preparation	• Requires user calibration • Time consuming • Optimization of instrument for different NPs
FCS	Fluorescent fluctuations	• High sensitivity • Fast measurement time • Can use *in vitro*	• Requires sample labeling • Tedious set up and calibration • Requires extensive user knowledge to analyze data

In regards to microscopy, traditional light microscopy cannot be used to study the size NP particles. This is due to the diffraction limitation of light, which limits technique resolution to

approximately 200 nm [141]. To overcome this obstacle, other forms of microscopy are needed. Electron microscopy (EM) is able to overcome this limitation by using electrons that have shorter wavelength compared to photons, and pushes resolution of microscopy to the atomic scale. Transmission electron microscopy (TEM) and various derivations (cryo-TEM and freeze-fracture TEM) have been used for the detailed studies of size and shape of the delivery systems [41, 142, 143]. Although structures could be studied in stunning detail using TEM, samples sometimes require fixation in resin prior to imaging. Due to the soft nature of the non-viral system being studied, increases the risk of preparation artifacts.

Scanning probe microscopy (SPM), another form of microscopy to study delivery systems, is a form of atomic force microscopy (AFM). AFM is a powerful tool able to investigate NPs in a variety of environmental conditions, most importantly liquid, making it a versatile technique. AFM utilizes a probe attached to a sensitive cantilever that measures the vertical deflection of the probe as it interacts with its environment [144]. In a sense, AFM allows the user to "feel" the topology of various materials. A resolution of 1Å is possible; however resolution is limited by the sharpness of the tip. AFM has gained particular attention as an alternative to TEM since it does not require the extensive sample preparation and harsh conditions as such with TEM (conditions that may affect the morphology of the delivery systems). Although the sample preparation is less invasive, it is not free from artifacts. One example of AFM application is the study the surface morphology of functionalized liposomes [145].

Although the resolution of both TEM and AFM give for stunning images of individual or small populations of particles this window is quite small. Therefore due to the heterogeneity observed with NP preparations, great care must be taken in selecting the number of particles to sample and measure to avoid bias. Furthermore due to the high cost of specialized equipment and operations, it is difficult to obtain large number of images. Generally this number will be orders of magnitude smaller than total number of particles yet, too small a sample size can result in bias and misleading data. Therefore to inquire into the population distribution of NPs other techniques are required.

Techniques that are routinely used to monitoring of size and distribution are dynamic light scattering (DLS), flow-field fractionation (FFF) and NP tracking analysis (NTA). These techniques indirectly measure the hydrodynamic diameter which is based on the Stokes-Einstein equation below. Where k is Boltzman constant (1.38×10^{-23}J/K), T is absolute temperature in Kelvins and η is viscosity of medium.

$$D_H = \frac{kT}{3\pi\eta D} \quad \text{(Eq 1)}$$

Each technique utilizes different methods to determine the diffusion coefficient (D), with each having their own advantages and disadvantages. Dynamic light scattering (DLS, or photon correlation spectroscopy, PCS), a frequently used method, is used to determine size and size distribution of NPs [135, 146-150]. DLS uses light (in form of a laser) which is directed at a suspension of particles and a record is taken from the fluctuation caused by scattering-based Brownian motion. This autocorrelation function (ACF) is then fitted by a mathematical model which is used to determine the diffusion coefficient. Due to its simplicity of use, DLS is a widely used technique in the study of NP size and dispersion. One consideration of the DLS is that it does not reveal the true physical size of the particles, but rather it evaluates the hydrodynamic diameter based on NP movement through solution. Although DLS is suitable for determining particle size distribution or polydispersity of relatively homogenous samples, and more heterogeneous samples can result in measurement errors. Furthermore the presence of larger particles (causing larger amounts of scattering compared to smaller particles) can lead to an over-estimation of particle size.

Nanoparticle tracking analysis (NTA) is another popular technique that is similar to DLS in that they both measure the scattering generated from particles in solution. But unlike DLS (which uses ACF) NTA uses a charged-couple device (CCD) camera (a high resolution camera) to monitor the trajectory of individual particles as a means to determine diffusion coefficient [151]. Since each particle is measured individually, NTA is not as prone to partiality due to the presence of larger aggregates. This makes it a more suitable technique for the study of poly-dispersed systems. A disadvantage of NTA is that NP need to be labeled which is not required for DLS. Although both DLS and NTA are simple to use for routine analysis, there are limitations

Field-flow fractionation (FFF) is another technique used for sizing NPs [152-155]. FFF and its sub-techniques are chromatographic techniques that pump sample through a ribbon-like channel, where an external force (dependent on the sub-technique, could be centrifugal, thermal, electrical or hydrodynamic) is applied perpendicularly to the flow [156]. This results in the separation of particles based on size, density or surface functionalize in the presence of the external force. From this, the diffusion coefficient can be used and particle size is determined via the Stokes-Einstein as mentioned previously.

While these techniques allow for the study of population of NPs there are some limitations. One consideration is that these techniques do not reveal the true physical size of the particles, but rather their hydrodynamic diameter based on NP mobility movement through solution. Furthermore another consideration for these techniques as the Stokes-Einstein equation used to determine size based on mobility is under the assumption the particles are spherical. Another factor that needs to be considered is the polydispersity or how uniform the particles are. While one of the advantages of these techniques is the ability to study larger populations of particles and determine their distribution, there are limitations. For instance with DLS, the presence of larger particles or aggregates cause significant increase in input signal which can mask smaller particles. This results in an over-estimation of the reported particle size for both DLS and NTA (although the effect is not as severe with NTA). This make NTA more suitable for analysis of poly-dispersed systems compared to DLS. Overall, these methods work best with mono-dispersed systems, while the size values from very poly-dispersed systems must be interpreted with care.

1.6.2 Other physical characterization

Another key factor that is routinely monitored in delivery system characterization is the surface charge or zeta potential. Zeta potential (ζ) is a measure in colloidal science that describes the electrical potential that exist within the electron double layer of the particle specifically, at the sheer plane with respect to the electroneutral bulk medium. In theory, the magnitude of zeta potential, both positive and negative, can be used to predict the stability of the suspension [157]. Electrophoresis can be used to determine the zeta potential by monitoring the mobility of the charged particles in the presence of an electric field. This electrophoretic mobility or velocity can be used to calculate the zeta potential.

To study the internal structure of NPs, techniques such as small-angle x-ray scattering (SAXS) have been used. SAXS makes use of a high-energy x-ray, generally produced by a synchrotron, and produces a scatter pattern which reveals the pattern of organization of components. SAXS has been used to characterize DNA-liposome complex and reveal several polymorphic structures exist [136, 158-162].

From a pharmaceutical production stand-point, a lack of understanding of the interactions that govern a cationic delivery system limits the control of the stability of these formulations. There are several methods that have been used to counter this and allow for the study of interactions within the delivery systems.

1.6.3 Characterizing interactions of nanoparticle components

Besides surface features and transfection efficiency of NPs, other traits can also be examined. One of the key requirements of good NP design is study of the interactions between the various components that make up the NP.

One of the simplest techniques that can be used to study the interaction of the carrier with DNA is dye exclusion assay. Dye exclusion assay utilizes a nucleic acid dye, typically ethidium bromide (EtBr) that only fluoresces when bound to DNA. Therefore if the assembly process affects the conformation of the DNA, this can affect the binding sites for the dye. Therefore the degree of signal detected can be used as an inverse measure of affinity of the carrier to DNA [116, 132].

For a more quantitative measure of the energies involved in the assembly of the NP systems other techniques can be employed. Isothermal titration calorimetry (ITC) is a technique used to monitor the change in enthalpy (ΔH) of biomolecular interactions. By using the change in enthalpy, in combination with stoichiometry, ITC can indirectly monitor the stability of the delivery system in such situations, such as in the binding of DNA with its cationic carrier [163-165]. Another technique utilizing thermodynamics, is differential scanning calorimetry (DSC), which measures the shift in heat capacity (C_p). Deviations in these values can be used to identify conformational states of the molecules and determine changes in packing or structural fluctuations [166]. For both ITC and DSC, thermodynamic properties can be monitored without additional modification to the sample.

Fluorescence microscopy has been widely used in studying gene delivery systems despite having lower resolution than EM and light microscopy. One of the major applications of fluorescence microscopy is the study of transfection effectiveness of gene delivery system. In general, a gene that expresses a fluorescent protein, is monitored for the amount of fluorescent expression. The amount of fluorescence can be used to study transfection efficiency of one system versus another [167]. The delivery system and cargo can also be labeled with specific fluorescent dyes to study other properties of gene delivery systems. One application involves using the fluorescent-labeled components as reporters. These reporters determine the sub-cellular location of labeled molecules, such as delivery system components or nucleic acid cargo [82, 168]. Other examples of fluorescent techniques are Fluorescence Recovery After Photo-Bleaching (FRAP) and Fluorescence (Förster) Resonance Energy Transfer (FRET); both techniques utilize the phenomena of fluorescence to determine biophysical parameters such as diffusion, unpacking and interactions of non-viral delivery systems. [82, 84, 169, 170]

Important in delivery system design, secondary structures of DNA-carrier complex were shown to have an effect on transfection. Circular dichroism (CD) and Fourier Transform Infrared Spectroscopy (FTIR) are two techniques are that able to measure secondary structures of DNA-carrier complexes. CD uses polarized light to study the secondary structure of DNA-carrier complex [121, 171, 172]. FTIR can also be utilized to study the effect of cationic complexing agents on the secondary structure of DNA inside the NPs [118, 173].

1.7 Gemini nanoparticles as gene delivery system

1.7.1 Introduction to gemini surfactants

The initial study of gemini surfactants by Menger's group in the 1990s generated significant interest in both industry and academic circles due its remarkable properties. The basis of this interest is linked to its unique dimeric structure. In structural comparison, monomeric surfactants are composed of a single hydrophobic tail that is attached to a polar head-group, while gemini surfactant are composed of two hydrocarbons tails with two polar heads linked by a rigid spacer as shown in Figure 4 [174].

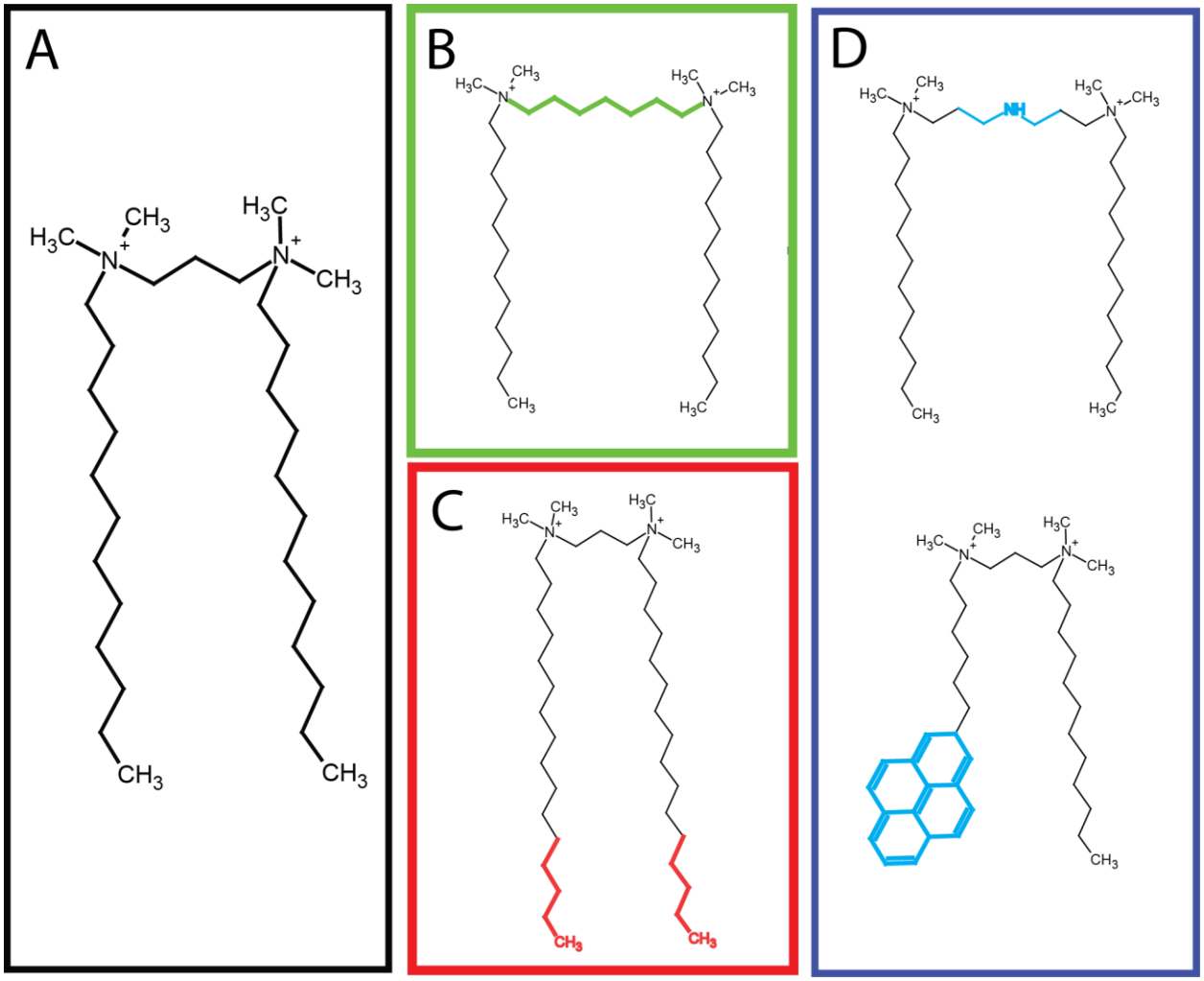

Figure 4 General chemical structure of gemini surfactants. Gemini surfactants are composed of two hydrophobic tail with charged head group linked by a spacer (A). To change their properties various structural modifications can be made. These include changes to spacer length (B), tail length (C) and addition of various functional groups (D).

The dimeric structure gives it remarkable aqueous properties when placed in solution and provides advantages to gemini surfactant NPs. Compared to monomeric counter-parts, gemini surfactants possess a significantly lower critical micelle concentration (cmc), increased solubilization, high surface activity and better wetting and foaming properties [175, 176]. Simply, a small amount of gemini surfactant can have dramatic effects. In terms of formulation development, this is an advantage in that less material is required to form NPs therefore reducing cost and potentially toxicity. Additionally, gemini surfactants can be easily synthesized at a low cost which adds another economical advantage. Furthermore, studies have demonstrated that the properties of the gemini surfactants can be adjusted by modifying their structure. As a result, a wide array of morphological structures can be obtained, giving gemini surfactants greater flexibility [177, 178]. This flexibility has been demonstrated by their

widespread application in various fields such as cosmetics, cleaning agents, nano-engineering (used a scaffold for gold NPs), anti-microbial agents, enhancing oil recovery, preparative chemistry, and nano-sensors (carbon nanotubes with gemini) to detect containments in food products [179-193]. Lastly, another application related to Foldvari research group is the application of gemini surfactant in drug delivery, which will be further discussed in the following section.

1.7.2 Gemini surfactants as cationic delivery agents

Research has shown that a sub-group of gemini surfactants, the cationic gemini, can be utilized as novel delivery systems for gene therapy. Unique physical properties, due to the dimeric structure of gemini surfactants, makes them ideal candidates for non-viral delivery systems [175]. One advantage of gemini surfactants is low cmc that allows gemini surfactant to readily associate with DNA at low concentrations. From a drug delivery system point this is advantageous because a low concentration of surfactant would mean lower cytotoxicity levels.

Studies by the Foldvari group have also revealed other desirable properties of gemini NPs. As with other non-viral delivery systems, gemini surfactants have been shown to be effective pre-complexing agents by effectively neutralizing the anionic charge of DNA. Although gemini surfactants on their own have shown cytotoxicity, with the addition of a phospholipids, gemini NPs become an effective delivery system for gene delivery [194, 195]. Several studies have also shown that the effectiveness of the gemini NPs can be tuned through structure modifications to the gemini surfactant. These studies have shown that short spacers and longer tails have been correlated to higher transfection efficiency [195]. Modifications, like the addition of various chemical groups have been shown to add necessary functions to the gemini NPs, such as response to pH and increased biocompatibility [196, 197].

With every new generation of gemini, there has been an increase transfection efficiency compared to parent compounds. SAXS studies on internal structures have revealed that gemini NPs assume a unique, cubic-lamellar phase which has been correlated to increase transfection efficiency [161]. In addition, physiochemical studies have found these phases to be safe in cutaneous gene therapy in mice [162].

1.8 Current status of gene delivery

A wide variety of commercial transfection systems based on non-viral delivery systems are available for *in vitro* cell studies [198-202]. As shown in Table 5, the majority of commercial transfection systems utilize a non-viral delivery system, rather than a viral vector. Although this is a promising application for non-viral gene delivery, it reflects their applications to ex vivo, instead of *in vivo* therapies [203]. This trend is also supported by the clinical applications of non-viral delivery systems (see Table 5). As of 2012, less than 6% of gene therapy clinical trials worldwide utilize lipid-based non-viral delivery systems, versus 66% which use viral vectors [9]. One of the major reasons for this discrepancy is transfection efficiency. Unlike viral vectors that have adapted mechanisms to bypass host defenses, non-viral delivery systems do not have these mechanisms and currently have *in vivo* issues which are related to pharmacokinetics and intracellular trafficking [39, 66, 67]. There is active research in the field of non-viral gene delivery, but additional information is needed concerning the mechanism of crossing the delivery barriers. This information is necessary for the rational design of suitable non-viral delivery systems for clinical use [67, 82-84, 204]. An additional issue is that majority of the study of non-viral delivery systems is based on *in vitro* studies and studies have shown that *in vitro* results do not reflect the efficacy in *in vivo* studies [95]. Therefore to overcome this hurdle and improve the clinical efficacy of non-viral delivery systems, further studies must be performed *in vivo* to gain more useful information.

Table 5: List of commercial transfection reagents for *in vitro* applications.

Non-viral		
Name	*Formulation*	*Manufacturer*
Convoy™	Cationic Polymer	ACTgene
GeneCellin™	Cationic Polymer	Bio Cell Challenge
Lipofectamine®	Cationic Lipid	Invitrogen
Effectene	Non- liposomal	Qiagen
Superfect	activated dendrimer	Qiagen
Fugene 6®	Non-liposomal	Promega
TransIT	Not disclosed	Mirus Bio
TransFast™	Synthetic cationic lipid	Promega
JetPEI®	PEI	Polyplus Transfection
ExGen 500™	Linear PEI	Fermentas/Thermo Sci
TurboFect	Cationic Polymer	Fermentas/Thermo Sci
Escort™	Cationic Liposome (DOTAP DOPE 1:1)	Sigma Aldrich Co. LLC.
NeuroPORTER™	Cationic lipid	Genlantis
HiFect®	Biochemical trasnfection agent	Lonza
X-tremeGENE	Non-liposomal reagent, synthetic	Roche
Genejuice®	Not disclosed	Millipore
Glycofect	Not disclosed	Kerafast
Viral		
Name	*Formulation*	*Manufacturer*
SMARTvector	Lenti Virus	Thermo Sci
Virapower™	Adenovirus or lentivirus	Invitrogen
Polybrene®	Retrovirus	Millipore
rAVE™	AAV	Gene Detect

1.9 Studying intracellular trafficking of non-viral delivery systems

Extensive research in the field of non-viral delivery systems has revealed that to improve our design of carrier requires additional insight into their intracellular behavior. Techniques such as PCR and separation of cellular components through ultracentrifugation are generally labor intensive and cannot provide real-time data about the dynamics of the vectors in the cellular environment [205, 206]. Currently, most intracellular studies routinely use fluorescence techniques to gain insight into the critical steps in trafficking processes [207, 208].

1.9.1 Confocal laser scanning microscopy

Confocal laser scanning microscopy (CLSM) has become one of the fundamental tools in studying the mechanism of non-viral delivery systems due to its high degree of sensitivity, resolution and ability to generate 3D images in living cells with minimal disturbance. With labeled-delivery system components, CLSM has been used to study the localization and trafficking of delivery systems within cells. Adding multi-fluorophores for instance, an organelle stain and labeled nucleotides, it is possible to determine the interaction of NPs components with a high degree of spacial resolution through a technique known as co-localization [209]. Transfection efficiency of non-viral delivery systems can also be monitored using CLSM. This is accomplished by loading delivery systems with reporter plasmids that express a recombinant protein, and using them to transfect the cell. The degree of expression can be visualized by an increase in the signal for that fluorescent protein and can be used to gauge the effectiveness of a specific delivery system. Although CLSM is widely used in studies of trafficking, there are limitations. One limitation is the need for image processing which prevents the study of particles in true real-time. The second issue relates to the diffraction limit of light. Although co-localization is a useful technique to show that two molecules are close together, due to limit of resolution, it is impossible with CLSM to distinguish if the two molecules are just close (<200 nm) or actually interacting. Since many NP used for gene therapy are smaller than 100 nm, this limits CLSM applications in studying interactions between a NP components and DNA for example. To gain insight into the biophysical properties of NPs other fluorescent techniques have been used.

1.9.2 Fluorescence recovery after photobleaching

One technique that is used to determine mobility of molecules is FRAP. FRAP utilizes a high intensity laser to photobleach all labeled molecules in a select region; followed by it monitoring the time required for fluorescence to return therefore measuring the mobility of the molecules [210]. FRAP has

been applied to measure different regions of the cell and to determine which components, such as the extracellular matrix (ECM) affect diffusion of DNA. This enables the identification of possible barriers to gene delivery [169, 211, 212]. The drawbacks of FRAP is that it can only measure the average movement of a high concentration of molecules over large distances. Therefore this limits the resolution of FRAP to study the interactions and movement of the delivery systems within a cell. Furthermore, the use of high intensity lasers poses the risk of damaging cells and or the components of the gene delivery system. These limitations reduce its application in studying intracellular diffusion since many non-viral complexes are not present in high enough concentrations for FRAP to be performed. Also, due to the Rayleigh limit, it is not possible to confirm the physical interaction of the molecules using traditional microscopy technique, meaning that two molecules could be very close to each other (<200 nm apart) but not interacting [207]. To obtain precise information on the physical interactions of molecules, beyond the resolution of light based microscopes, another technique is required.

1.9.3 Förster resonance energy transfer

FRET occurs when two distinct fluorophores, the donor and acceptor, are in close proximity (< 10 nm). If the emission spectrum of the donor overlaps with the excitation spectrum of the acceptor, a non radiative transfer of excitation energy from the donor to the acceptor can occur. Since FRET only occurs within 1-10 nm this makes it suitable for studying dynamic molecular interactions of non-viral delivery systems [213]. FRET enables to obtain data beyond the resolution of optical techniques; it has become a very popular technique in the study of non-viral delivery systems. FRET's ability to detect when two molecules are in close proximity is applied quite frequently to study the stability of non-viral carriers. By labeling the complexing agent and the cargo (e.g. plasmid) with separate fluorophores, FRET should only appear when the NP is intact. Therefore by monitoring the quenching of the donor and the excitation of the acceptor by FRET, the state of the complex can be determined [82, 84]. Although FRET is a powerful tool in studying interactions, it requires a careful set of design parameters of the system to ensure FRET only occurs under controlled conditions. This includes the selection of FRET dye pairs and their strategic placement which is difficult in the spontaneous assembly of DNA complexes. This section shows that a variety of techniques are needed to complement each other in order to gain information of intracellular trafficking of delivery systems. Therefore to expand our understanding, additional techniques need to be used to gain deeper insight into the nature of the non-viral delivery systems.

1.10 Introduction to fluorescence correlation spectroscopy

One technique that is able to study the molecular dynamics of the molecules in solution, while being minimally invasive is fluorescence correlation spectroscopy (FCS). Developed in the 1970s, FCS is a technique that measures the minute fluctuation in fluorescence intensity in a small population of molecules around equilibrium [214]. From these fluctuations patterns, one can extract various biophysical properties of molecules. Fluctuations can occur at wide variety of time ranges and include shifts in molecular orientation (picoseconds), blinking or triplet state transitions (microseconds) and molecular interactions such as binding and chemical reactions (milliseconds).This section will introduce the theory of FCS and discuss why FCS can be a powerful tool in the study of non-viral delivery systems. For the context of this thesis, a brief description of the FCS theory and set up is shown in Figure 5. For more information, several excellent reviews cover the in-depth theory and instrumentation of FCS [214-217].

1.10.1 Instrumentation and data collection

FCS is a time-dependent statistical analysis of the minute spontaneous fluorescent intensities that fluctuate around equilibrium. To be able to resolve the fluorescent fluctuations at a single molecular level, the number of individual particles being measured must be decreased order to increase the significance of each fluctuation. To achieve this level of detection in a bulk solution, the focal volume is spatially limited by means of a confocal set-up (Figure 5A). This provides a high degree of spatial resolution and allows for the selective exciting and monitoring of a small number of fluorophores. Streams of photons are taken from florescent samples and are recorded by the avalanche photodiode detector (APD). It is indexed based on arrival times, generating raw intensity data (Figure 5B). This raw data contains all the information that can be determined by FCS, but requires additional processing to extract the biophysical parameters of interest.

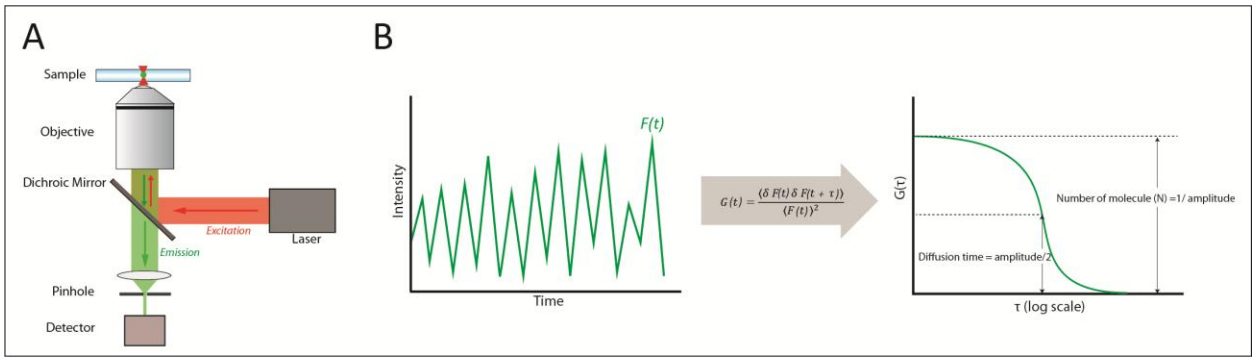

Figure 5: A brief introduction to FCS. (A): Instrumental set-up of FCS system using a confocal microscope: laser excitation enters the object from behind and is focused on the sample. Emission from sample is collected through the objective and is separated from excitation via a dichroic mirror. Emission is then focus in front of pinhole place in front of the Avalanche Photodiode (APD) to remove out of focus fluorescence. This provides FCS the ability to focal volume of less than one femtoliter. (B) Principle of FCS measurements: fluorescence fluctuations are recorded by the APD as the fluorophores diffuse through the focal volume. The temporal recording is subjected to the autocorrelation function (ACF) and generates a correlation curve (G(τ)) which is used to reveal parameters of about the fluorophore [218].

1.10.2 Autocorrelation function

The first phase of analysis is the preparation of the ACF in conjunction with the raw photon data. The ACF (Eq. 2) describes the time-dependent decay of fluctuations around an average value at equilibrium.

$$G(t) = \frac{\langle \delta F(t) \delta F(t+\tau) \rangle}{\langle F(t) \rangle^2} \quad \text{(Eq. 2)}$$

Where $\delta F(t)$ and $\delta F(t+\tau)\rangle$ are the amplitude of fluctuations from the mean at time (t), and $(t+\tau)$ and $\langle F(t)\rangle$ is the mean fluorescence signal. To simplify, ACF is a plot of the degree of self-similarity (that is how similar a molecule is to itself in terms of fluorescence) between its signal and a signal at some other time interval (Figure 6).

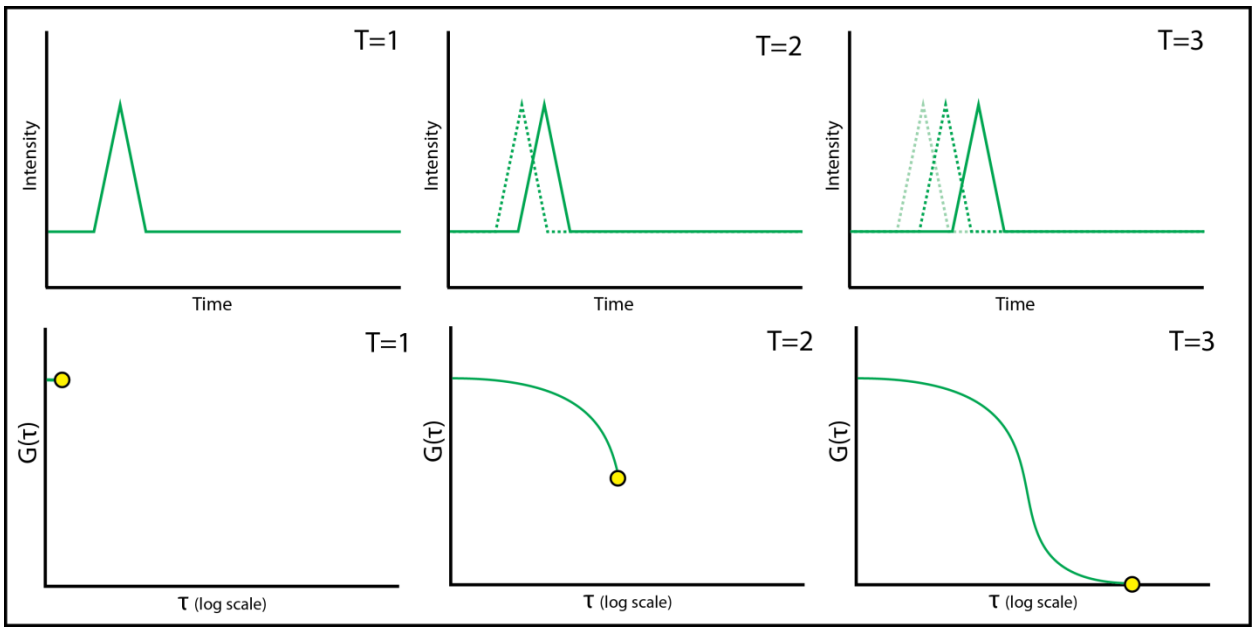

Figure 6: Schematic diagram of the principle of autocorrelation calculation of a single molecule. As the fluorophore passes through the focal volume, the degree of self-similarity (G(τ)) will decay relative to residual time of the molecule. This rate of decay at equilibrium for numerous molecules is interpreted as the ACF.

The degree of self-similarity will decay at a rate based on the resident time of the molecule in the focal volume that is recorded as the ACF. Depending on the time frame of the measurement, various parameters can be determined from the ACF (Figure 7).

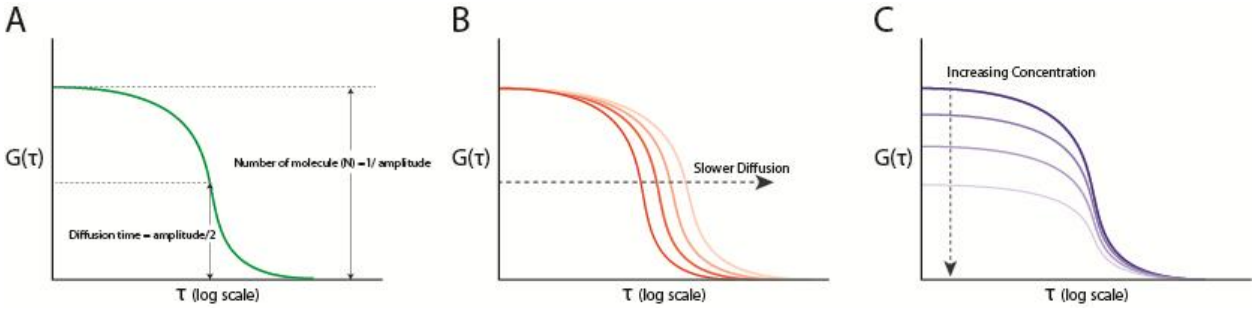

Figure 7: Anatomy of the autocorrelation function. Various properties of the molecule can be determined by analyzing the ACF. A) For this study, the main interest is the diffusion time of the molecule, at half amplitude of the curve, and the number of molecules or concentration which is inverse to the maxima of the amplitude. Shifts in the ACF can also reveal changes in the behavior of the molecule such as change in the mobility (B) and shifts in concentration (C).

For most practical applications, the parameter of interest is the time it takes for a molecule to pass through the focal volume. This is known as the decay time or diffusion time (τ_D) of the molecule (used to determine the diffusion coefficient) to study the mobility of the molecules. Shorter fluctuations (pico-and

micro-seconds) can arise within the focal volume (a 3-dimensional space from which the fluorescent measurement is being taken) which can be significant in describing other internal dynamics of molecules, such as rate of blinking and molecular rotations. Furthermore, based on Poisson distribution, theoretically, there is an inverse relationship between the time-zero of the ACF and the number of particles in the focal volume. To obtain quantitative data based on the shape of ACF additional processing is required.

To produce analytical data, the ACF needs to be fitted to mathematical models to obtain quantitative biophysical data such as diffusion time of molecule. In terms of the fitting parameters of the mathematical model, they are designed to report for various molecular and instrumental factors, which determine the quality of data extracted. The parameters can be set up to account for variables such as population types (homogenous or heterogeneous), diffusion types (passive or active) and focal volume characteristics. Several publications are available for an in-depth coverage of various models of fitting ACF [219, 220]. As the data extracted will depend on the fitting parameters that make up the fitting model, the user must take great care in selecting the appropriate model. To select the appropriate parameters, the user must understand the system and account for as many variables as possible to generate the best possible fit. In short, to be able to interpret the FCS data, the researcher is required to have some previous knowledge of the system being studied in order to apply the correct interpretation based on the fitting model [221].

1.10.3 Applications of FCS

The point of interest of FCS is to determine the source of fluorescent fluctuations created by the molecule in question. By using FCS one can distinguish the source of these fluctuations that occur, such as protein binding, molecular rotations of small molecules, changes in triplet state of the fluorophores due to changes in the micro-environment; all of which are intramolecular dynamic and chemical reactions [219]. For FCS to achieve great results, however, it is necessary to understand the ability of this technology with which it operates.

One of the goals of FCS is to monitor the minute fluctuation of fluorescence as small molecule moves through the focal volume. Therefore it cannot accurately measure the diffusion of large, slow-moving molecules in such a small focal volume. Photo-damage may pose a threat to these large molecules if left too long in the focal volume, or may not be detected due to their slow diffusion and fast acquisition of FCS. In addition, with FCS being highly sensitive, the addition of fluorophores to non-fluorescent molecules requires tactful management to minimize artifacts and invalid results. Careful experimental design with sufficient controls in place is essential to ensure the measurement represent a specific mechanism is occurring. A second consideration is that FCS can monitor binding events if significant changes in mobility of the labeled molecules occur. This is explained by dependence of diffusion coefficient (D) on the molecular weight of the molecule based on the Stokes-Einstein equation.

$$D = \frac{kT}{3\pi\eta D_H} \quad \text{(Eq. 3)}$$

Where the diameter (D_H) is related to molecular weight (MW) with a specific gravity ($\bar{\upsilon}$) as shown below:

$$D_H = \frac{3MW\bar{\upsilon}^{\frac{1}{3}}}{4\pi} \quad \text{(Eq. 4)}$$

These equations demonstrate that the relationship between diffusion coefficient and molecular weight is quite weak. To simplify a 10-fold change in molecular weight of the particles is required to show a 2-fold increase in diffusion coefficient [222]. If these concerns are not addressed, it can provide poor autocorrelations and unreliable data. With proper experimental design, and knowledge and use of the technology, FCS can be a powerful investigative tool.

In the field of gene delivery, FCS has been applied to study two key biophysical properties of non-viral delivery systems. The first property, mobility, can reveal information about the state of the delivery system. Factors that affect mobility include the size of delivery system due to binding/releasing events, changes in the viscosity of the micro-environment and the effect of active transport. These events can all be monitored with great detail and are important to consider in order to overcome barriers to gene delivery [90, 223-225]. Secondly, FCS can be utilized to monitor local concentrations of specific molecules (DNA) and to determine localized concentrations, for example, DNA concentrations on either side of a lipid membrane. Both of these properties are vital to aid in the determination of barriers to gene delivery [209]. In the context of this thesis, FCS will be used to determine the stability of different gemini NP compositions in solution.

2.0 Motivation of the study

The scope of the project was to study the biophysical properties of a series of gemini NPs using FCS. The first goal is to determine the proper method of labeling of the gemini NPs and to optimize FCS measurement parameters. The second goal of this study was to evaluate the effect of the chemical structure and physicochemical properties of each gemini surfactant component on the properties of the formed respective NPs and to assess the limitations of FCS to study these properties. FCS application to NP characterization would introduce a powerful analytical tool to study the assembly of gemini NPs in a wide variety of environments in real-time. Overall, a better understanding of biophysical properties of NPs will aid with the rational development of non-viral gene delivery and improve efficiency, effectiveness and safety.

3.0 Research hypothesis and objectives

This thesis describes the development of FCS method to probe the assembly of gemini NPs. The main hypothesis is that due to the condensation properties of gemini surfactants, FCS will be able to monitor the assembly of the gemini NP. In order to evaluate the FCS the following objectives have been established.

- Optimize the labeling and instrumental settings required to monitor gemini NP using FCS.
- Evaluate the ability of FCS to monitor changes in NP assembly compared to other techniques such as DLS, zeta potential and dye exclusion assays.
- Study the effect of gemini surfactant chemical structure on gemini surfactant-plasmid complexation and gemini NP assembly using FCS.

It is believed that a thorough understanding of the assembly of gemini NPs will provide crucial information that will contribute to the rational development of non-viral gene delivery systems with improved efficiency, effectiveness and safety.

4.0 Materials and methods

4.1 Plasmids

gWiz GFP (5757 bps) and gWiz Luc (6732 bps) were purchased from Aldevron (Fargo, ND, USA). Plasmids were routinely checked for purity and topology using spectroscopy and agarose gel electrophoresis, respectively.

4.2 Gemini surfactants

A series of gemini surfactants listed in Table 6 were previous synthesized as described elsewhere [121, 165, 226]. The gemini surfactants in this study were systematically selected to investigate change to spacer and tail length and functionalization. Gemini surfactants were prepared to a final concentration of 3mM with milli-Q grade water. Aliquots were stored at 4°C and used immediately after warming to room temperature.

Table 6: List of gemini surfactants used in the study. Gemini surfactants are separated based on category of modification.

Gemini surfactants series		
Spacer-series	*Tail-series*	*Functionalization -series*
12-3-12	16-3-16	12-7NH-12
12-6-12	18-3-18	Py-3-12
12-7-12		
12-10-12		
12-16-12		

4.3 Lipids

DOPE (1,2-di-(9Z-octadecenoyl)-sn-glycero-3-phosphoethanolamine) and DPPC (1,2-dihexadecanoyl-sn-glycero-3-phosphocholine) were obtained from Avanti Polar Lipids (Alabaster, AL, USA).

4.4 Nucleic acid labeling

Plasmid DNA (gWiz GFP; 5757 bps) was labeled with Cyanine 5 fluorophore (Cy5) using the Cy5 LabelIT® Tracker kit from Mirus Bio LLC (Madison, WI, USA) at 0.25:1 (w/v) labeling reagent-DNA ratio. Labeled gWiz GFP (Cy5-gWiz) was purified by ethanol precipitation and filtration through Amicon Ultra centrifuge filters (3kD cutoff) from Millipore Corporation (Billerica, MA, USA). Labeling density was determined by determining the ratio of base to dye using the equation:

$$Base{:}\,Dye = \frac{\left(A_{nucleic\ acid} \times \varepsilon_{Cy5}\right)}{\left(A_{Cy5} \times \varepsilon_{nucleic\ acid}\right)} \quad \text{(Eq. 5)}$$

Where $A_{\text{nucleic acid}}$ and A_{Cy5} are the absorbance measured at 260 nm and 649 nm respectively. The extinction coefficients for nucleic acid and Cy5 dye were previously determined to the values ε_{Cy5} = 250 000; $\varepsilon_{\text{nucelic acid}}$ = 6600. A correction factor (CF_{260} = 0.05) was included to the $A_{\text{nucleic acid}}$ measurement using the equation $A_{\text{nucleic acid}} = A260 - (A_{cy5} \times CF_{260})$.

4.5 Confirmation of super-coiled plasmid and purity

Purity of unlabelled and labeled gWiz GFP was determined by spectrophotometry by measuring absorbance at 260 nm and 280 nm on the Nanodrop 2000C (Thermo Scientific, Wilmington, DE, USA). The topology of Cy5-gWiz was determined by electrophoresis on a 0.8% agarose gel run at 80V for two hours (VWR International, Mississauga CA). Supercoiled DNA was quantified using densitometric analysis with ImageJ software (National Institutes of health, Maryland, USA).

4.6 Liposome preparation

Liposomes (neutral phospholipids) composed of either pure DOPE or DOPE and DPPC at a ratio of 0.25:0.75 (DD 1:3) were prepared by thin-film method. Lipids were dissolved in 100% ethanol in a round bottom flask. Thin-films were deposited by removal of solvent with a rotary evaporator under vacuum at 50°C at 150 rpm. Trace amount solvent was removed by freeze-drying (Labconco) for 4 hours. Lipid thin-film was re-hydrated to 3mM concentration with a 9.25% w/v sucrose solution adjusted to pH7 and pH 9 for DD 1:3 and DOPE respectively at 50°C for 30 minutes to produce crude/multi-lamellar liposomes. pH of all liposomes were determined using a Fisher Accumet pH meter (Thermo Fisher Scientific Inc., MA, USA). Crude liposome solutions were sonicated for 30 minutes in a bath sonicator

(VWR 75D, VWR International LLC,PA, USA) or until solution was clear. Liposomes were filtered through a 0.45μm cellulose filter prior to use. Liposome size was routinely checked by DLS using Zetasizer Nano (Malvern Instruments Ltd, Worcestershire, UK) to be approximately 150 nm.

4.7 Gemini nanoparticle preparation

Gemini NPs were prepared in a two-step process. Primary assembly consists of the addition of gemini surfactant to 0.5 μg of Cy5-gWiz to obtain a charge ratio (N/P) of 10:1 and incubated at room temperature for 15 minutes to form the gemini-plasmid complex (GP). The secondary assembly requires the addition of 75μL of 1mM DOPE:DPPC liposome to GP and further incubation for an additional 30 minutes to form GPL or gemini NP.

4.8 Fluorescence correlation spectroscopy experimental set-up

FCS measurements were performed on a commercial Zeiss LSM 710 microscope with Confocor 3 system (Zeiss, Jena, DE). Cy5 was excited by a 633 nM HeNE laser at approximately 50 μW and reflected by a dichroic beam splitter (488/633) and focused 200 μm into the sample to avoid reflection of the laser on the glass through a 40x Zeiss Apochromat NA 1.2 water-immersion objective lens. Emission spectra were collected through a 580 nm long-pass filter and record by an avalanche photo-detector (APD). Out-of-focus emission was blocked by a pair of confocal pinholes set at 45 μm. The lateral diameter of the focal volume for 633 nm laser was determined by a calibration dye (Cy5-NHS-ester) to be 250 nm. FCS measurements were carried out in 200 μL volumes of diluted gemini NP in a 4-well CELLview coverslips (Grenier-Bio One, Frickenhausen, DE). NP samples were prepared in triplicates for FCS and measurements were taken for 10 s, twenty-five times for each sample. Calibration of the system was performed with a 50 nM Cy5 solution. Using the known diffusion coefficient of rhodamine G6 ($3.2 \times 10^{-10}\ m^2\ s^{-1}$), the laterial ($\omega_R$) and axial ($\omega_z$) radii of the focal volume was determined to be respectively of 0.25 and 1.6 μm, giving an focal volume of 0.19 fL using the equation below (Eq. 6).

$$V = \frac{\pi^{3/2}}{2} \omega_R{}^2 \omega_z \quad \text{(Eq. 6)}$$

4.9 FCS data analysis

The ACF was determined from count rate collected from APD as described elsewhere [219]. Assuming a three-dimensional Gaussian excitation intensity distribution, the free diffusion of a single species was calculated using the formula:

$$G(t) = \frac{1}{N}\left(1 + \frac{\tau}{\tau_d}\right)^{-1}\left(1 + \frac{\tau}{S^2\tau_d}\right)^{-1/2} \quad \text{(Eq. 7)}$$

Where N is the mean number of molecules in the excitation volume, S is the ratio between the equatorial and axial radii of the focal volume, and τ_d is defined as the characteristic diffusion time of the particle. Diffusion coefficients (D) were determined using the equation shown below.

$$D = \frac{\omega_R{}^2}{4\tau_d} \quad \text{(Eq. 8)}$$

Where ω_R is the lateral radius of focal volume experimental determined by measuring the diffusion time of calibration dye (τ_{dCy5}) with a known diffusion coefficient (Cy5 NHS-ester; D_{Cy5}=3.2 × 10-6 cm^2/s). τ_d for the sample is obtained from the fitted ACF. FCS data was analyzed using Confocor 3 Software Zen 2009 (Jena, DE). Files were exported into Origin 7.5 (Microcal, MA, USA) to plot ACF and intensity histograms. All reported diffusion coefficients were averaged based on four separate batches of formulations and each measurement repeated 25 times.

4.10 Particle size and zeta potential measurements

Particle size and zeta potential measurements were performed simultaneously using the Zetasizer Nano (Malvern Instruments Ltd, Worcestershire, UK). Particle size was determined using DLS and zeta potential was determined using laser doppler micro-electrophoresis (LDME). Gemini NPs were prepared at a charge ratio of 10:1 as described previously. Measurements were carried out with 70 µL of aqueous solution in micro-cuvette (Brandtech Scientific, CT, USA). Samples were prepared in triplicates and four aliquots were measured five times for DLS and LDME. pH of all formulations were determined using a Twin compact pH meter (Horiba Scientific, Kyoto, JP). pH of GPs and GPLs were between 6.5-7.1.

4.11 Dye exclusion assay

Gemini NPs were prepared at a charge ratio of 10:1 as described previously. For PicoGreen dye exclusion assay NPs were diluted 10-fold in water and incubated in PicoGreen dye prepared as recommended by the manufacturer for 5 minutes prior to measurement. NPs were diluted 5-fold in water for EtBr assay in water and incubated in EtBr (Bio-Rad Laboratories Ltd., Hercules, CA, USA) dye was prepared at final concentration of 1 µg/mL for 5 minutes. Fluorescence measurements were made on the Spectramax M5 spectrophotometer at 485 nm and 560 nm for PicoGreen and 250 nm and 605 nm for EtBr [227]. To assess the quantity of DNA, a standard curve was prepared from gWiz Luc for both PicoGreen and EtBr dye exclusion assays to determine amount of detectable DNA in NPs.

4.12 Statistics

Statistical analysis was performed using SPSS V 17.0. For FCS data sets, data was log transformed to account for non-normality prior to two-way ANOVA analysis. One-way ANOVA was used to determine the significance for particle size, zeta potential and transfection studies. Significance was determined between experimental groups with a p-value less than 0.05 level of significance.

5.0 Results

5.1 Development of FCS method for nanoparticle characterization

5.1.1 Confirmation of labeled plasmid DNA

The results of the labeling of gWiz GFP at 0.05:1, 0.25:1 and 0.5:1 labeling ratios are presented in Table 7 and Figure 8. The most optimal labeling was achieved at 0.05:1 and 0.25:1 labeling ratios, resulting in a similar diffusion coefficients and high preservation of SC form ($D_{0.05}$=3.6±0.3x 10^{-12} m^2/s) and $D_{0.25}$=4.2±0.2 x10^{-12} m^2/s). However at the 0.5:1 labeling ratio, a large portion of the plasmid (at least 40%) was nicked into an open circular form resulting in a shift in the diffusion coefficient (Figure 8, lane 3; $D_{0.5}$=7.1±0.7 x10^{-12} m^2/s).

Table 7: Analysis of gWiz GFP labeling reaction. gWiz GFP plasmid was labeled at three dye:base pair ratios. The labeling density, topology was measured by two different analytical techniques (fluorescence and densitometry) and FCS diffusion time were also recorded. The diffusion coefficient could not be determined for control sample due to lack of fluorescent label.

Lane	***Labeling ratio***	***Base-dye ratio***	***Degree supercoiled DNA (%)***		***Diffusion coefficient***
			Spectroscopy	*Densitometry*	*(10^{-12} m^2/s)*
1	Control	-	84%	85%	-
2	0.05:1	N/A	82%	83.5%	3.6±0.3
3	0.5:1	196.76	65%	40%	7.1±0.7
4	0.25:1	400	83%	83.4%	4.2±0.2

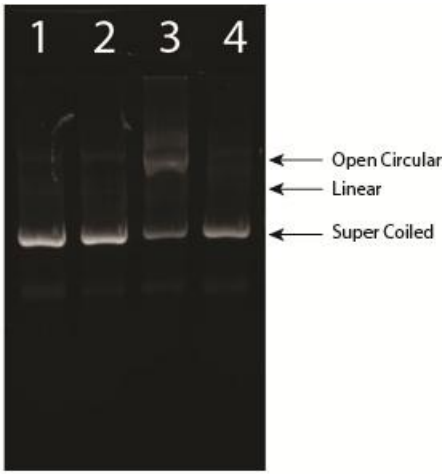

Figure 8: Gel electrophoresis of gWiz GFP with various degree of labeling with Cy5 on 0.8% agarose gel. Samples were arranged as followed: 1) Control, 2) 0.05:1, 3) 0.5:1 and 4) 0.25:1 Cy5-gWiz GFP.

The reproducibility and yield was highest with 0.25:1 labeling ratio, hence these conditions were used to prepare the Cy5-labeled gWiz GFP plasmid for the FCS experiment. The comparative studies using DLS, zeta potenail and dye exclusion were also performed using the same batch of Cy5-gWizGFP plasmid.

5.1.2 FCS measurement of individual nanoparticle components

To better understand the gemini NP, Cy5-gWiz GFP, gemini surfactants and phospholipids were examined individually by FCS to create an independent profile of their behavior. Cy5-gWiz was studied at a concentration of 2 ng/µL which was experimentally determined to be optimal for FCS measurements to achieve a mean particle number (N) of 1. It should be noted that due to the Zen2009 software, the mean particle of 1 on the G(τ) scale is expressed as 2. The ACF for Cy5-gWiz GFP (open squares) was satisfactorily fitted to the model described in (Eq. 7 (Figure 9). The diffusion coefficient of Cy5-gWiz GFP, with a labeling ratio of 0.25:1 (D_{pDNA}) was calculated to be 4.2±4.76% x10^{-12} m^2/s (n=4).

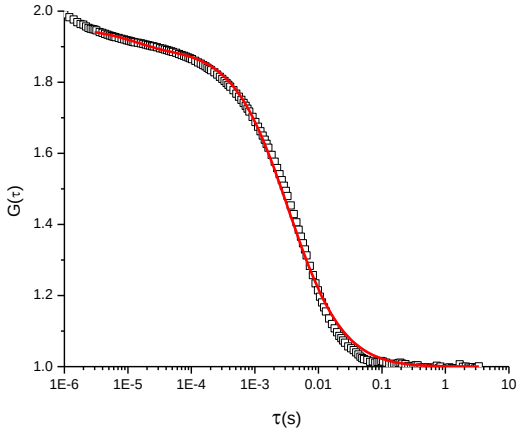

Figure 9: Autocorrelation function (ACF) from the FCS measurement of Cy5-gWiz GFP. ACF of Cy5 labeled gWiz GFP. Open squares show the experimental signal and red line represent the fitting model to ACF. DNA was prepared at 2 ng/μL for all experiments; calculated diffusion coefficient: 4.2±0.2 x 10^{-12} m^2/s (n=4).

To gain additional insight into the distribution of fluorophores on the plasmids, raw intensity count rates from the APD were also analyzed. The raw intensity data (Figure 10A) was plotted as a histogram to show the distribution of the photons intensity (Figure 10B). The intensity histogram shows that Cy5-gWiz GFP had an average intensity of 250 kHz with the majority of the peaks between 150-300 kHz. Figure 10B also shows a long tail of the histogram as a result of a small number of measurements ranging up to 5000 kHz. This variation in peak intensity is indicative of different degrees of labeling, or the presence of small populations of aggregates. To ensure this was not an artifact due to the presence of free dye or dye aggregates, additional purification steps by ethanol precipitation and centrifugation were performed. This additional purification did not remove the larger signal peaks and resulted in the decrease of the diffusion coefficient due to increased DNA degradation (data not shown). Furthermore, the agarose gel did not reveal the production of a significant amount of aggregation in the plasmid DNA due to the labeling process. Overall, the presence of the brighter peaks in the Cy5-gWiz GFP did not interfere with the quality of the FCS measurement and confirmed that the only source of fluorescence was due to presence of the labeled plasmids.

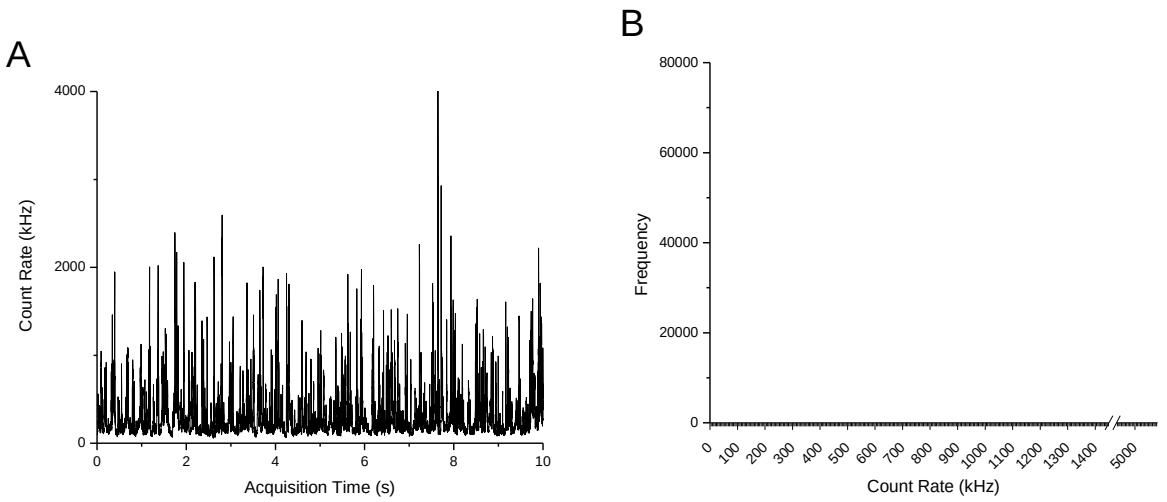

Figure 10: Raw intensity count rate for Cy5-gWiz GFP. A) Count rate measurement for Cy5-gWiz GFP (10 seconds of 250 second measurement shown). B) Intensity histogram of Cy5-gWiz count rate measurement.

Individual solutions of gemini surfactants and phospholipids were also evaluated at the same final concentration found in NPs (30 nM and 300 nM, respectively). Gemini surfactant and phospholipid samples showed no background fluorescence was found in the NPs and that only Cy5-gWiz GFP was being monitored by FCS. Milli-Q water was used for all experiments and was also measured on FCS to establish the baseline or background fluorescence.

5.1.3 Systematic screening of GPs and GPLs with FCS

Gemini-plasmid complexes (GPs) and gemini nanoparticles (or gemini-plasmid-lipid complexes; GPLs) were prepared as described in Figure 11.

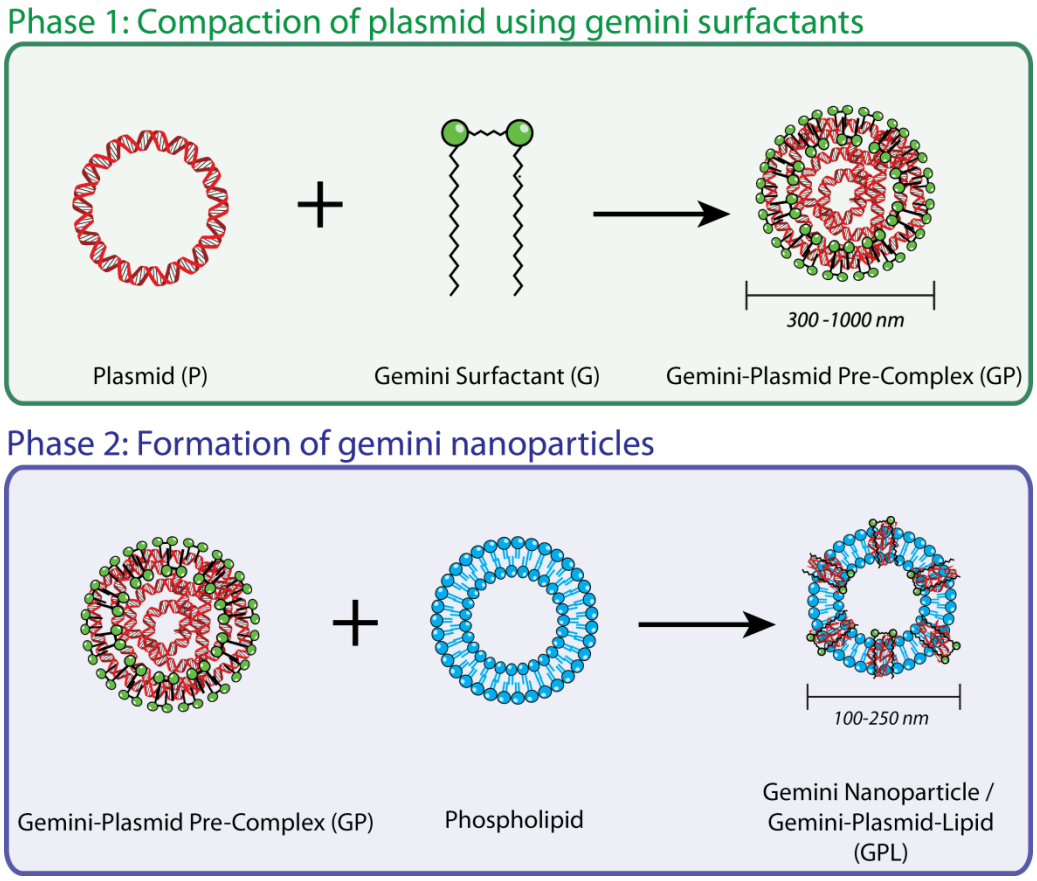

Figure 11: Schematic diagram of gemini nanoparticle assembly. Plasmids are pre-compacted by the addition of cationic gemini surfactant to form GP. The GPs is then stabilized through the addition of the helper lipid to form the completed gemini nanoparticle (or GPL).

A systematic screening of GPs and GPLs based on different gemini surfactant structure (increasing spacer and tail length and the addition of functional groups) and addition of different phospholipids (DD 1:3 and DOPE). The ACFs and intensity histograms profiles for all GPs and GPLs are shown in Figure 12, Figure 13 and Figure 14.

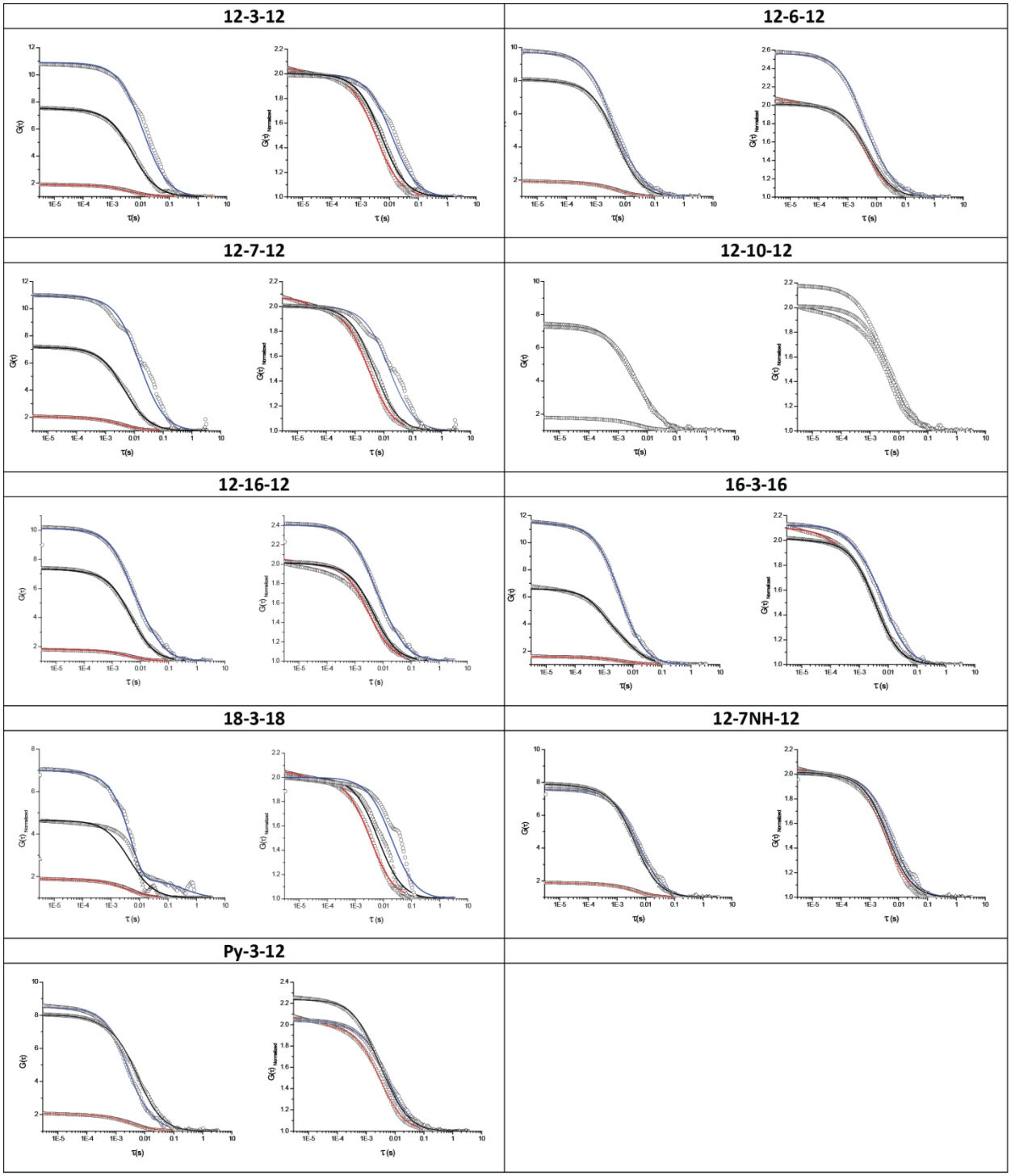

Figure 12: Systematic screen of gemini NPs prepared with DD 1:3 using FCS. Autocorrelation curves of free Cy5-gWiz GFP, GP and GPL (open square, circle and triangle respectively) organized by gemini surfactant. ACF is shown on the left and a normalized ACF is shown on the right to highlight shifts in diffusion coefficient. Curves represent an average of 25 measurements repeated with three individual samples (n=3).

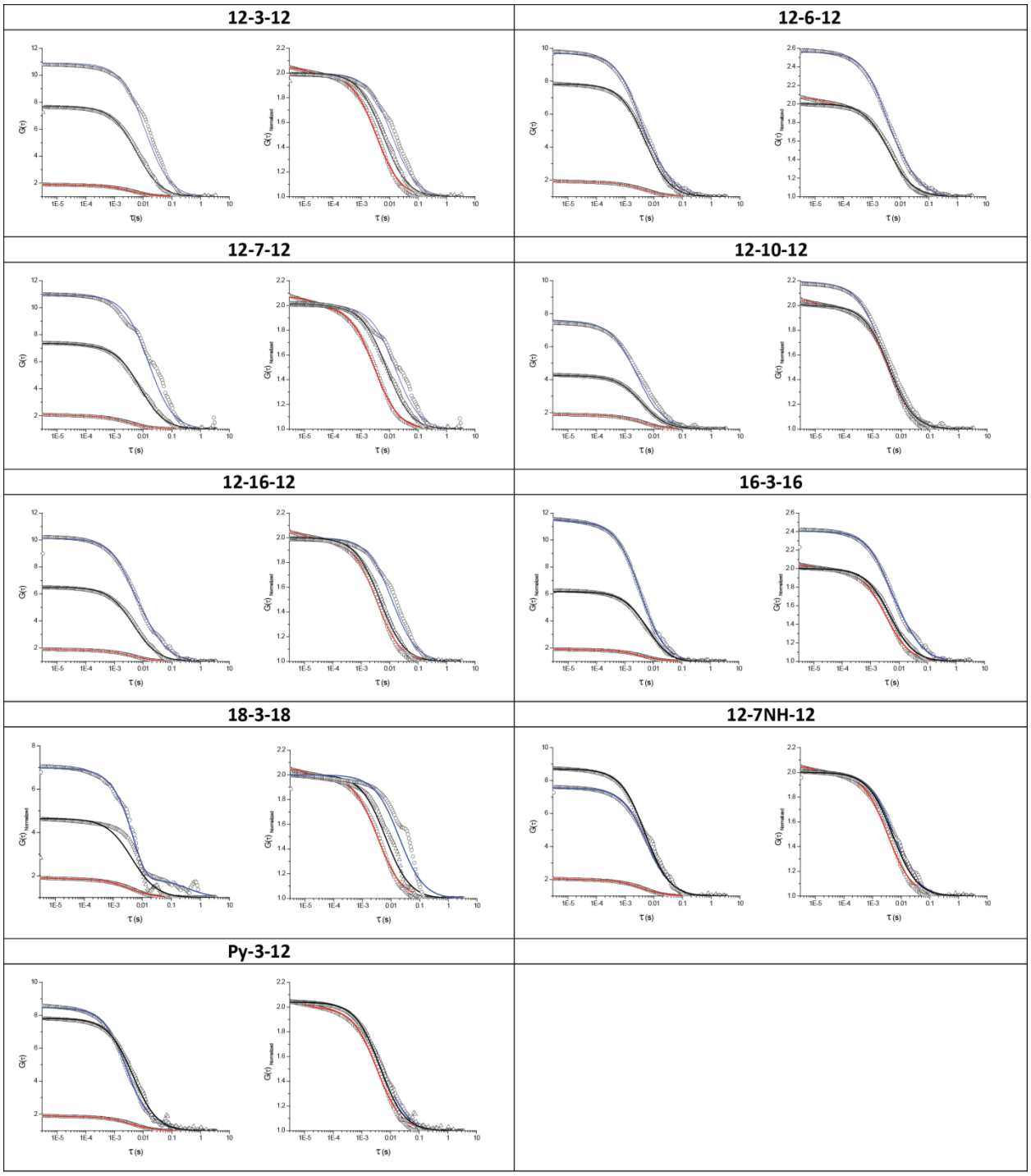

Figure 13: Systematic screen of gemini NPs prepared with DOPE using FCS. Autocorrelation curves of free Cy5-gWiz GFP, GP and GPL (open square, circle and triangle respectively) organized by gemini surfactant. ACF is shown on the left and a normalized ACF is shown on the right to highlight shifts in diffusion coefficient. Curves represent an average of 25 measurements repeated with three individual samples (n=3).

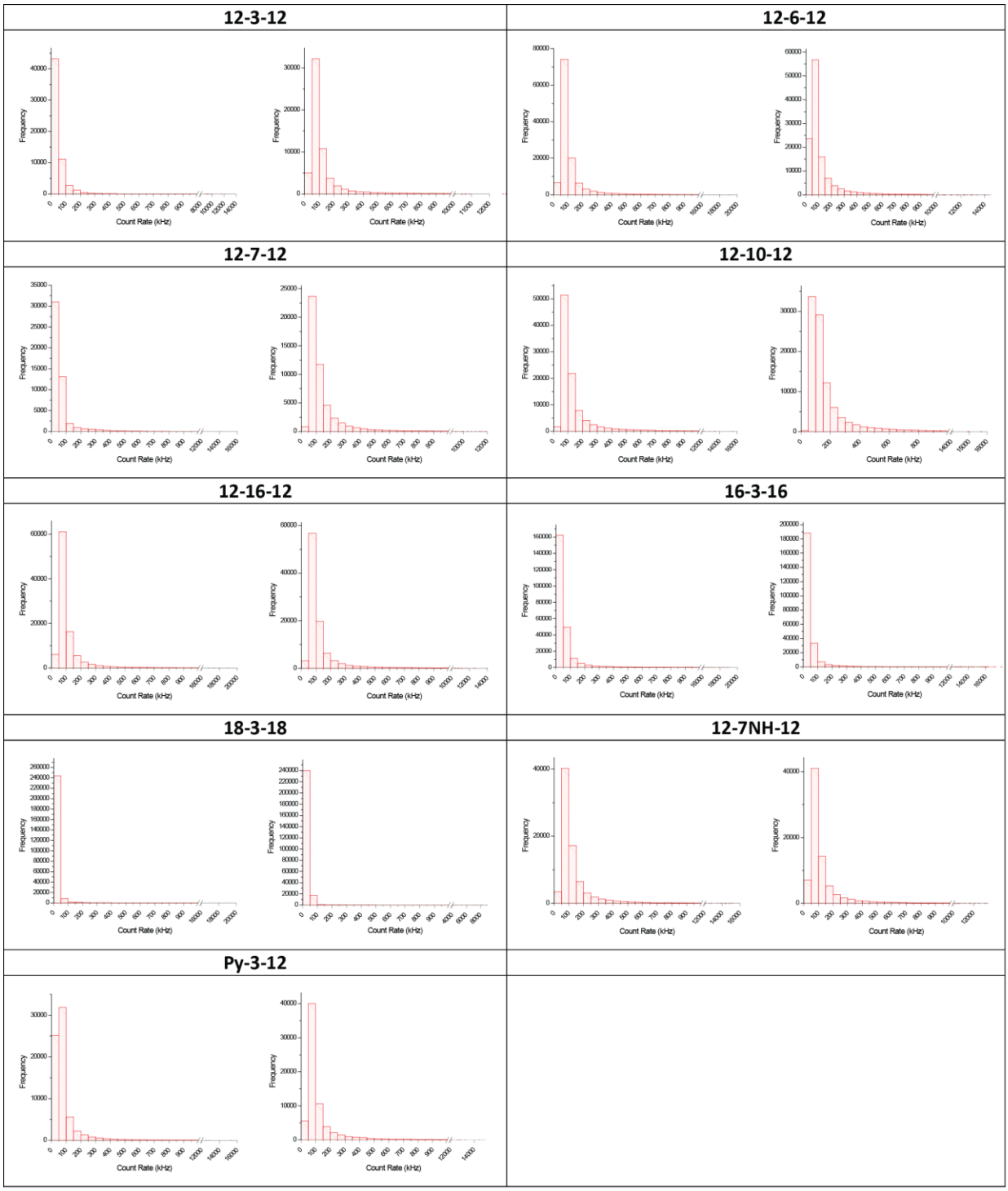

Figure 14: Intensity histograms from systematic screen of various gemini NPs. Representative samples of GPs (left) and GPLs (right) are organized by gemini surfactant. GPLs are prepared with DD 1:3 phosopholipid. DOPE values were similar and therefore not shown. Histogram represent an average of 25 measurements of one sample (n=1).

5.1.4 FCS measurements of gemini-plasmid complexes

FCS was performed on GPs with Cy5-gWiz GFP and unlabelled gemini surfactants prepared at 10:1 charge ratio as described in Section 4.8. Samples normalized to a final DNA concentration of 2 ng/µL for all FCS measurements as optimized previously in Section 5.1.2. Therefore any changes to FCS profiles of plasmid were due to interactions during NP assembly and not concentration differences in plasmid. Figure 15 below shows the ACF of Cy5-gWiz GFP in the absence and presence of gemini surfactant 12-3-12.

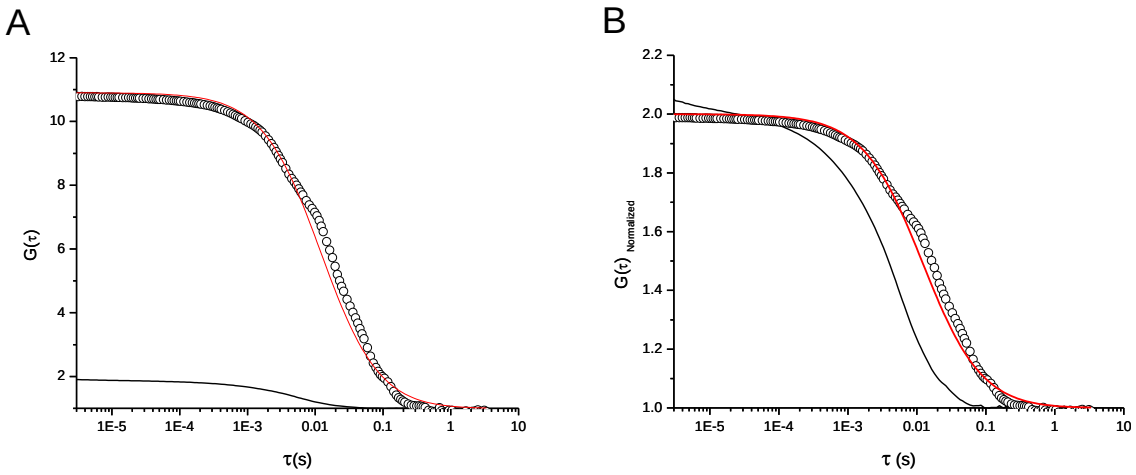

Figure 15: FCS measurement of GPs at charge ratio of 10:1 with 12-3-12. Open circle shows the experimental signal and red line represent the autocorrelation for GP. Cy5-gWiz GFP (solid line) are added as references. DNA concentration for both samples was 2 ng/µL. A) Original ACF B) Normalized ACF, sample were normalized to one particle on Zen 2009 software. Calculated diffusion coefficient: 0.98±0.31 x 10^{-12} m^2/s (n=4).

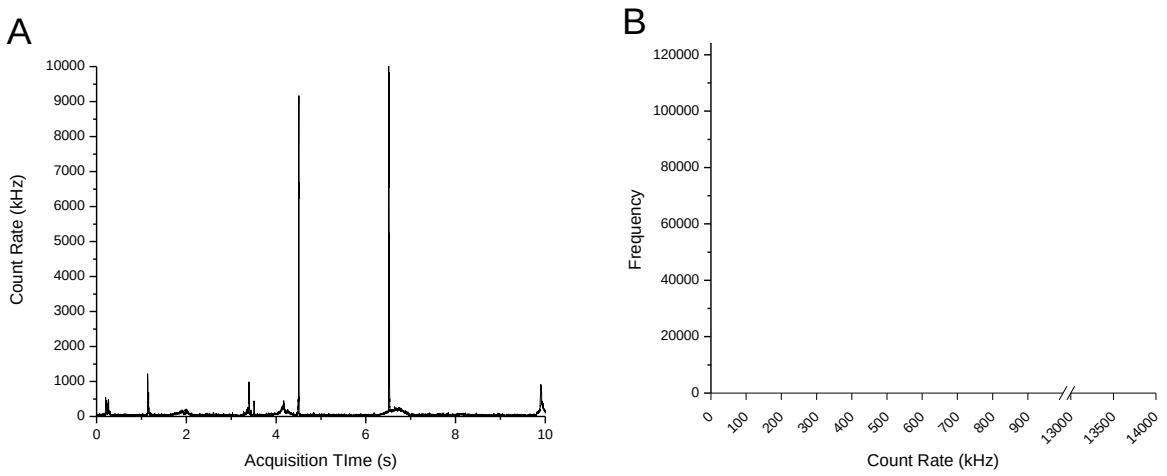

Figure 16: Raw intensity count rate for GP prepared with 12-3-12. A) Count rate measurement for GP (10 seconds shown). B) Intensity histogram of GP count rate measurement.

Figure 15 (open circle) demonstrates the two key parameters that can be observed from the ACF. With the addition of the 12-3-12 gemini surfactant, two major shifts are seen compared to the free Cy5-gWiz GFP ACF (Figure 15, solid line). The first is a significant upward translation of the curve which represents decrease in the mean number of molecules in the focal volume as shown in Figure 15A. Recall this number corresponds to the inverse of the $G(\tau)$. This indicates that there was a decrease in the number of fluorophores in solution passing through the focal volume. The second change was a horizontal translation of the curve of the right. To emphasize the shift in diffusion time between free Cy5-gWiz GFP and GP the mean number was normalized to 1 (Figure 15B). This indicates a deceleration of the Cy5-gWiz GFP with a diffusion coefficient of $0.98\pm0.31\text{x}10^{-12}$ m^2/s (n=4). The diffusion coefficient of the other GP formed from the remaining gemini surfactants is shown below in Table 8.

In addition to the FCS analysis, the raw intensity profiles can also provide insight into the morphology of the GPs. Figure 16A shows that the addition of 12-3-12 resulted significant changes in raw intensity profile compared to in the free Cy5-gWiz (Figure 10A). One of the major changes is a decrease in the number of fluorescent fluctuation as seen in Figure 16A. This is quantified by an intensity histogram in Figure 16B due to the increase in the 0-50 kHz counts that was established previously as background, and indicates a lack of fluorophores in the focal volume. This indicates a drop in mean number of particles, as shown previously in the FCS data in the previous section by the upward translation of the ACF (Figure 15A). Attempts were made to increase the amount of labeled plasmid in order to increase the concentration of GP in order to increase fluorescence fluctuation to improve data

quality of FCS measurements. This resulted in significant increase in high intensity spikes and an increase in saturation of the detector (data not shown). Figure 16 shows that the maximum intensity increases dramatically (well over 15,000 kHz in most cases). This indicates the formation of very bright particles, due to aggregation of multiple fluorophores. This suggests an aggregation and formation of multi-plasmid system for GP. GP composed of other gemini surfactants were also measured using FCS by the same procedure. A summary of the ACF and diffusion coefficients are shown in Figure 17 and Table 8.

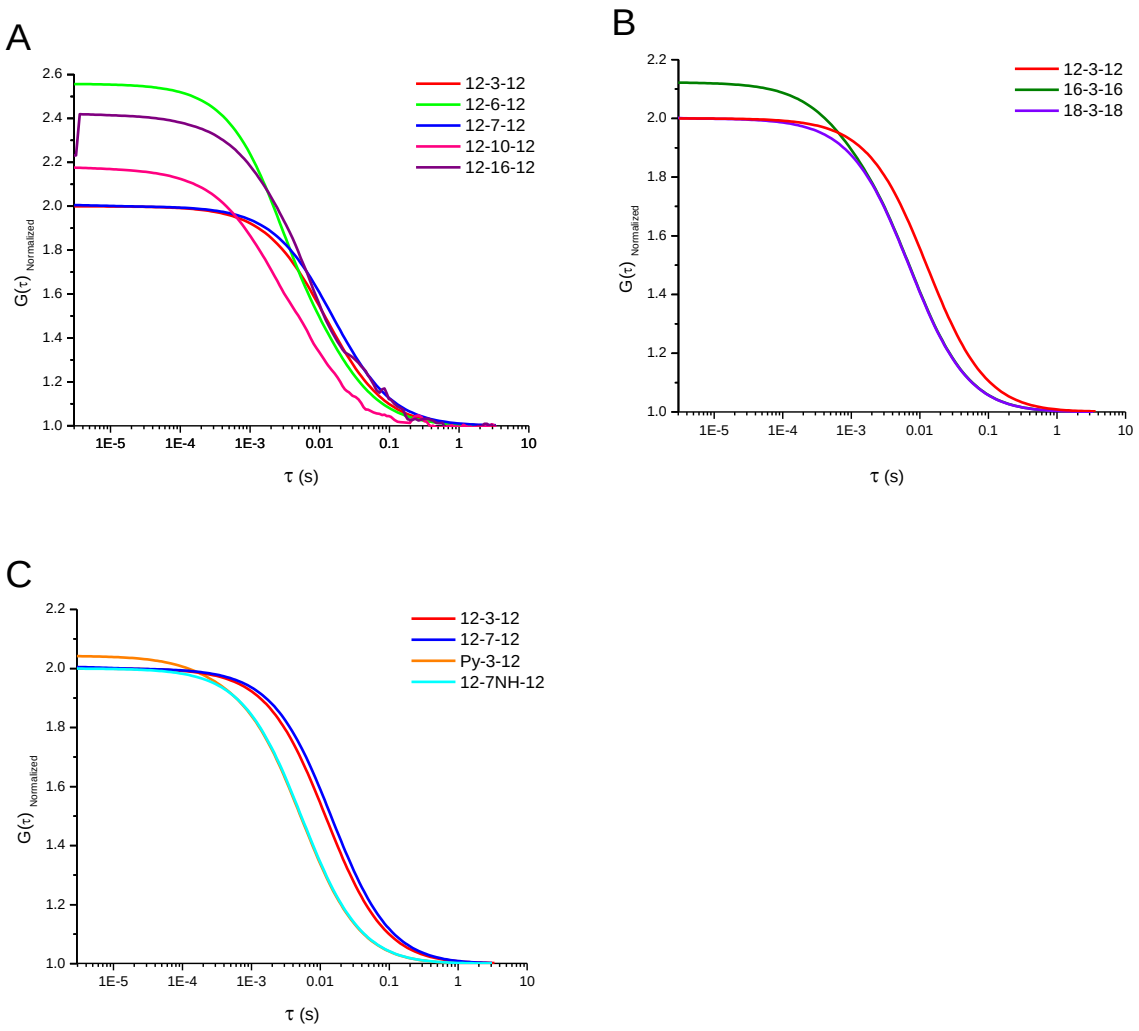

Figure 17: ACF of GPs prepared with different gemini surfactants. A) Effect of gemini spacer length. B) Effect of gemini tail length. C) Effect of gemini functionalization.

Table 8: Diffusion coefficients of various GPs from FCS measurements (n=4)

Sample	***Mean diffusion coefficient (10^{-12} m^2/s)***	***CV (%)***
12-3-12	0.98	31.66
12-6-12	1.36	21.76
12-7-12	1.03	32.82
12-10-12	4.15	23.20
12-16-12	1.37	24.35
16-3-16	1.91	14.98
18-3-18	0.17	175.59
12-7NH-12	3.06	8.65
Py-3-12	2.03	6.04

Although the diffusion coefficient could be calculated from the ACF, the fitting represented in Equation 1 provided a poor fit for the majority of the GPs such as 12-3-12, 12-6-12, 12-7-12, and 16-3-16. 18-3-18 also had the poorest fit, but this was due to the presence of flocculation in the sample. Several other fitting models where tested to account for other parameters, such as additional populations and diffusion rate, but did not produce a tighter fit for the ACF (data not shown). The reason for the large deviation is not based on the fitting model but the quality of the raw intensity data. Recall that FCS is fundamentally a study in the fluctuation of molecules as they diffuse through the focal volume. As shown in Figure 16, the GP resulted in higher intensity peaks, but decrease in the overall number of fluctuations. This in turn directly impacts the calculation of ACF making the GP samples difficult to analyze by FCS. Another issue was the saturation of the APD due to the larger intensity values which resulted in the termination of the measurement. The issue of the presence of high intensity peaks has also been reported by other groups studying gene transfer by NPs that can impede the use of FCS [228]. Therefore due to the lower particle count and high degree of saturation it made the reproducibility of GP measurements by FCS difficult. Also the presence of the extreme high intensity peaks also resulted in deviations in the normalized ACF as seen by the difference in starting positions of a some GP on the X-axis in Figure 17A. Although quantitative fitting is not possible, the diffusion coefficients can still be interpreted but with a degree of caution.

Although a majority of the GPs were hard to monitor using FCS, there are exceptions. As shown in Figure 17A-C, 12-10-12, 12-7NH-12 and Py-3-12 GP showed a different ACF profiles. These ACF show a shift to the left compared to other GPs indicating a faster diffusion coefficient. In addition the lower deviation of the overall intensity of the peaks was also not as large, resulting in less saturation of the detectors. These two factors results in significantly better fit compared to the previous model (Eq. 7) and more confident assessment of diffusion coefficient. These changes can be explained in part by studying the intensity profiles of these select GPs. As seen in

Figure 18B, an increase in number of measured fluctuations which is shown by the drop in 0-50 kHz counting indicating fewer background measurements. Another trend noticed is a drop in average intensity closer to 150 kHz, compared to 250kHz seen for the free labeled plasmid, but the shape of the distribution is similar.

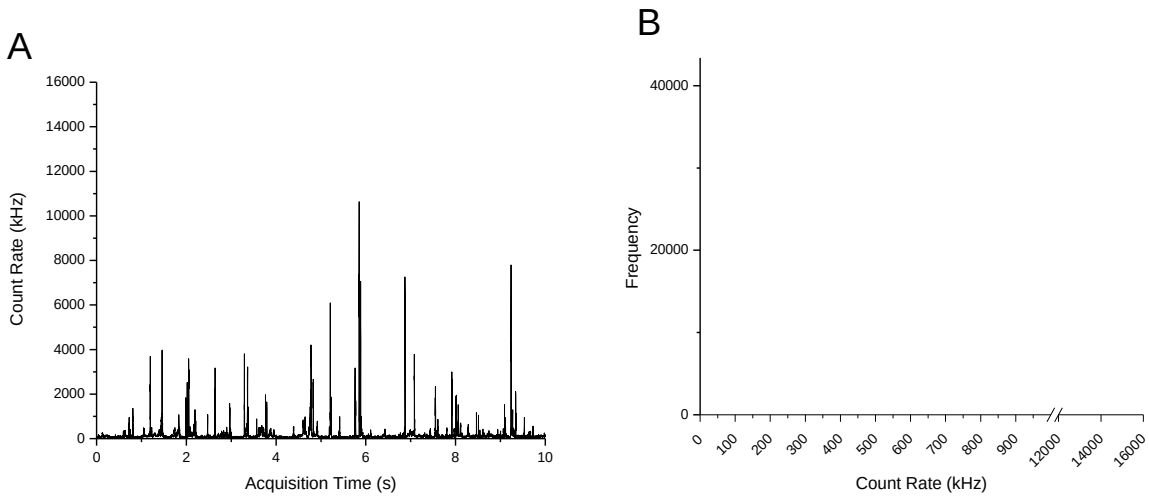

Figure 18: Raw intensity count rate for GPs prepared with 12-7NH-12. A) Count rate measurement for GP (10 seconds shown). B) Intensity histogram of GP count rate measurement.

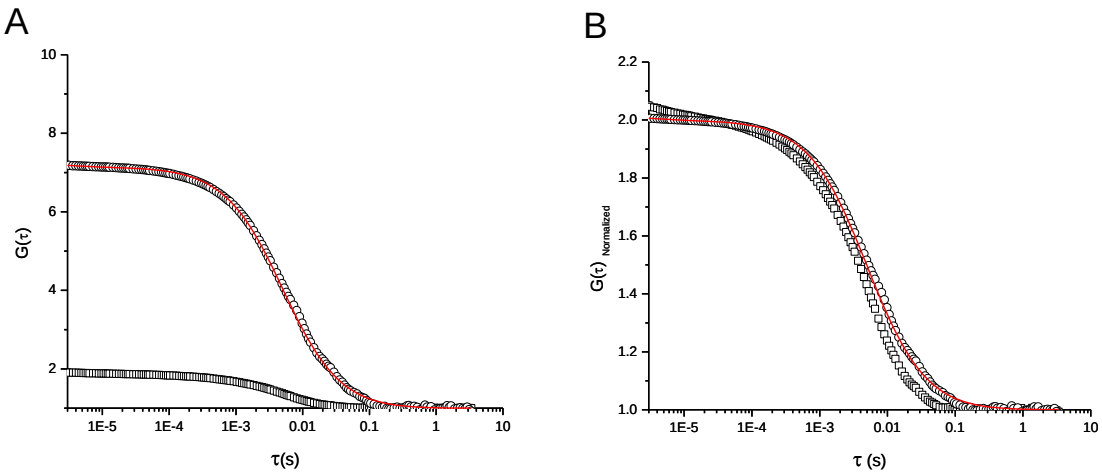

Figure 19: FCS measurement of 12-7NH-12 GP at a charge ratio of 10:1. Open circle shows the experimental signal and red line represent the fitting model to ACF for GP. Free Cy5-gWiz GFP is shown for comparison (open squares). DNA concentration for both samples was 2 ng/µL. A) Original ACF B) Normalized ACF; samples were normalized to one particle on Zen 2009 software. Calculated diffusion coefficient: 3.06±0.26 x 10^{-12} m^2/s (n=4).

In addition to studying the mobility, the hydrodynamic diameters of the GPs were also calculated using the Stokes-Einstein equation (Eq. 8), from the diffusion coefficients shown in Table 8.

Table 9: Particle size of GPs determined from FCS data using the Stokes-Einstein equation.

Gemini compound	*Mean diameter (nm)*	*CV (%)*
12-3-12	502.24	31.66
12-6-12	359.32	21.76
12-7-12	475.38	32.82
12-10-12	117.88	23.20
12-16-12	358.05	24.35
16-3-16	255.76	14.98
18-3-18	2836.96	175.59
12-7NH-12	159.89	8.65
Py-3-12	241.33	4.33

Table 9 shows that the chemical structure of the gemini surfactant has effect on the size of GP. Changes to the spacer length of the gemini surfactant did not significantly affect the particle size of GPs except with C-10 where smaller particle formed. The effect of tail length modifications to gemini surfactant was shown to have a greater effect on the particle size of GP. Compared to spacer length modification of similar length (4C increase for 12-7-12 from 12-3-12), the 16-3-16 gemini surfactant produced smaller particles ($D_{H\ 12\text{-}7NH\text{-}12}$ = 475.38±32.82 nm and $D_{H\ 16\text{-}3\text{-}16}$ = 255.76±14.98 nm respectively). This trend was not observed though with 18-3-18 GP due to presence of large particles (DH 18-3-18 = 2836.96±175.59) that were observed in the sample as flocculation. One explanation for the flocculation is due to the 18-3-18 significantly lower cmc compared to other gemini surfactants (

Table 16). A study has demonstrated that surfactant concentration can affect the stability of emulsion, where flocculation can occur at a concentration above the cmc [229]. The effect of functionalization has also shown to have a significant effect on the final size of GP. Both modifications to spacer and tail of gemini surfactant resulted in significantly smaller GPs compared GPs prepared with parent un-functionalized GPs. Overall the compaction of the plasmid was most effective with 12-10-12, 12-7NH-12 and Py-3-12 resulting in smaller particle size.

5.1.5 FCS measurements of GPLs

Following the study of GPs, a FCS study was carried out on GPLs prepared with the addition of phospholipids vesicles composed of pure DOPE or mixture of DOPE and DPPC at 1:3 molar ratio (DD 1:3). GPLs were prepared at 10:1 ratio as described in section 4.7 to reproduce NPs previous studied by our research group [121, 195]. DNA concentration was normalized to 2 ng/µL as described in previous FCS measurements of Cy5-gWiz GFP and GPs (Section 5.1.2 and 0). Figure 20 below shows an example of the ACF from GPLs prepared with 12-3-12 and DD 1:3.

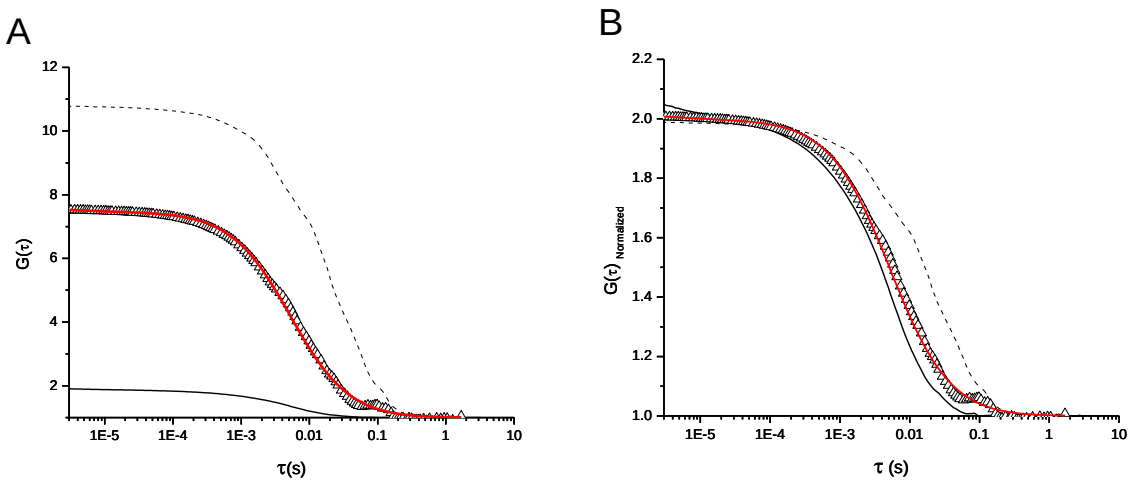

Figure 20: FCS measurement of GPLs at charge ratio of 10:1 with 12-3-12 and DD 1:3 phospholipid. Open triangles shows the ACF and red line represent the fitting model for the ACF for GPL. Cy5-gWiz GFP (solid line), GP (dashed line) are added as references. DNA concentration for all samples was 2 ng/µL. A) Original ACF B) Normalized ACF.

Figure 20 demonstrates that the addition of the phospholipids causes significant shifts to the ACF. Compared to GPs (Figure 17), the GPLs show both a downward and right shift of the curve. This indicates an increase in the number of particles and that the particles also move faster through the focal volume ($D_{GPL\text{-}12312}$=3.1±0.4 x10^{-12} (n=4), $D_{GP\text{-}12312}$=1.0x10^{-12} ±0.3 (n=4)). An additional difference is in the overall quality of the ACF. Figure 20A shows that the model described by (Eq. 7) fitted to ACF very well. Furthermore the measurements were more reproducible, which is demonstrated by the smaller standard deviation in the subsequent derivation of diffusion coefficient from the ACFs (Table 10). This suggests that the addition of the phospholipid produces smaller and more homogenous particles.

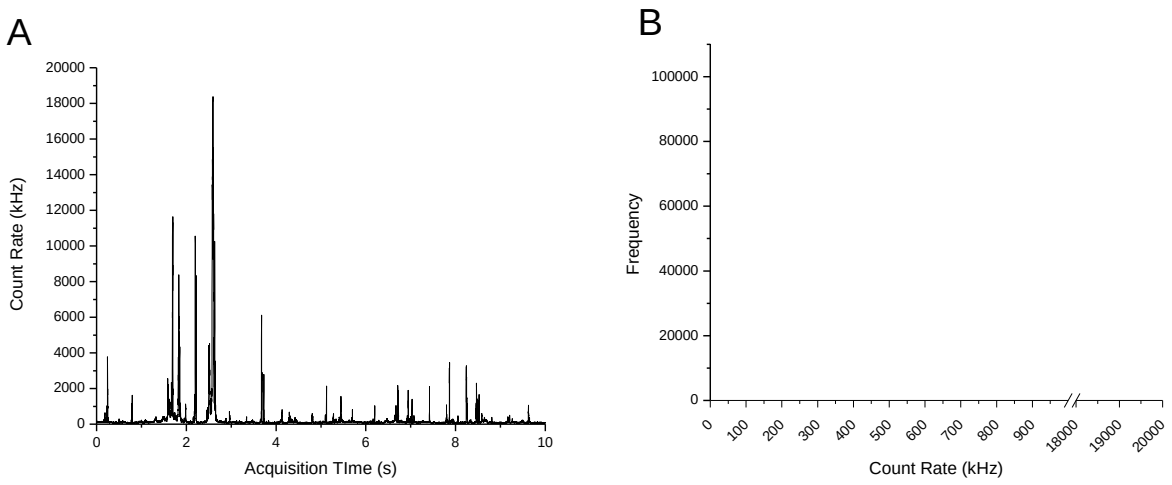

Figure 21: Raw intensity count rate for GPLs with 12-3-12 and phospholipids DD 1:3. A) Count rate measurement for GPLs prepared with DD 1:3. B) Intensity histograms measurement for GPLs prepared with DD 1:3.

These finding were also supported by a change in profile of the intensity histogram that showed a decrease in the number of background signals (0-50 kHz) and an increase in the 100 and 200 kHz peaks as shown in Figure 21B and D. The raw intensity diagram in Figure 21A and C also show the increase in the number of fluorescence fluctuations and decrease in the intensity of the higher peaks. The test shows that reduction in the number of measurements had no effect on overall distribution of the intensity histograms.

The fitting model (Eq. 7) also showed a tighter fit for the GPLs compared to the GPs counterpart, partly due to the increase in fluctuations and decrease in high intensity peaks that provide more suitable data for the ACF analysis. Additional fitting models with more variables were also tested on the ACF for the GPLs but did not result in a better curve fitting (data not shown). FCS measurements performed for all ten GPLs with two different phospholipids (DOPE and DD 1:3) are presented in Table 10 and Table 12.

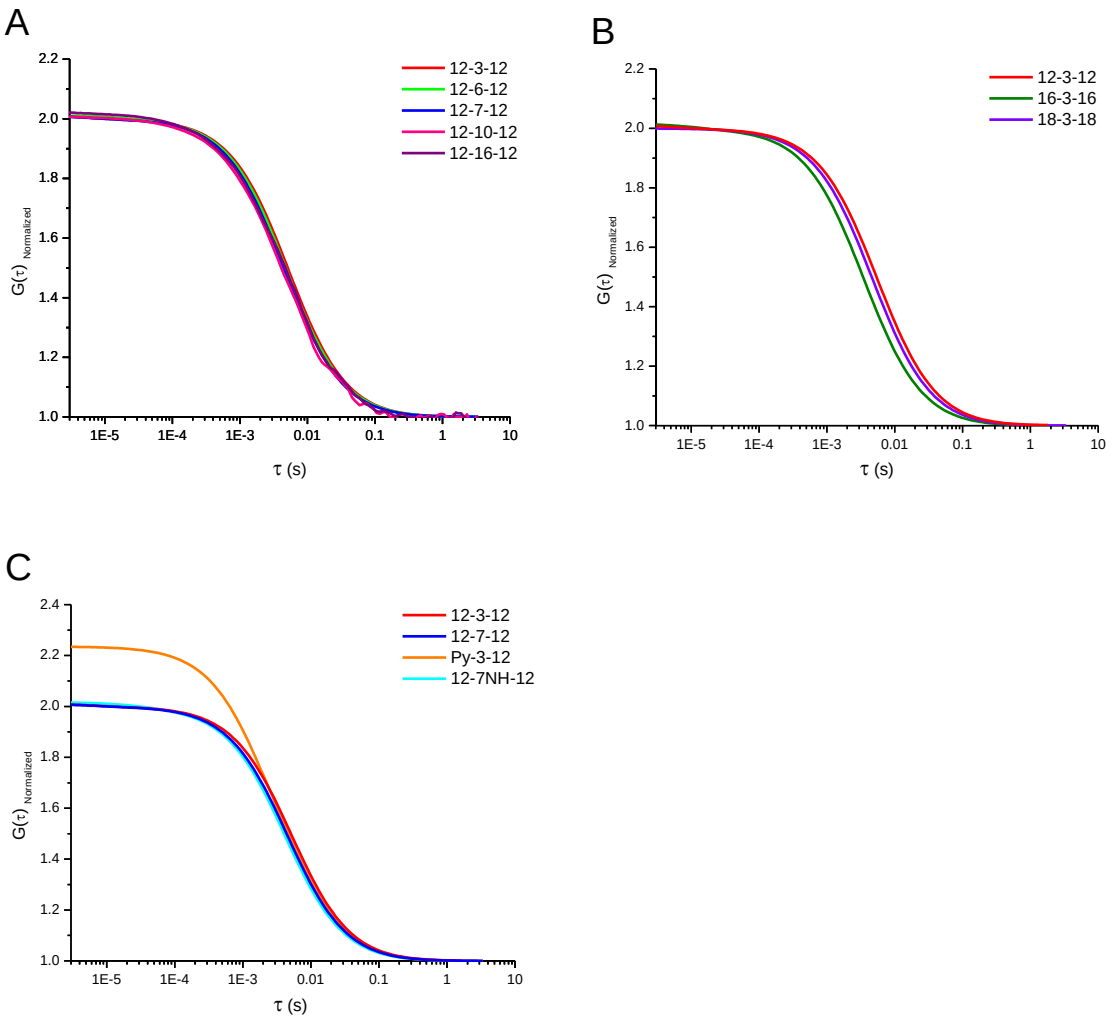

Figure 22: ACF of GPLs prepared with various gemini surfactants and DD1:3 organized by A) effect of gemini spacer length B) effect of gemini tail length and C) effect of gemini functionalization.

Table 10: Diffusion coefficient of GPLs prepared with DOPE:DPPC 1:3 phospholipids

Gemini compound	*Mean diffusion coefficient (10^{-12} m^2/s)*	*CV (%)*
12-3-12	3.11	13.18
12-6-12	3.21	19.46
12-7-12	3.76	6.32
12-10-12	3.84	13.56
12-16-12	3.47	14.12
16-3-16	3.68	17.34
18-3-18	2.36	79.62
12-7NH-12	4.33	8.38
Py-3-12	3.57	6.63

Table 11: Particle size of GPLs prepared with DOPE:DPPC at 1:3 molar ratio phospholipids determined by FCS calculated using the Stokes-Einstein equation. Dimensions are expressed as diameter in nm.

Gemini compound	*Mean diameter (nm)*	*CV (%)*
12-3-12	157.50	13.18
12-6-12	152.46	19.46
12-7-12	130.38	6.32
12-10-12	127.51	13.56
12-16-12	140.97	28.15
16-3-16	133.18	17.34
18-3-18	207.16	79.62
12-7NH-12	112.99	8.38
Py-3-12	137.25	6.63

Table 12: Diffusion coefficient of GPLs prepared with DOPE phospholipids

Gemini compound	*Mean diffusion coefficient (10^{-12} m^2/s)*	*CV (%)*
12-3-12	3.21	19.11
12-6-12	3.24	15.25
12-7-12	2.64	13.90
12-10-12	4.60	6.40
12-16-12	3.06	15.71
16-3-16	2.85	12.66
18-3-18	0.58	66.68
12-7NH-12	3.92	6.17
Py-3-12	3.80	14.32

Table 13: Particle size of GPLs prepared with DOPE phospholipids determined by FCS calculated using the Stokes-Einstein Equation. Dimensions are expressed as diameter in nanometers.

Gemini compound	*Mean diameter (nm)*	*CV (%)*
12-3-12	152.48	19.11
12-6-12	151.35	15.25
12-7-12	185.50	13.90
12-10-12	106.46	6.40
12-16-12	160.00	15.71
16-3-16	171.99	12.66
18-3-18	849.68	66.68
12-7NH-12	124.87	6.17
Py-3-12	126.06	14.32

Figure 22 shows that addition of DD 1:3 to the GPs results in ACF with very similar curve profile. A similar trend was also observed with addition of DOPE and no significant difference in the ACF between DD 1:3 and DOPE GPLs (data not shown). As shown in Table 10 and

Table 12 the addition of either class of phospholipids resulted in GPL with similar diffusion coefficient. The trends observed for GPs regarding the structure of the gemini surfactants was not as evident. Overall, the diffusion coefficient of most GPL was an average of 3.2-3.3x10^{-12} m^2/s. As a result, the calculated particle size for the majority of GPL were also quite uniform with an average of approximately 120 ±30 nm as shown in Table 11 and Table 13. This uniformity is also reflected in the ACF of the phospholipids as shown in Figure 22. This suggests that in contrast to the GP, composed of large and heterogeneous particles (Table 9; 300-500 ±20-30% nm), the addition of phospholipid normalized the size and produced smaller and more uniform NPs (Table 11 and Table 13; ~120-150 (± 10-20%) nm).

As shown in Figure 21, the addition of the phospholipids increased the number of fluctuations, but there were some larger peaks still present. To help identify these high intensity peaks a control was run using Cy5-gWiz and DD 1:3 in the absence of pre-compaction with gemini surfactant.

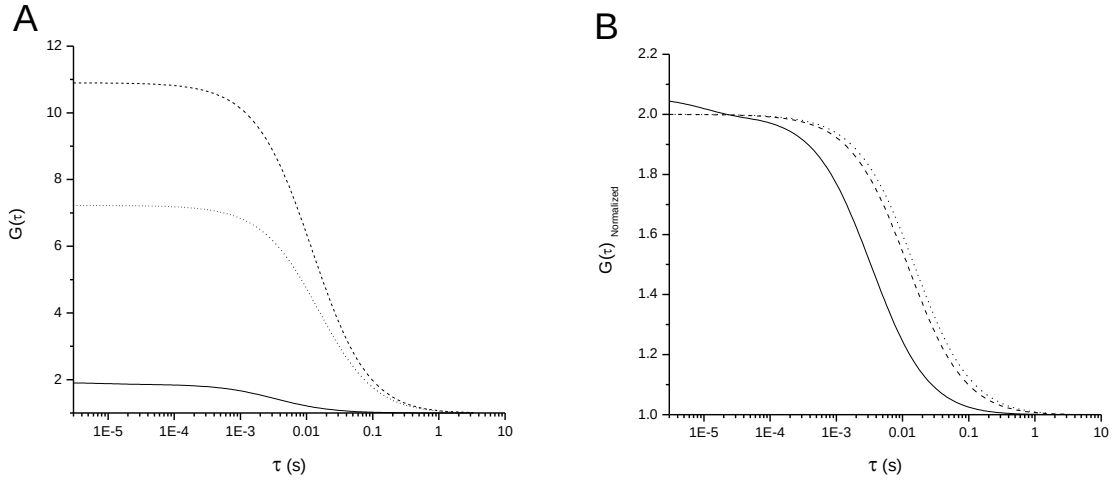

Figure 23: FCS measurement of DD1:3-plasmid vesicles (dotted line). DNA concentration for all samples was 2 ng/µL. A) Original ACF B) Normalized ACF. Free Cy5-gWiz GFP (solid line) and 12-3-12 GP (dashed line) was shown for comparison. Diffusion coefficient of DD 1:3 was calculated to 1.39x10^{-12} (±40%) m^2/s (n=4).

The DD 1:3-plasmid complexes had a diffusion coefficient of 1.39x10^{-12} m^2/s with a CV of 40% (n=4; Figure 23). The encapsulation of the plasmid DNA by the phospholipids is suggested by the decrease in particle number shown by the increase in the maxima of the ACF in Figure 23A. Although the DD1:3 are slow moving like other GPs, Figure 23A shows that there were more particles in solution like GPLs. Based on the FCS information, it is not possible to determine the source of the small populations of aggregated particles found in the GPLs preparation since there is no method to determine which element of gemini NP the plasmid is interacting with.

5.2 Additional physicochemical characterization of GPLs

To validate FCS as a tool to monitor physiochemical parameters of GPLs, additional techniques were also used in parallel to monitor these parameters. Key physical characteristics of GPLs such as particle size and zeta potential were measured using DLS and DLP for various compositions at various stages of assembly. The results are presented in two major sections: particle size and zeta potential.

5.2.1 Evaluation of particle size by DLS

5.2.1.1 Optimization of particle size measurement

The first experiment was to determine the size for the various individual components of GPLs. This includes the labeled-plasmid, gemini surfactant and phospholipids vesicles. As expected, size distribution of Cy5-gWiz GFP, was heterogeneous, 300 nm ± 400 nm, with a high PDI 0.5±0.3 (n=4). This demonstrates that free plasmid alone is not compacted and the measurement is of low reliability based on the DLS correlogram. Gemini surfactant solutions contained particles (micelles) of average diameter of 250-300 nm. Vesicles prepared with phospholipids DOPE and DD 1:3 by thin-film method had a final average diameter of 120±30 nm and 140±20nm (n=4) and narrow size distribution with PDI of 0.2 and 0.23, respectively.

5.2.1.2 Effect of dilution on particle size of GPLs

The purpose of this experiment was to evaluate the effects of dilution on the size of prepared NPs. This was important because the sub nano-molar concentration required for FCS measurement to monitor if any artifact can occur due to dilution. Figure 24 shows the effect of dilution on the particle size of both GPs and GPL complexes measured by DLS.

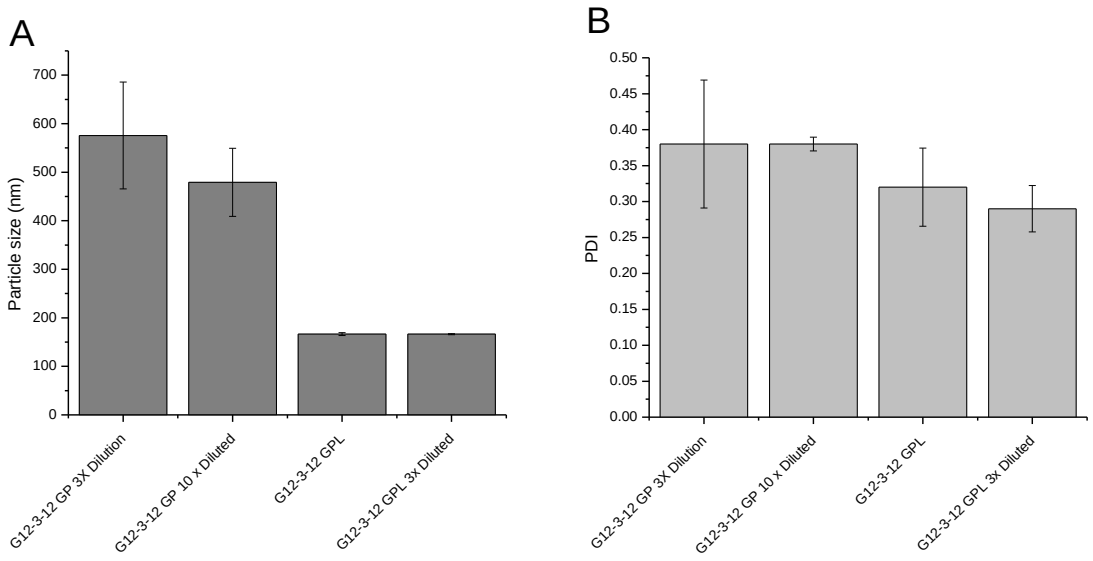

Figure 24: Effect of dilution on particle size measurement of GP and GPL. A) Diameter of gemini assemblies B) PDI of gemini NP assemblies (n=4). GP could not be measured undiluted and therefore a 3x and 10x dilution were used.

In the case of GP, the first step in the assembly process of the GPLs; three samples were tested: undiluted GP (6.28 ng/μL), samples diluted to 2ng/μL for FCS analysis (GP) and 10x diluted (0.628 ng/μL). This initial study showed that undiluted gemini DNA complexes were quite large; with diameters over 20, 000 nm an PDI of 0.98 (data not shown). This indicates that the system is very heterogeneous and a PDI value over 0.7 indicates that this sample is unsuitable for DLS analysis. A three-fold dilution brought the concentration to the range used FCS analysis (2ng/μL) and showed that GP forms complexes were ~500 nm with a PDI of about 0.35 (Figure 24A and B). Further dilution (10-fold) showed no significant effect on particle size and PDI. These results indicated that a certain degree of dilution was required to acquire adequate measurement for GP complex. These initial studies suggests that the initial condensation of plasmids by gemini surfactants results in large particles. The second set of measurements were performed with the completed GPL particle (Figure 24A and B). Measurements with undiluted GPL showed that GPLs have an average size of about 166 ±2nm and PDI 0.38. Upon a three-fold dilution, no significant change was observed in size or size distribution. A 10-fold dilution was also performed and no significant change was observed (data not shown). The results confirm that no dilution-related artifact occurred due to sample preparation for FCS. This demonstrates that there is an upper limit for measurement of GP due to the concentrations of particles, and heterogeneity of the population of particles. The effect of dilution is minimal between application range and FCS range for GPLs.

5.2.1.3 Effect of gemini surfactant composition on particle size of GPs

The aim of this part of the research was to study the effect of compositional changes in GPL assembly, in particular, the effect of gemini surfactant structure on particle size and size distribution. Figure 25 shows the effect of gemini surfactant structure on the size and size distribution of GP.

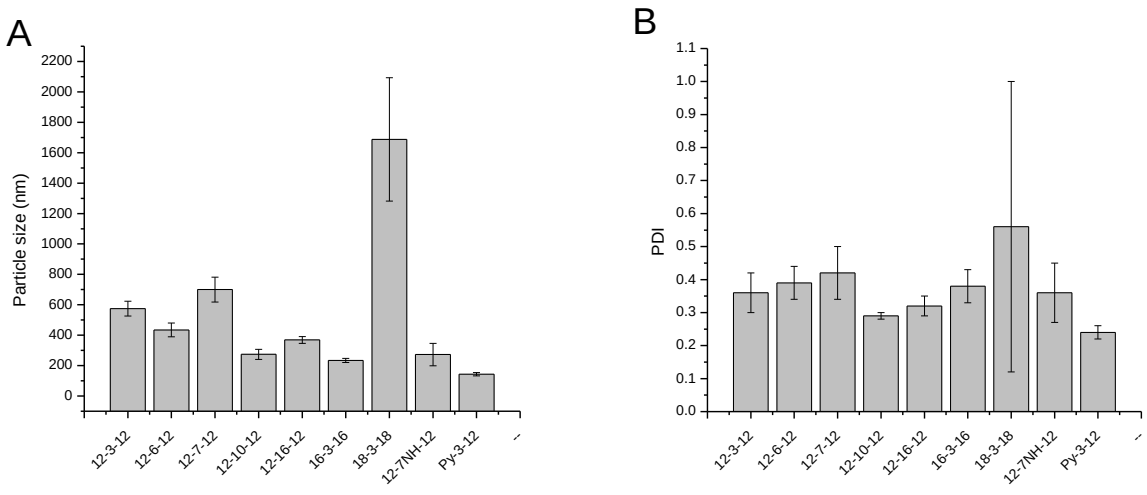

Figure 25: Particle size and distribution of GPs prepared with various gemini surfactants. DLS measurements were performed and the diameter of the NP and PDI were reported. A) Particle size of various GPL B) PDI of various GPL.

Figure 25 shows the particle size and PDI of GP formed from different gemini surfactants and Cy5-gWiz GFP at a charge ratio (N/P) of 10:1. Overall, the average size of GP was approximately 650±40 nm with PDI greater than 0.3. The structure of gemini surfactants was also found to play a role in modulating the size of the GP. The effect of spacer length begins with 12-3-12 and size decreases until 12-10-12 (with the exception of 12-7-12) and rises slightly with 12-16-12. Overall, the size distribution does not significantly change for spacer length 3, 6 and 7. Increasing the tail length from 12C to 16C generated significantly smaller GPs. In contrast, 18-3-18 produced significantly larger GP. This can be explained by the flocculation in the sample. Functionalization of the gemini surfactants also had an effect on particle size. As seen in Figure 25, Py-3-12 produced the smallest pre-complexes (143 nm compared to 543 nm for its parent gemini surfactant) and PDI of 0.24. This suggests that Py-3-12 is capable of producing NPs without the aid of a phospholipid (data shown in following figures). This is significant, because of its similarity to gemini NPs. The pH-sensitive functionalization 12-7NH-12 showed an insignificant difference compared to the parent compound (12-7-12). When compared to free-plasmid, it is evident that overall the DNA is being compacted into a more organized form than it was previously.

The raw intensity data in some measurements shows the presence of a larger species of GP (Figure 26). These complexes typically appear in all GP, with the exception being Py-3-12. This minor species typically consist of larger particles (4000-5000 nm) and makes up 9% of the GP in those runs (data shown in Appendix 0), which could represent free-DNA or lesser organized form of the gemini-plasmid complex.

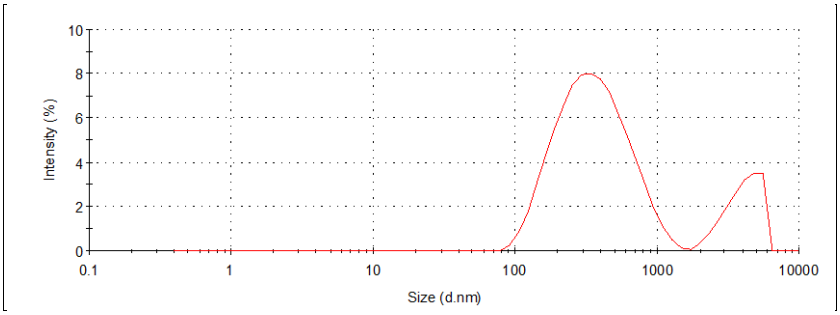

Figure 26: Size distribution by intensity for 12-3-12 GP. Graph is an average (n=4) and exported from Zetasizer Nano software.

5.2.1.4 Effect of helper neutral phospholipids on the size of nanoparticles

GPLs were prepared by the addition of phospholipid vesicles to the GP. For this experiment, two different composition of phospholipids, DOPE and DOPE:DPPC at 1:3 ratio (DD 1:3) were used to explore its effects on the formation GPLs.

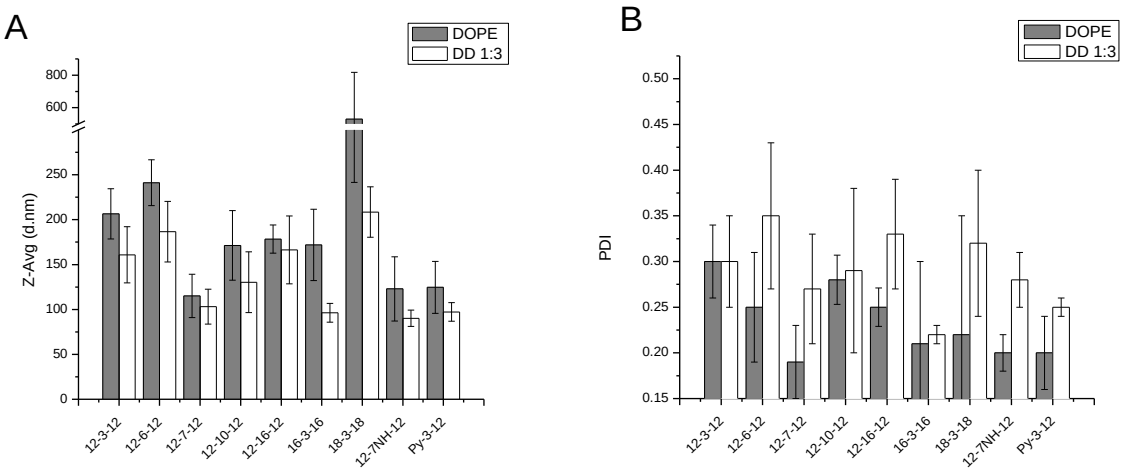

Figure 27: DLS measurement of GPLs. A) Particle size and B) PDI of GPLs prepared with a series of gemini surfactants neutral phospholipids DOPE and DD 1:3. Values are expressed as mean±SD, n=4.

GPLs in general have a diameter between of 100 -200 nm (Figure 27). Overall, the type of phospholipids used to prepared the GPL resulted in a small change in size ($Z\text{-}Avg_{GPLDD1:3}$=159±47 nm and $Z\text{-}Avg_{GPLDOPE}$=168±42 nm), but statistically insignificant between the two groups. The only exception to this trend is with the imine gemini surfactants (12-7NH-12) where the DD 1:3 GPL was significantly larger than the GPL prepared with DOPE. Within each groups of GPL, trends arise once again based on the gemini surfactant used previously to compact the plasmid. As shown in Section 5.2.1.3, gemini spacer length shows a trend of decreasing size from starting 3C spacer (206±8 nm) down to a minimum at 7C spacer (115±24) with increase in particle size up to 12-16-12 (178±15 nm). Similarly increase in the tail length of the gemini surfactants resulted in decrease of particle size (172±40nm). Again this trend could not be extended onto 18-3-18 due to the presence of flocculation in the sample. The addition of functional groups to both the spacer and tail region of the gemini surfactants in the form of the 12-7NH-12 and Py-3-12 also resulted in smaller GPLs (123±35 nm and 125±28 nm respectively).

Figure 27B also demonstrates that the gemini surfactant structure have an effect on the polydispersity of the GPL. This suggests that gemini surfactants do not only aid in the production of smaller, but also more uniform particles depending on specific structural modifications. Furthermore GPLs prepared from DD1:3 were smaller in size but showed a larger PDI compared to their DOPE counterparts. One explanation for this larger size distribution could be due to the mixing of different lipids. This could result in polymorphism in lipid vesicles and in turn result in a greater diversity of GPLs [51, 230]. Compared to GP which had a broad size distribution and larger particle sizes (PDI_{avg}=0.38, 450 nm), the addition of neutral phospholipids creates a more homogenous population of smaller particles (PDI_{avg} =0.28, 150 nm). This trend is reflected upon in Figure 28 that demonstrates that not only are GPLs are more homogenous compared GPs (Figure 26) but also that there is a reduction of the large minor population.

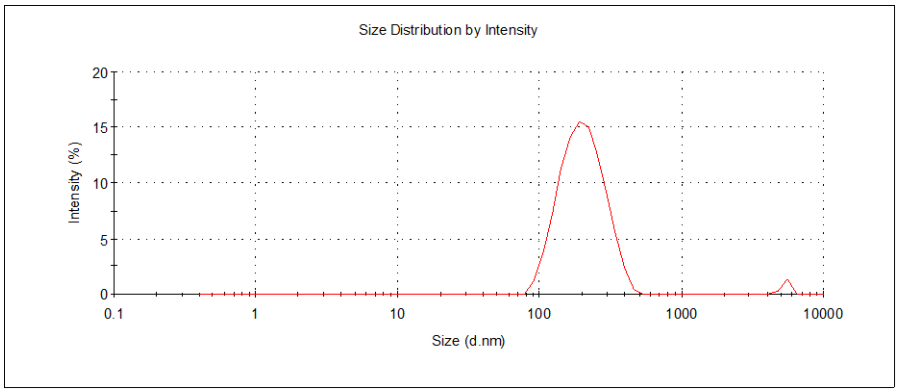

Figure 28 : Size distribution by intensity for 12-3-12 GPL prepared with DD 1:3. Graph is an average (n=4) and exported from Zetasizer Nano software.

5.2.2 Evaluation of surface charge of nanoparticles

The aim of this section was to determine the effect of composition on surface charge (zeta potential) of gemini NPs at various stages of assembly. Measurements were performed on the Zetasizer Nano using laser Doppler velocimetry (LDV) which was used to determine the electrophoretic mobility of a particle in solution. The zeta potential was then used as an indicator of thermodynamic stability (with surface charge greater than ±30 mV generally being considered as stable) [231].

The shifts in zeta potential during NP assembly are summarized in

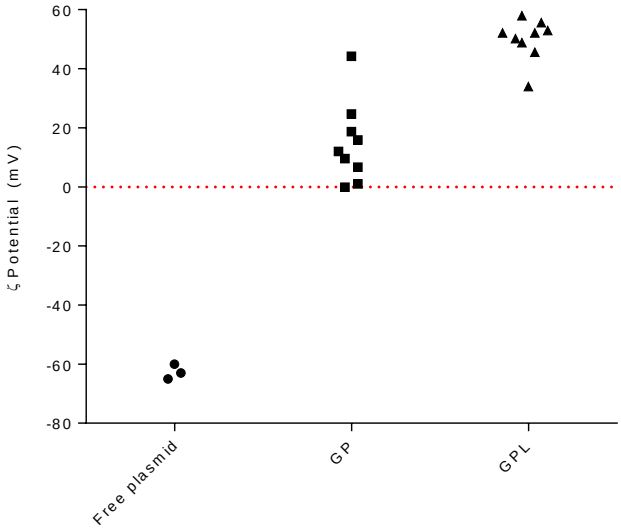

Figure 29 using 12-3-12 as a model. Initially, it shows that the plasmid has a strong negative charge (-63 mV) due to the phosphate backbone. With the addition of gemini surfactant, the negative charge is neutralized. The low zeta potential (~ 0 mV) suggests that these initial complexes are not stable and are

also prone to aggregation. After the addition of the phospholipids, the zeta potential of NPs increased to around +30 mV. This suggests that the phospholipids aid in stabilizing the initial complex formed between gemini surfactant and DNA, therefore making them more uniform. The following sections will provide a deeper evaluation of the effect of gemini surfactant structure on the zeta potential.

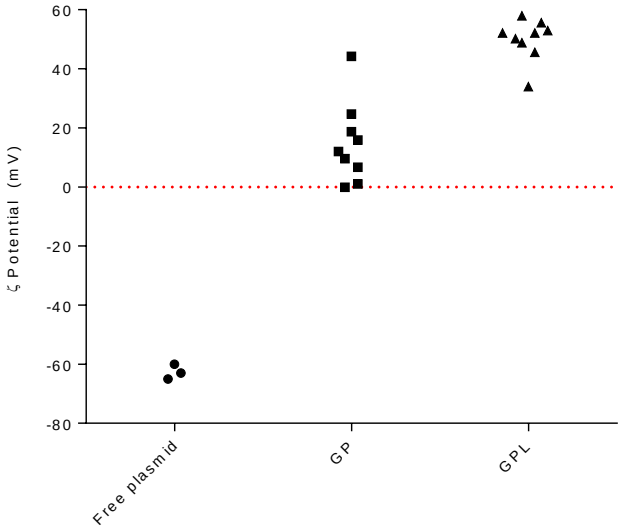

Figure 29: Zeta potential measured at different stages of gemini NPs assembly. Dotted red line indicates a neutral charge. Plasmid DNA has a strong negative charge (Circle; -63 mV). The addition of gemini surfactants neutralizes the negative charge of the plasmid to form the GP (Square; 0-25 mV). The addition of phospholipid (e.g. DD 1:3) forms the stable GPL (Triangle; 40-50 mV).

5.2.2.1 Effect of gemini surfactant composition on surface charge of GPs

The goal of this study was to investigate the relationship between gemini surfactant structure on the overall stability of the GP and to investigate the process of NP assembly. Figure 30 shows the effect of chemical structural modification of gemini surfactants on the surface charge of the GP.

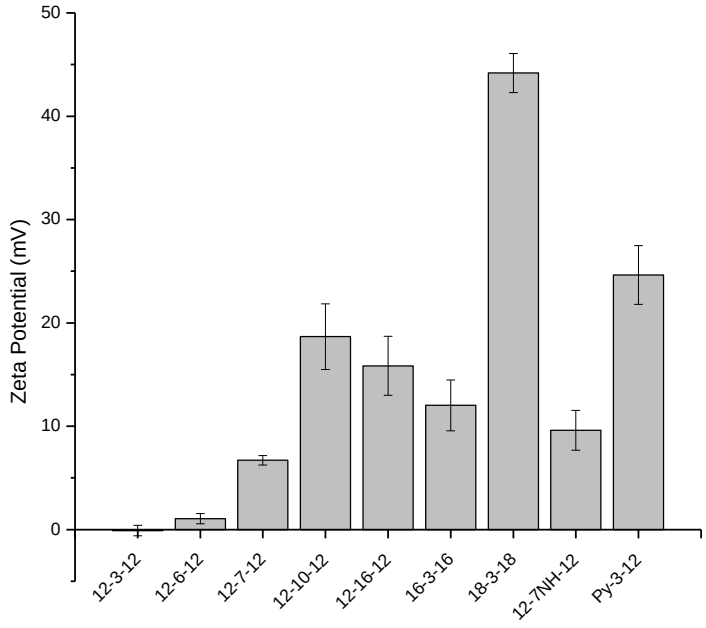

Figure 30: Effect of gemini surfactant structure on zeta potential of GPs. Values expressed as mean±SD (n=4).

All gemini surfactants in this study were able to effectively neutralize the negative charge of the plasmid (-63 mV, Figure 30). Beyond neutralizing the plasmids, it was shown that the structure of the gemini surfactant also governed the final charge of GPs. Overall increase in the alkyl chain length of either the spacer or the tail region of the gemini surfactant resulted in a significant increase in zeta potential. Overall, modifications to the tail regions resulted in greater changes compared to spacers ($\delta_{18\text{-}3\text{-}18}$=+44mV, $\delta_{12\text{-}10\text{-}12}$=+20 mV). The 18-3-18 was previously shown to produce highly charged GPs (+44 mV) but the quality of the measurement was poor due the presences of flocculation in solution. The introduction of functional groups was also shown to have a significant effect on the surface charge. GP complexes made either with 12-7NH-12 (9.6±2 mV) or Py-3-12 (24.64±2.8 mV), had significantly higher surface charges compared to their parent compounds ($\delta_{12\text{-}7\text{-}12}$=6.71±0.4 mV and $\delta_{12\text{-}3\text{-}12}$=0.09±0.4) respectively).

5.2.2.2 Effect of phospholipid on surface charge of GPLs

The role of neutral phospholipid components of gemini NPs on their zeta potential was investigated in detail. The effect of two lipid compositions, DOPE or DD 1:3 are shown in Figure 31.

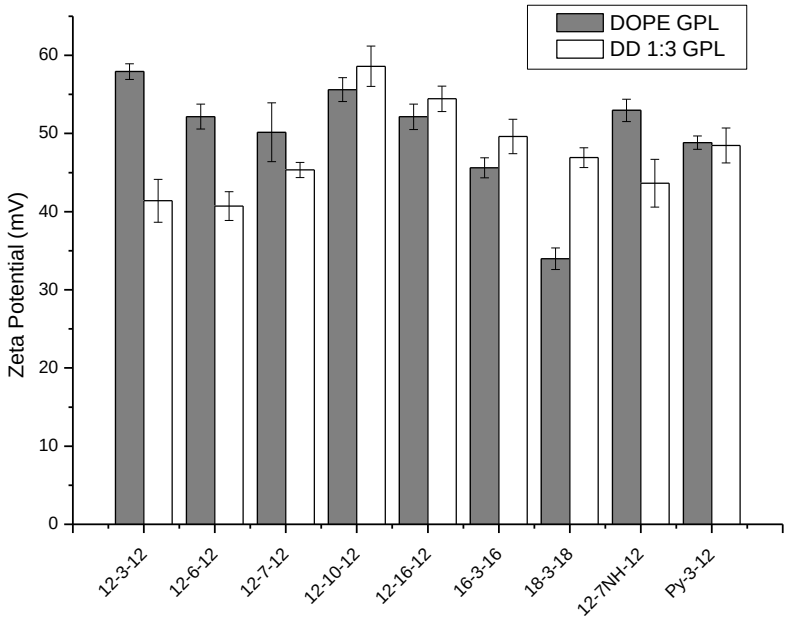

Figure 31: Surface charge of GPLs prepared with DOPE and DD 1:3 phospholipids. Surface charge is expressed as the zeta potential (mV). pH of DOPE and DD 1:3 GPLs was between 6.5-7.1.

Regardless of gemini surfactant structure, all GPLs possess a positive surface charge above +30 mV (Figure 31). Generally, GPLs prepared with DOPE and DD 1:3 GPLs had similar zeta potential values (between +40-60 mV). Only in the cases of 12-3-12, 12-6-12 and 12-7NH-12 GPLs prepared with DOPE showed a higher zeta potential compared to GPLs made with DD 1:3. The effect of spacer length on the zeta potential showed a bimodal pattern (two peaks at C3 and C10), with tail length resulted in a slight decrease of the surface charge. Also, compared to the GP, the effect of gemini surfactant structure was not as pronounced as the trends observed in Figure 30. Furthermore, the zeta potential for both DOPE and DD 1:3 NP were more uniform than their GP counterparts. This suggests that the lipid composition played a major role in governing the final surface charge of the NPs.

5.2.2.3 Effect of dilution on surface charge of GPLs

Table 14 shows the effect of dilution on the zeta potential measurements of 12-3-12 GPL prepared with DD 1:3. These results show that zeta potential was not affected by dilution in water. This demonstrates that GPLs were stable when measured at sub-nanomolar concentrations that are required for FCS.

Table 14: Effect of dilution on zeta potential of G12-3-12 GLP.

Dilution	***Avg ζ (mV)***	***± S.D. (mV)***
2-fold	39.28	2.11
3-fold	41.80	2.71
4-fold	40.27	3.08

5.3 Dye exclusion assay

Dye exclusion assays, using both PicoGreen® and EtBr, were used to investigate the microenvironment around the nucleic acid cargo within the NP. This was to gain a deeper understanding of the role of NP composition in the self-assembly process. Dye exclusion occurs when cationic agents compact DNA which results in an increase in DNA rigidity, thus denying the dye access to the DNA [232, 233]. This results in a decrease in fluorescence intensity which is used to monitor the degree of compaction of the plasmid by the NP. Experiments were performed using gWiz Luc plasmid to conserve labeled gWiz GFP for FCS experiments. Controls were performed to ensure the degree of dye exclusion was not affected by the labeling (data not shown). As a side note, due to similar size of gWiz GFP to gWiz Luc plasmid, the difference in size was considered negligible (5757 bp vs. 6730 bp).

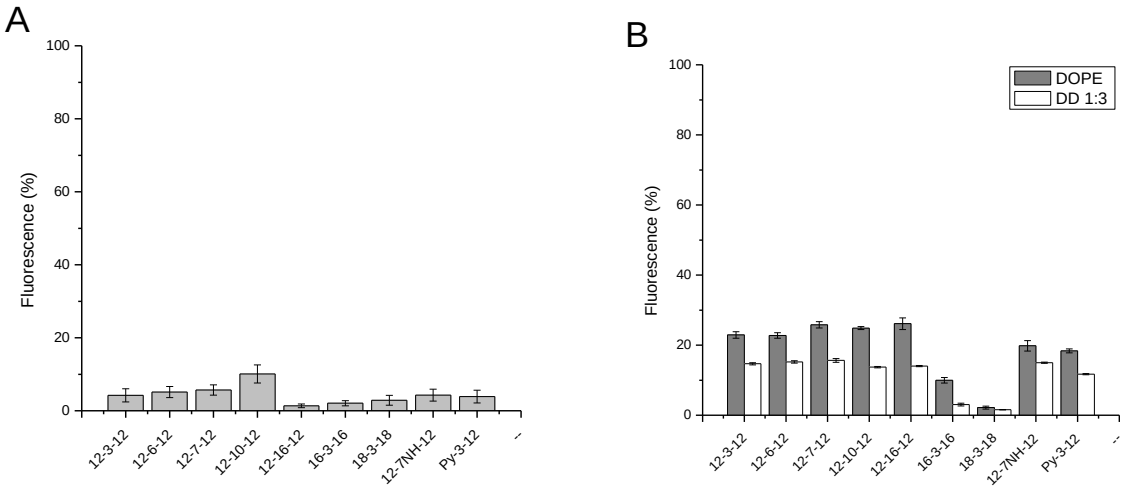

Figure 32: PicoGreen dye exclusion assay for various GP and GPLs. Results reported as percentage of fluorescence remaining relative to free DNA. Values expressed as mean±SD (n=4). A) Degree of fluorescence blocked by GP with different gemini surfactant B) Degree of fluorescence blocked by GPLs with DOPE and DD 1:3 GLP.

Figure 32 shows the ability of GP and GPLs to block the fluorescence of PicoGreen. Overall, GPs were found to have significantly lower fluorescence compared to the GPLs counterparts. GPs were capable of blocking approximately 95% of fluorescence that suggest a very high degree of DNA compaction occurred at this phase (Figure 32A). The modification of gemini surfactant has generally minor effect on dye blocking with GPs. Increasing spacer length in gemini surfactants from 3C (4.2±1.8%) caused a slight increase of fluorescence up to 10C spacer (10.1±2.5%), followed by a significant drop at 16C spacer (1.4±0.5%). Modification to the tail region of the gemini surfactants provided a significant shift in dye blocking (16-3-16=2.1±0.7%, 18-3-18=2.9±1.2%). The GPs prepared from functionalized gemini surfactants 12-7NH-12 and Py-3-12 also did not provide significant shift in degree of dye block (4.3±1.3 and 3.9±1.8 respectively). shows that the addition of phospholipids normalized the degree of fluorescence exclusion among the final GPLs (Figure 32B). Compared to GPs (Figure 32A), where gemini surfactants determined the degree of dye blocking, the majority of the GPLs showed a similar degree of dye blocking with a mean for most GPLs of around 20%. A significant shift was seen with GPLs prepared from gemini surfactants with longer tails; 16-3-16 and 18-3-18 gemini surfactants produced significantly higher degrees of fluorescence. These results, along with the trend observed with GPs (Figure 32A) would suggest that the hydrophobic regions of the gemini surfactants played a key role in controlling the compaction of the DNA. Furthermore, the composition of the phospholipid did not only normalize the GPs, but it also governed the final degree of dye blocking. It was observed in Figure 32B that GPLs

prepared from DD 1:3 had an overall lower fluorescence compared to DOPE counter-parts. In addition to PicoGreen, a second dye exclusion assay with EtBr assay was also performed.

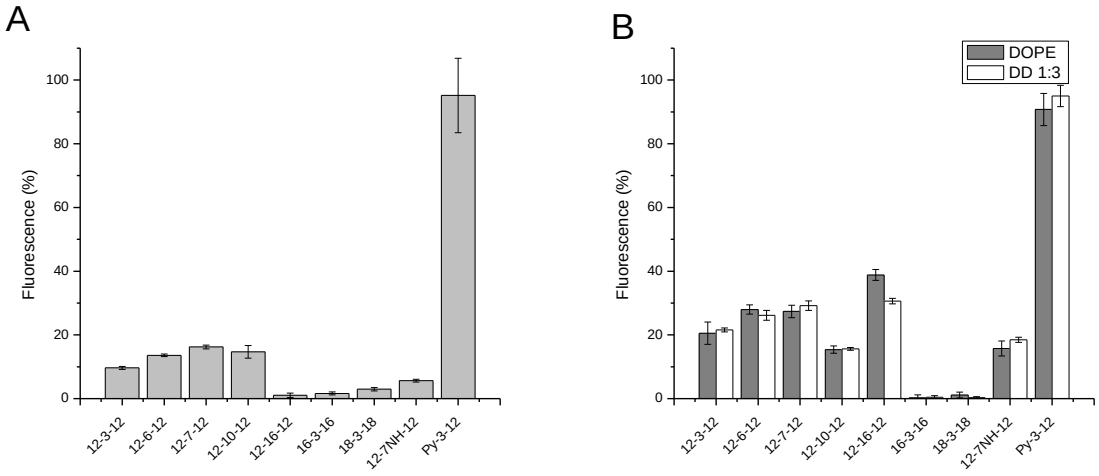

Figure 33: Ethidium bromide dye exclusion assay for various GP and GPLs. Results reported as mean ±SD percentage of fluorescence remaining relative to free plasmid. Values expressed as mean±SD (n=4). Degree of fluorescence from GPs with different gemini surfactant B) Degree of fluorescence from GPLs prepared with DOPE and DD 1:3 GLP.

EtBr provided similar results to PicoGreen® in dye exclusion assays, such as the increased blocking of GPs relative to GPLs. However, in the case of Py-3-12, the two assays showed significantly different result for both GP and GPL (Figure 32 and Figure 33 respectively). In the PicoGreen® assay, GP and GPL prepared with Py-3-12 gemini surfactant was able to effectively block PicoGreen®. However with EtBr, no fluorescence blocking was observed at all. Controls were also performed to ensure the unique Py-3-12 surfactant did not interact with EtBr which would cause the resulting fluorescence.

6.0 Discussion

6.1 Preparation of fluorescently labeled gemini nanoparticles

6.1.1 Selection of labeled nanoparticle component

The first step in the development of the FCS methodology is to label the molecule of interest. Since the gemini NP is composed of three elements; plasmid, gemini surfactant and phospholipids, an important step in the optimization of the FCS experiment is ensuring the physical and spectral integrity of the fluorescent-labeled specimen of interest. Since FCS only monitors fluorescent fluctuations, the choice of labeled molecule in the gemini NP directly affect which parameter can be studied. Furthermore the labeling must also not interfere with the assembly of the gemini NP and must also be evaluated to ensure no artifacts occurring due to the labeling process.

For this study the plasmid was selected due to its key role as the cargo for gemini NP and its central presence in all phases of the gemini NP assembly. This allowed for a greater deal of flexibility in experimental design in terms of characterizing the gemini NPs. To study the interaction of plasmid with other components of the gemini NPs, it was essential to confirm that the process of labeling had no affect on the plasmid in order to provide a more accurate study of biophysical properties of gemini NPs. The first step was to determine the effect of labeling plasmids on the FCS measurements and optimize its labeling. Previous FCS experiments investigating other non-viral systems utilized smaller strands of nucleic acids such as oligonucleotide or siRNA [90, 209, 234-238]. In these cases, conjugation was performed at the terminal ends of the nucleic acids. This ensured a specific base-dye ratio – typically of one label per nucleic acid molecule. This was ideal for FCS because changes in fluorescent intensity and the number of fluctuation could be directly related to the concentration of the labeled species in solution. Plasmids, being larger and lacking of terminus (for SC form of interest), the labeling reaction involved further steps, such as binding grooves or intercalations between base pairs. This resulted in various degrees of labeling or labeling densities. The position of dye conjugation was one key difference noted from these previous experiments. This proved to be less consistent compared to reactions to linear forms of nucleic acids (due to the presence of N and C terminals). As shown in Table 7 the degree of labeling had an effect on the integrity of the plasmid topology. Furthermore, due to the sensitivity of the FCS technique, variation in the labeled and the quality of the plasmid needed to be controlled. This required extensive screening to verify the quality of the labeled plasmid, however it was considered the best

candidate for studying gemini NPs by FCS. This will be discussed in the following section (Section 6.1.1).

Labeling the other components of the gemini NP were also considered during the experimental design but were deemed not feasible for studying the biophysics of the gemini NPs that were previously studied by our group [121, 162, 226]. This is because the addition of any fluorophore to a gemini surfactant would modify the properties of the final GPL. Therefore any labeled gemini surfactant would not be a true representation of the unlabeled gemini surfactants. The phospholipid component was also considered for the evaluation of gemini NP. However, the reason why this component was not pursued in this study was because phospholipids are only added in the final step, and therefore would not provide information about the earlier stages of gemini NP assembly. Furthermore, with the addition of labeled lipids, or the integration of labeled lipids into the existing lipid vesicles, it has been shown in previous studies to have an effect on diffusion of the complexes [239]. Although the addition of any tracking moiety would have an effect on the system in study, effects were minimized in the presence of the plasmid, as examined in this section. Therefore an important part of this study was ensuring the labeling of the plasmid had no effect on the activity and interactions of the plasmid.

6.1.2 Evaluation of Cy5-gWiz GFP plasmid for FCS

Cy5-gWiz GFP was thoroughly evaluated to ensure that the labeling reactions had a minimal effect on the plasmids and was ideal for FCS measurements. To determine the effect of the labeling process on the plasmid, different labeling ratios were screened to observe the effects on the topology and diffusion coefficient. Agarose gel electrophoresis and fluorescent dye PicoGreen, developed by Levy and colleagues (SCfluro Assay), was used to evaluate and quantify the topology of the plasmid [240]. Table 7 shows that plasmid topology had significant effects on diffusion coefficient. Although claims by the manufacturer state that no degradation should occur due to labeling, studies by our group demonstrate that longer incubation times, or higher labeling density, resulted in degradation of the gWiz GFP plasmid. A possible explanation for this could be due to the labeling methods. The manufacturer's instructions require an incubation at 37°C for specific time intervals (to achieve 0.5:1 a one hour incubation is necessary). Therefore, one theory was that the longer exposure to the elevated temperature could result in the degradation that was observed. This was seen with the 0.5:1 base-dye reaction that had approximately 60% SC content with a diffusion coefficient of $7.1\pm0.7 \times 10^{-12}$ m^2/s. In comparison, ratios of 0.25:1 labeled-plasmid had less effect with SC content (83% compared to 85% for unlabelled) and diffusion coefficient of $4.2\pm0.2 \times 10^{-12}$ m^2/s. The experimental determined diffusion time of SC plasmid correlated

with findings from other groups, which was around 3.8±0.3 $x10^{-12}$ m^2/s [241]. The study also showed that the conjugation of the dye had little impact on the diffusion time of the plasmid. By comparing the ratios of 0.05:1 and 0.25:1, which had a similar degree of SC plasmid (85%), even though there was a 5-fold increase in the amount of label, there was an insignificant shift in the diffusion coefficient of the labeled plasmid. Since the mass of single a Cy5 fluorophore is 533 g/mol, the total mass of the Cy5 conjugated per plasmid can be approximated as 1519, 7462 g/mol and 15,457 g/mol for 0.05:1, 0.25:1 and 0.5:1 respectively, based on the base-dye ratio calculated in (Eq. 5). Therefore with the total mass of a plasmid being 3.74 $x10^6$ g/mol (5757 bp x 650 g/mol*bp), it would indicate that the mass of additional Cy5 would account for less (0.04%-0.4%) of the plasmid overall mass. Although the mass of the Cy5 used in this estimate could be smaller (the actual structure of labeling reagent with Cy5 unknown), it is clear that the mass of the dye has little effect on the diffusion of the plasmid

The next set of considerations focused on the optimization of FCS measurement conditions for labeled plasmid. With FCS being very sensitive and easily saturated, a successful FCS measurement is being able to achieve a low photon count. A low count rate would allow for longer measurement time which would increase the statistical validity of the FCS experiments [242]. A series of Cy5-gWiz GFP dilutions were prepared and it was determined that the optimal concentration of labeled plasmid was 2 ng/μL to achieve a mean particle number of 1. It was determined that this concentration was independent of the degree of labeling. The only difference was in the amplitude intensity of the signals. The optimal laser power was also experimentally determined by monitoring the brightness of the Cy5-gWiz GFP solution as a function of laser power.

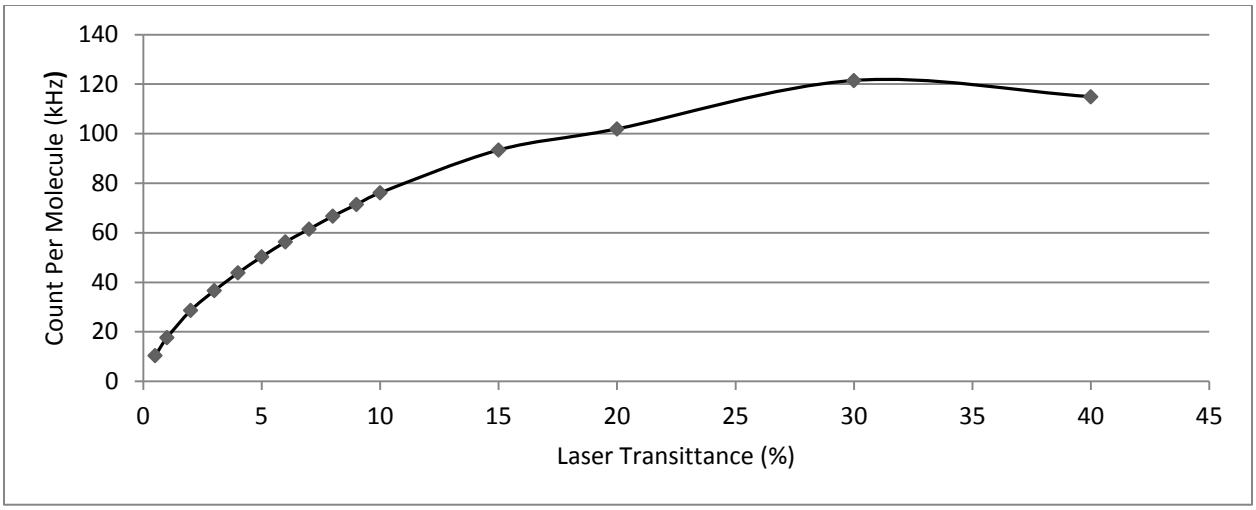

Figure 34: Determination of optimal laser power for Cy5. Count per molecule was recorded for individual sample at several different laser power ranging from 1-40%.

To reduce the possibility of photo-bleaching of the fluorophore and damaging the plasmid, a laser power setting of 5% laser was used for the FCS experiment. It provided a suitable number of photons or brightness for the calculation of ACF. Initial studies with 12-3-12 GPL also demonstrated the issue of intensity spikes (Figure 21A).Due to lower the intensity of measurement in GP and GPL complex, this resulted in the choice of 0.25:1 labeling ratio as the standard for experiment. A 0.05:1 batch was also prepared which had much lower intensity, but could not be re-produced in sufficient quantities for all the FCS experiments. Therefore to minimize variation in labeling densities, a larger batch of 0.25:1 labeling ratio plasmid, (referred to as Cy5-gWiz GFP) was prepared and used for the gemini NP FCS experiments.

6.2 Evaluation of FCS as method for characterization of gemini NPs

This section will talk about the applications of FCS as a tool to characterize gemini NP and discuss the advantages and limitations. In addition this section will compare techniques currently used within our group.

6.2.1 Monitoring assembly of gemini NP with FCS

One of the important prerequisites for a non-viral delivery system is the protection of the nucleic acid cargo through the process of encapsulation by the delivery system's soft material during assembly of the NP. To gain a better understanding of this process FCS was used to monitor the labeled plasmid during formation of the gemini NP. The initial study was performed using the 12-3-12 gemini surfactant and DD 1:3 phospholipid. The 12-3-12 based gemini NP was also selected as the first due it central role in screening of the remaining gemini surfactants, that will be discussed later.

The initial study with 12-3-12 demonstrated that formation of GPs and GPLs could be monitored by FCS. This was demonstrated by the significant right-shift of ACF for Cy5-gWiz GFP upon addition of the gemini surfactant (GP; Figure 15) and phospholipid (GPL; Figure 20). Furthermore, the FCS study was able to detect that two assemblies had distinct features based on the shape of ACF. Figure 15 suggested that the GP was composed of large and heterogeneous particles, as shown by the right-shift of the ACF, upon the addition of 12-3-12 to the free Cy5-gWiz GFP. This indicated a slower diffusion coefficient and a larger standard deviation compared to free labeled plasmid ($D_{12\text{-}3\text{-}12GP}$ = 0.98±31.66% x 10^{-12} m^2/s, $D_{Cy5\text{-}gWiz\ GFP}$ = 4.2±4% x 10^{-12} m^2/s). The second step involved the addition of phospholipid to the GP to form the GPLs (Table 10). The characteristic features of the GPLs were formation of smaller and more uniform NPs, which were relative to the previous GP. This was supported by the left-shift of the ACF which indicated a faster diffusion coefficient and lower standard deviation relative to GP ($D_{12\text{-}3\text{-}12GPL}$ = 3.11±13.18% x 10^{-12} m^2/s). This demonstrates that FCS has the ability to differentiate between the three phases of assembly of gemini NP based on changes to the mobility of labeled plasmid, as summarized in Figure 20. The next phase of the study was to determine if compositional changes to gemini NPs could be monitored using FCS.

6.2.2 Effect of GP composition on FCS measurements

The gemini surfactants in this study were selected to systematically evaluate three key modifications: spacer (12-s-12; s=3,6,7,10 and 16), tail (m-3-m; m=12,16 and 18) and addition of functional group (Py-3-12 and 12-7NH-12), based on studies performed previously by our group [195, 196, 226]. Overall, the majority of GP studied by FCS suggested a heterogeneous distribution of large particles (average of 324±132 nm) across all the gemini surfactants tested. FCS was able to monitor changes to ACF of the Cy5-gWiz GFP based on specific structural modifications to gemini surfactant (Figure 17). It was seen that with changes in the spacer length resulted in a non-linear shift in the diffusion coefficient of GPs. The diffusion coefficient for GP was highest at s=10 (4.15×10^{-12} m^2/s) and decreased as spacer got shorter or longer (Table 8). Similarly, increasing tail length also resulted in an increase in diffusion coefficient when comparing 12-3-12 to 16-3-16 (0.98 vs 1.91×10^{-12} m^2/s, respectively. This trend could not be extended onto 18-3-18 due to issue with aggregation caused by very low cmc, as discussed in section 0 [229]. The most significant change was observed with the introduction of functional groups. Both Py-3-12 and 12-7NH-12 formed smaller GPs compared to their parent gemini surfactant (12-3-12 and 12-7-12, respectively; Table 8).

6.2.3 Validation of GP measurements made with FCS

One of the interesting applications of the mobility values obtained from FCS was the ability to estimate particle sizes based on the Stokes-Einstein equation (Table 9). To validate the findings from the FCS study, in parallel, the samples were also analyzed using DLS. Figure 35 shows that although the general trends based on the structural activity relationship of gemini surfactant were observed using both techniques, there were some differences.

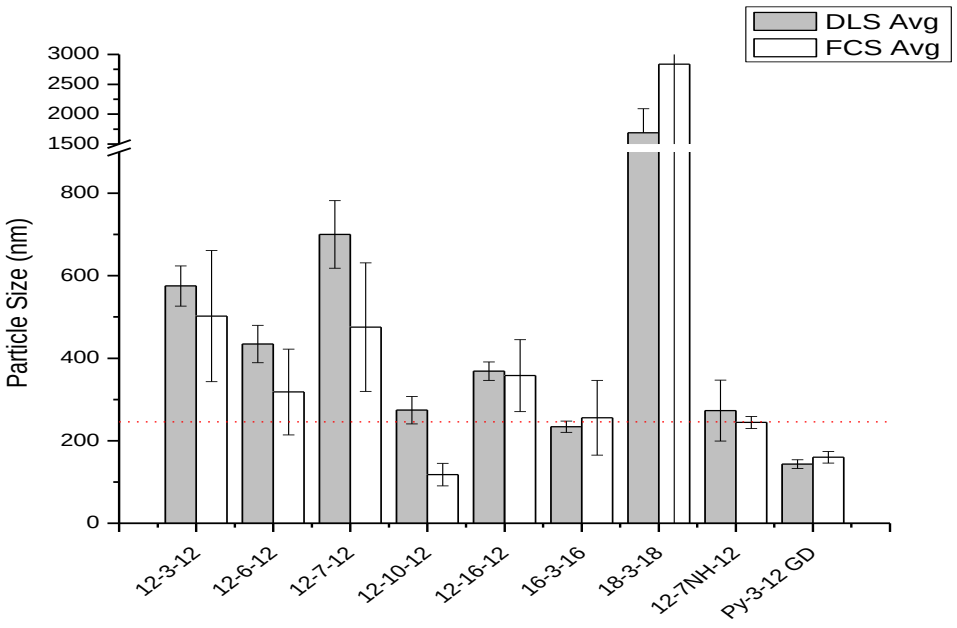

Figure 35: Comparison of particle size of GPs prepared with several gemini surfactants determined by DLS and FCS. DLS (grey) and FCS measurement (white) were performed on the same samples (n=4). Dotted red line indicates the beam width of focal volume (250 nm).

Overall the FCS and DLS provide similar estimates of particle size. FCS is particularly sensitive to the presence of particles greater than 300 nm and aggregates which is reflected in the significant increase in the standard deviation when compared to DLS. This trend was observed with 12-s-12 gemini GP (s=3,6 and 7) where the GP were greater than 400 nm. One reason for this large deviation was believed to be the suitability of FCS technique to measure larger NPs such as the GPs.

The original design of FCS was to monitor fast moving events at a single molecular level (at pico-microsecond range). To achieve this level of detection, a confocal light path is utilized to limit the focal volume. With a beam width calculated to be approximately 250 nm and GP sizes being greater than 250 nm, this caused monitoring difficulties using FCS. This was observed for larger particles where the deviation was larger, versus particles closer or below the 250 nm size-range had smaller deviations (502±159 nm vs. 256±90 nm for 12-3-12 and 16-3-16, respectively). Although the focal volume was a major factor in the quality of the measurement, this does not explain the variability of all the GPs. For example, 12-7NH-12 GP which is similar in size to 16-3-16, had a significant difference in their standard deviation (244±15 nm and 256±90 nm, respectively).

To understand this, the population distribution of molecules that make up the GP sample must be observed. It has been known that many self-assembling structures are not mono-distributed, or uniform in size [243-247]. This distribution can be demonstrated by DLS measurements where various sub-populations make up GP (see Appendix 9.3). These larger particles or aggregates are most likely composed of a large proportion of plasmid DNA, which resulted in a higher concentration of fluorophores (Figure 16). Due to technical limitations, these high intensity measurements could not be recorded due to the saturation of the APD detector. A saturation of the APD detector caused an automatic trigger of a safety shutdown on the APD. In addition, the larger peaks could not physically be measured by the FCS. This caused a reporting bias where the results that were shown were based on runs devoid of larger aggregates, and may have resulted in an under-estimation of the particle size. While biophysical values can still be extrapolated from the GP, these approximations should be interpreted with caution. Although this limits the quantitative analysis of the GP using traditional FCS, it does highlight a key feature of the assembly process of the gemini NPs.

During FCS analysis, there was varying degrees of difficulty in measuring each GP. Gemini surfactant 12-10-12, 16-3-16, 12-7NH-12 and Py-3-12 demonstrated smaller diffusion coefficients compare to other GPs, indicated by the left shifts in their ACF. In addition to the increased mobility, the reproducibility of these curves were higher, as demonstrated by smaller standard deviations compared to other GPs (Table 8). In Figure 19, 12-7NH-12 and Py-3-12, also had ACF that were different from the typical shape shown in Figure 15. These ACFs were unique due to their resemblance to the ACF of GPLs. This suggests that these gemini surfactants were more effective at condensing the plasmid, relative to the other gemini surfactants. This finding was also supported by a previous *in vitro* study that showed that GPs prepared with 12-7NH-12 were able to transfect cells due to increase stability of the complex [196].

Additional studies have also been performed to validate the FCS findings on GP systems. In Figure 30 the surface charge of all GPs were between 0 and +20 mV which suggests that the gemini surfactants were effective at neutralizing the DNA (-63 mV), but were unable to form stable complexes greater than +30 mV. This data supports the theory shows that the slow diffusion coefficients were caused by aggregates. It was observed that the surface charges changed based on the structure of the gemini surfactants. Both increased spacer and tail length resulted in faster diffusion coefficients and increased positive surface charges. This suggests that the increasing stability of the GP aids in reducing the degree of aggregation. In the case of 12-7NH-12 the zeta potential was lower than +20 mV, however it still had a relatively fast diffusion coefficients, whereas Py-3-12 which had the highest zeta potential for GP had a similar diffusion coefficient to 12-7NH-12 which had the lowest zeta potential. Overall, in both cases the

functionalized GP (Py-3-12 and 12-7NH-12) were faster than their non-functionalized parent GP (12-3-12 and 12-7-12). Furthermore, this suggests that other forces, other than surface charge, must also influence the stability of the NPs.

Furthermore, the presence of aggregates also explains the high intensity peaks observed in the raw intensity data (Figure 16). Since neutralization of phosphate backbone is known to result in condensation of DNA, this supports the theory that faster diffusion coefficients are in fact due to condensation of the labeled plasmid. This also supported by the dye exclusion data that show that the addition of gemini surfactants to the plasmid effective neutralizes the ability of both EtBr and PicoGreen to bind to DNA due to structural changes in the topology of the plasmid (going from free-plasmid to condensed plasmid).

6.2.4 Effect of GPL composition evaluated by FCS

Unlike the GPs that varied widely based on the chemical structure of gemini surfactant, the addition of phospholipids generated smaller NPs. These smaller NPs are more uniform and not as dependent on NP composition (either gemini or phospholipid component). This normalization of the NP is seen in ACF for all GPLs (Figure 22) when compared to ACF for GPs (Figure 17). This idea is supported by diffusion coefficients of GPL which span over a narrower range of 3-4 x 10^{-12} m^2/s compared to GP (0.98-4 x 10^{-12} m^2/s). Furthermore, standard deviation of each GPLs decreased significantly compared to GPs (±20-30% for GPs and ±10-17% for GPLs) that support formation of uniform NP.

A second phospholipid (DOPE) was screened to further investigate the role of the phospholipid on GPL morphology. Similar to the GPLs prepared with DD 1:3, the DOPE GPLs also resulted in the dispersion of the GP into a smaller more uniform particle, averaging 149±28 nm; 145±34 nm for DOPE and DD1:3 GPLs. The FCS measurements suggested that the type of phospholipid was not significant in governing the morphology of GPLs. The trends observed with GP were also seen with both GPL, but to a lesser degree. Also, recall that in Section 6.2.2, the FCS measurements suggested that certain GPs (e.g. 12-7NH-12 and Py-3-12) were capable of forming stable "GPL-like" complexes without the assistance of phospholipids. The addition of phospholipids in this case only resulted in a small decrease in particle size. Overall, this suggests that interactions between gemini and DNA formed during GP stages are still present during GPL stage.

6.2.5 Validation GPL measurements made with FCS

In terms of particle size, FCS reported an average of approximately 120-150 nm for the majority of GPLs screened in this study. To validate these findings, DLS was performed in parallel to verify GPL sizes reported by FCS.

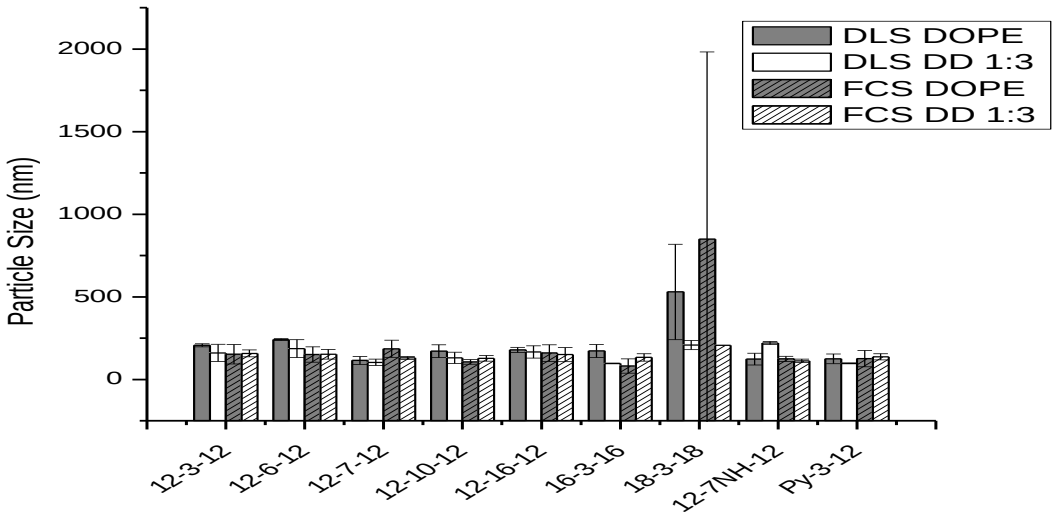

Figure 36: Comparison of particle size of various GPL determined by DLS and FCS. Values expressed as mean±SD (n=4).

Both DLS and FCS reported similar particle sizes for all GPLs which ranged between 100-200 nm (Figure 36). The surface charge of the majority of the GPLs was shown to be greater than +30 mV which is empirically accepted as the formation of stable particles in solution [231]. This finding supports the theory that an increase in diffusion coefficient from GP to GPL is in fact due to the formation of stable NP. This stabilizing effect of the phospholipid on GP is also supported by the dye exclusion data. The formation of GPL also strongly excludes both EtBr and PicoGreen® for most GPLs but the degree is slightly less than the corresponding GP. A possible explanation is due to the phenomena of self-quenching. This occurs when a high local concentration of fluorophores results in energy transfer between closely packed fluorophores resulting in a decrease in observed fluorescence. Therefore it is believe that in the GP, where many plasmids, and therefore fluorophores, are packed in close proximity, this phenomenon could occur. Once the phospholipid disperses the GP into smaller GPL this reduces the degree of self-quenching since few plasmids are in close proximity and result in an observed increase in

fluorescence. This supported the finding from the FCS data that also show the drop in intensity of the Cy5-gWiz GFP peak when transitioning from GP to GPL. Also this phenomena has been reported in the literature with other NPs loaded with fluorophores [248].

6.2.6 Effects of compositional changes on gemini assembly

The FCS study suggests that modifications to the basic structure (m-s-m) increase in the hydrophobicity of the of the gemini surfactants results in smaller and more stable GPs. A longer tail length would affect the overall hydrophobic nature of the gemini surfactant. Although the spacer are traditionally associated with the polar region of the amphiphilic molecule, spacer length have also been previous shown to cause changes to the hydrophobicity. Literature has suggested that beyond a critical spacer length, the alkyl chain can fold, therefore incorporated into the hydrophobic region [249]. Shorter spacers (s=3-8) on the other hand have lack the flexibility and therefore cannot integrate into the hydrophobic region [250]. This mechanism explains the smaller GP and in turn GPL formed from s=3-10. However, this does not explain why the 12-16-12, which has a longer spacer, produces smaller GP compared to 12-10-12. One theory is due to the packing arrangement between gemini surfactant and DNA. A previous study by our group had shown that head group area (a^a), the distance between cationic head groups of the gemini surfactant, has an effect on the binding properties of the gemini surfactant with DNA (Table 15).

Table 15 Head group area of various gemini compounds. Modified from Badea et al, 2005 [195]. 12-8-12 is used to approximate 12-7-12 since data was not available. a^a = Head group area

Gemini Compound	***(a^a) [nm^2/molecule]***
12-3-12	0.98
12-6-12	1.40
12-8-12	1.78
12-10-12	2.16
12-16-12	1.44

The increase in diffusion coefficient of the final GP can be correlated to an increase in the head group areas. This is unexpected because as the head group areas increases, one would believe based on sterics, that the overall number of molecules that can come in contact with the DNA would decrease. A theory as

to why diffusion coefficient increases with fewer gemini surfactants is related back to the issue of gemini concentration. It was reported that an excess of cationic surfactants can results in aggregation and results in larger NPs as measured by FCS [229]. This parameter was shown to be important in governing the interaction between DNA and gemini surfactant. A study by Chen and colleagues have also demonstrated that surface properties, such as molecular area of GP is not linear and reaches a maximum around s=6, with longer spacer assuming a new conformation [251]. This further suggests that the interaction between DNA and gemini changes upon the spacer folding. This theory of a new confirmation is supported by surface charge data. Figure 30 shows that 12-10-12 has the highest zeta potential ($\delta_{12\text{-}10\text{-}12}$=+18.7 mV) compared to other gemini compounds. This higher surface charge would result in higher repulsion and therefore more stable particle that would resist aggregation and explain the smaller size. 12-3-12 on the other hand had a smallest a^a and very low surface charge ($a^a_{12\text{-}3\text{-}12}$=0.98 and $\delta_{12\text{-}3\text{-}12}$=+0.09 mV) which would suggest weak force between particles. This could promote aggregation and result in the larger GP particles and therefore smaller diffusion coefficient. While no data exist to our knowledge of the tail length and functionalization, the initial finding suggests that the compaction of DNA, which was believed to be a simple neutralization, is based on electrostatic interactions and stoichiometry. This suggests that interaction between gemini and DNA is complex and that multiple factors come into play to govern the final shape of the final particle.

One such factor that was studied previously is the critical micellar concentration (cmc). Cmc for gemini surfactants were established previously within our research group (

Table 16).

Table 16 Critical micellar concentration for various gemini surfactants

Gemini surfactant	***cmc (mM)***
12-s-12	
12-3-12	0.98
12-6-12	1.08
12-7-12	0.85
12-10-12	0.62
12-16-12	0.12
m-3-m	
16-3-16	0.03
18-3-18	0.013
m-NH-m	
12-7NH-12	1.29
Pyrenyl	
Py-3-12	0.22

Key observations from this study are that the relationship between alkyl length and cmc is not linear. This is evident with spacers as an increase does not result in large change until longer spacers are achieved.

Table 16 also shows that the location of the modification is also essential. By comparing 12-7-12 and 16-3-16, both had an addition of 4C but have different cmc. This demonstrated that similar increase in alkyl chain length to the tail region results in greater shifts to the cmc values. This occurs because it is known that modification to the tail regions, which affects the hydrophobic region or the surfactant, has more dramatic effect on packing arrangement of the micelle. This also explains why gemini surfactants with long spacer (10 and 16C) also have significant changes.

While basic structure is one factor that governs gemini surfactant interaction with DNA, other factors can also influence the self-assembly process. This was observed with significant shifts in diffusion coefficient that occurred with functionalized gemini surfactants. While their cmc is lower than their counter parts, compared to their parent gemini surfactants (12-3-12 and 12-7-12) both Py-3-12 and 12-7NH-12 showed significant increase its diffusion coefficient 2.00 and 3.06 x 10^{-12} m^2/s respectively). This

demonstrates that several different forces are at work that can all be utilized to govern NP formation. It is this versatility of chemical modifications of gemini surfactants provide many opportunities to fine-tune their activity and possibly the properties of the resulting NPs.

6.2.7 Evaluation of particle size determined by FCS

FCS was originally designed to study the dynamics of small molecules at a single molecule scale which is primarily determined by the dimension of the focal volume. Although the NPs are indeed small, in the realm of single molecule detection the NPs are relatively large. This issue of size measurement was seen in the study of the GPs which exceed the focal volume and severely limits the analytical validity of the FCS measurement for particles exceeding the pre-determined focal volume. The size of the NP complicates the FCS analysis in two ways. First these NPs, especially the GP, move relatively slowly (in the micro-millisecond range) and therefore longer measurements times are required to acquire sufficient data to generate an ACF. Beyond the physical limit of the focal volumes, the condensed labeled DNA poses another issue. The condensation of a plasmid increases the local concentration of fluorophores and significantly increases the brightness of each individual particle under study. This increases the molecular brightness and runs the risk of overwhelming the detector that affects validity of the ACF. This issue becomes even more significant if multiple plasmids are condensed which further increase the molecular brightness. This is highlighted in Table 8 by the large standard deviations seen with a majority of the GP studied due to the presence of large spikes. These issues are most evident while studying GP but are also present in to a degree with GPLs.

To overcome these issues, different set-up to FCS were considered and evaluated. One common modification is to change the dimension of the focal volume. This set-up is generally based on system being measured. For instance, small molecules (single fluorophores and intramolecular dynamics) require smaller pinholes to maximize the resolution of the FCS technique. The focal volume can be enlarged to track larger or slowly moving complexes at the cost of resolution. The reduction in resolution is due to the increased number of particles passing through the focal volume which reduces the significance of each individual fluctuations used to calculate the ACF [242]. Therefore to account for the larger GPs, the use of a larger pinhole (500 nm, compared to 250 nm) was evaluated. The experiments showed that although the number of fluctuations did increase, it also increased the difficulty in making a measurement. This is because with a larger focal volume, more fluorophores could be monitored for longer periods of time that aids in collecting fluorescent fluctuation for the calculation of ACF. But since the brightness of each individual GP was very high, the increase in number of molecules resulted in the saturation of the detector

and the canceling of the measurement. Since laser power was already optimized to minimize damage to labeled DNA this option could not be used to help with saturation issues. Therefore due to these technical limitations, using a larger pinhole to monitor the GP was not feasible. Although no strict upper limit has been reported in the literature, similar issues have been reported by other groups which have demonstrated that FCS is not well suited for the analytical evaluation of self-assembled complexes larger than 500 nm [228, 252]. Therefore to be able to extract meaningful values such as diffusion coefficient and size, from the FCS one need to study the data carefully in order to validate it. This provides a significant learning curve when developing new FCS methodology as a lot of firsthand experience is needed to understand each system. Another complication with the interpretation of FCS data is based on the way particle size is determined.

To be able to extract meaningful data, particle size data from FCS the limitations of the Stokes-Einstein equation must also be considered. A careful examination of the formula shows that particle size is calculated assuming the particles are spherical. Since non-viral delivery systems can assume a variety of shapes using the Stokes-Einstein equation without knowing the physical morphology of the particles being evaluated this model could be too simple and any measure of diameter of the particles could be erroneous. While other groups have addressed other shapes by using modified equations, a researcher still needs to know the physical morphology in order to apply the appropriate corrections. Generally, a direct method of visualizing the NP is required to confirm the actual morphology being studied prior to evaluation of sizing using FCS. For the GPLs, previous studies in our research group have also utilized both TEM and AFM to study gemini NP. A TEM images shown in Figure 37 revealed that GPLs prepared from 12-3-12 and 12-7NH-12 are in fact spherical and the particle size are consistent with the findings in this study by FCS and DLS.

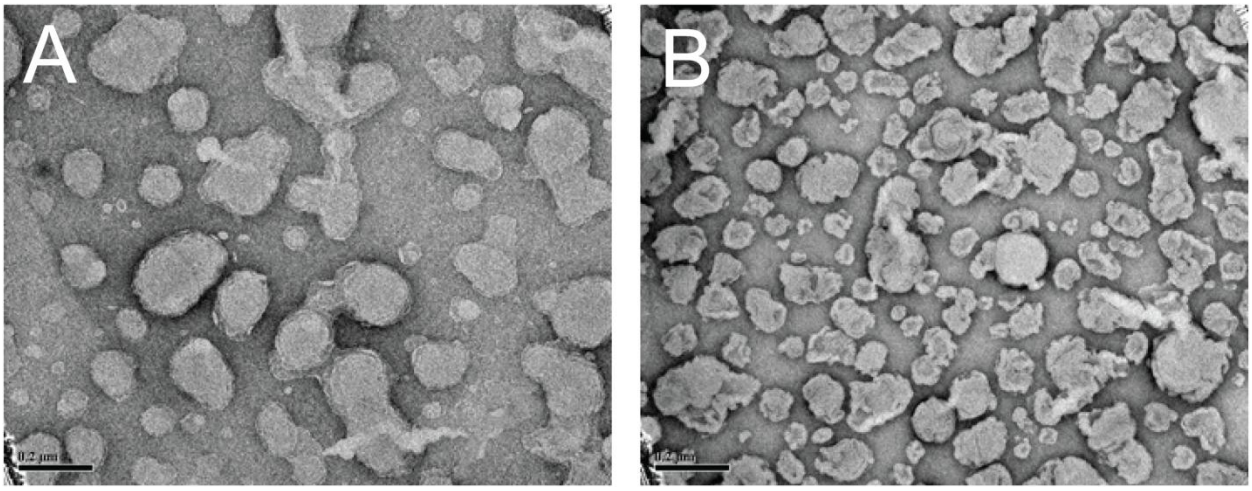

Figure 37: Transmission electron microscopy (TEM) by negative staining of the structural morphology of 12-3-12 A) and 12-7NH-12. B) GPL prepared at N/P 10:1 with DOPE. Scale bar corresponds to 200 nm. Images were taken by a JEOL 2010F TEM at the Canadian Centre for Electron Microscopy at McMaster University (Ontario, Canada) by M. Foldvari.

Additional studies by AFM confirmed the morphology of other GPLs. A study performed on 16-3-16 GPL also confirms the morphology of 16-3-16 GPL to be spherical NP. Furthermore this particle size approximated by AFM (100-200nm) also supports the values from the FCS and DLS study [195].

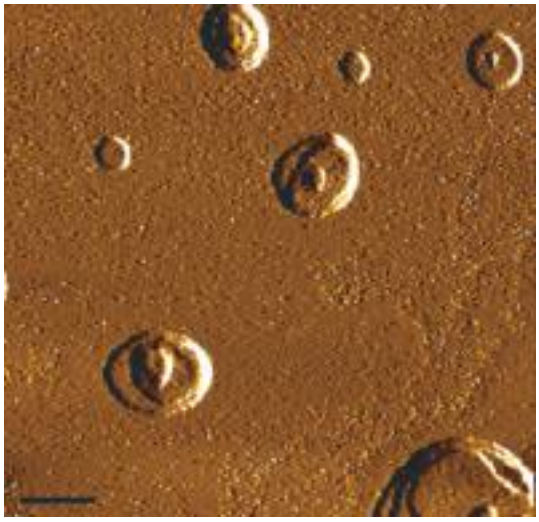

Figure 38: Atomic force microscopy (AFM) image of 16-3-16 GPL prepared at N/P 10:1 with DOPE. Bar represents 200 nm. Image reproduced from Badea et al, 2005 [195].

Both the TEM and AFM study show a small window into the polydispersity that is observed with spontaneously self-assembling structures. As seen in both the FCS and DLS study the presence of a small population of large aggregates that could skew the average upwards. Overall, the GPL monitored by DLS

were rigorously tested to ensure the maximum uniformity with a major population being over 98% with aggregates forming less than 2%. Therefore, the effect of these large particles was minimal and can be overlooked. This verification of FCS as particle sizing tool highlight that no one technique was free of artifacts and that each one had to be understood and evaluated carefully to ensure the results reported where correct [253]. Therefore it is recommended that multiple techniques be used.

To conclude this section we will also evaluate the FCS as particle sizing technique against the current standard DLS. Both FCS and DLS are based around the extrapolation of the particle size based on diffusion coefficients obtain from an ACF. The key difference between FCS and DLS is the values used to construct the ACF (fluorescence fluctuations vs light scattering and the sensitivity of the detectors). Overall both are biased by the presence of large aggregates which generates stronger signals (both fluorescence and light scattering) that can mask smaller signals. This demonstrates the limitation of these measurement values which are intensity-weighted [254]. Therefore the artifacts experienced by FCS also need to be considered when analyzing DLS data. While both techniques are best suited for studying small mono-dispersed systems, their size range do vary. Traditionally FCS is focused on smaller molecule interactions or even intramolecular changes, while DLS is better suited for the study of larger NPs in the range of 10-1000 nm. Technical requirements are also quite different from between the DLS and FCS platforms. Currently DLS instrumentation is easy to use and automated, able to quickly calculate ACF and extrapolate values with minimal user input. FCS on the other hand requires careful calibrations and for size measurements are not automated and require custom software or exported FCS data into other programs to calculate size. This makes for a steeper learning curve as hinted earlier in this section. While DLS is still a benchmark for the routine size analysis, FCS does have specific advantages. One of the advantages of FCS over DLS is small sample size. Since the focal volume of FCS extremely small (~1 fL), technically any size sample could be used as long as there is an appropriate cover slip to control factors such as evaporation. In the literature and discussion with other groups indicated that FCS can be routinely performed with as small as 10-20µL of sample or less [255, 256]. In the early phase of drug development, this is critical as the raw materials may not be in excess (e.g. synthesis of a new gemini surfactant). Although there are many technical parameters that need to be accounted for during FCS set-up, the actual acquisition time for each measurement is very fast [253]. Furthermore these parameters can be saved to aid easy subsequent set-up. Along with automation and fast measurement time makes ideal for high-throughput screening. A unique advantage of FCS has over DLS is the ability to simultaneously size and monitor compaction of plasmid. Other techniques such as DLS can also provide particle size of the GPL, it cannot conclusive confirm if nucleic acid is actually present in the various complexes. To deduce the compaction of nucleic acids, a secondary measurement, such as zeta potential, is necessary to

monitor the charge shift of the nucleic acids and dye exclusion study or centrifugation method is needed to confirm the encapsulation of the nucleic acid within the NP. This is useful for future solution studies to monitor the assembly and disassembly properties of GPL systems.

6.2.8 Additional characterization of gemini NP by FCS

While particle sizing by FCS may not be as practical compared to other routinely used techniques such as DLS, FCS provides other unique advantages. This section will discuss these unique advantages and their applications towards characterizing gemini NPs.

6.2.8.1 Monitoring the structural state of gemini NPs

Most traditional particle size techniques lack is the ability to monitor the structural state of NPs. By measuring the zeta potential of NPs at various stages the self assembly process can be determined. By correlating the surface charge with the ACF of the corresponding GPL and GP, one can indirectly monitor the state of the NP. This a powerful tool since FCS can monitor changes in real-time and under various environmental conditions. For example, changes in the environment such as pH, ionic strength and presence of additives can be recorded as a series of ACF and the changes to the NP structural state can be mapped.

6.2.8.2 Estimation of the number plasmids inside gemini NPs: Intensity histogram analysis

In addition to monitoring the conformation of labeled plasmids, other factors can be determined by having a deeper look at the raw data. FCS photons are collected and the fluorescent fluctuations are analyzed in a time-dependent manner to extract values such as the diffusion coefficient. This allows one to distinguish between different species of particles based on their mobility and is the basis of the spectral fingerprinting established for free plasmid, GPs and GPLs. These same photons also carry a specific intensity or molecular brightness that is also recorded but is ignored in FCS-based analysis as shown in Figure 10. As shifts in the mobility of the molecules can be utilized to characterize molecules with FCS, changes in the intensity of the peaks or molecular brightness can also be used to extract other characteristics of the molecules. In the context of studying assembly of gemini NPs, these shifts in intensity are used to approximate the distribution of plasmid at each stage of gemini NP assembly. By evaluating the intensity histograms of the free plasmid, GP and GPL and comparing the changes that occur one can gain insight into the distribution of the plasmid within the NP. Figure 10A shows the raw photon stream from APD for free Cy5-gWiz GFP. This plot shows that although the peaks fluctuate randomly, they are equilibrated around average value, or baseline at approximately 250 kHz. Some of the

fluorescent fluctuations are more intense that the others and this is due to the uneven labeling of plasmid. This artifact resulted in small spikes in intensity, but was shown not to affect analysis since the ACF could be calculated and fitted. To gain a better understanding of the distribution of intensity peaks, the data were re-plotted in the form of a histogram. The majority of the peaks have an intensity of approximately 250 kHz (Figure 10B), which correlates with observed baseline in Figure 10A. Since the concentration of free Cy5-gWiz GFP was determine to be approximately 1, this suggests that on average most plasmids passing through the focal volume have an intensity of approximately 250 kHz. The intensity histogram also has a specific shape that can reveal other characteristics of the molecules. The Cy5-gWiz GFP generally has a bell-shaped distribution with a significantly long tail on the right-side of the maxima. This suggests that brighter molecules also exist within the population of plasmids. One source of these high intensity peaks are due to the presence of uneven labeling as described earlier. Another reason could due to the morphology of the plasmid. Since the SC form of the plasmid is a tightly wound coil, it is possible that labeled regions can overlap and therefore increase the number of fluorophores in the focal volume. Although these peaks are significantly larger than average, these events were rare and had little impact on the calculation of the ACF. Since all the samples in the FCS study contained the same amount of Cy5-gWiz GFP any changes in the characteristics of the intensity histogram profile can be related to the addition of the gemini surfactant and neutral phospholipids.

The GPs were described as large particles based on the aggregation of plasmid and gemini surfactant during the initial neutralization (see the intensity histogram in Figure 16A), furthermore these aggregates are composed of a large number of plasmids. Evidence of multi-plasmids complex is seen in Figure 16A which shows a significant upward shifts in the intensity histogram profile of the Cy5-gWiz GFP upon the addition of gemini surfactant. The intensity histogram (Figure 16B) reveals a very long tail to the right and shows a major increase in the brightness of the GP (from 5000 kHz for free Cy5-gWiz GFP to well over 10,000 kHz for GP). Since the focal volume is restricted, it must indicate that these labeled plasmids must in fact be concentrated with in very close proximity (<250 nm) to cause these large spikes in intensity. Since previously it was established that each plasmid has an average brightness of 250 kHz, the large peaks seen in Figure 16A suggest that larger peaks with intensities of 10,000 kHz, must contain over 40 plasmids. The intensity study also reveals that the addition of the gemini surfactants effectively encapsulates all the plasmids in solution. This is supported by data in Figure 16B that shows a loss of the previous maxima (250 kHz for Cy5-gWiz GFP) and a left-shift of the maxima to between 0-50 kHz that was previously determined to be background (Section 5.1.2). This indicates there are long intervals with no fluorophores (plasmids) in the focal volume. This supports the idea of a multi-plasmid assembly within the GP since this would result in the depletion in free plasmid in solution. Not only do

GP contain multi-plasmids, but they are very few in number. This shown in Figure 16A as significant decrease in the number of fluorescence fluctuations. These finding support the theory that addition of the gemini surfactant results in aggregation of the multiple plasmids to form the GPs. While the majority of the peaks are quite large, a small sub-fraction of peaks is still evident between 100-300 kHz. The source of these fluorescent fluctuations could due the presence of smaller GP that formed. Another possibility is that these are the large particle that did not pass directly over the focal volume resulting in a lower florescence burst. While it may be possible these peaks represent some free plasmids in solution due to the excess gemini surfactant added it is unlikely that this is the case. Furthermore the zeta potential data shows that in all GP charge is at least neutral (close to 0 mV to +20 mV) that does not suggest the presence of negatively charged free DNA.

The addition of phospholipids results in the formation of GPL that have fewer plasmids then the GP particles (Figure 21). As the focal volume is limited, this relative decrease in intensity suggests that GPL particle have fewer plasmids then GP. The GPL not only contain fewer plasmids, but are also more numerous compared to GP. This is seen as the increase in the number of peaks (Figure 21A). While the peaks are smaller and more numerous than the GPs some larger peaks still existed around 5000-15,000 kHz. Whether these larger peaks are based on the presence of GPL aggregates or the remainder of GP cannot be verified during this study. This is because the fluorescence represents one species (plasmid) and we cannot comment on the present or absence gemini and lipid in the focal volume.

This insight into the quantity of plasmids in NPs is unique to FCS. For instance, although DLS can reveal the overall size of the NPs like FCS, while assumed, it cannot say for certain that the NP in fact contains DNA. This can only be confirmed by performing a second experiment to monitor the state of the DNA. These experiments could include zeta potential or dye exclusion assays to monitor changes in the state of the nucleic acid based on the presence of the gemini NP components but cannot quantify the amount of plasmid that exist within each complex.

While this initial study allowed us to understand that distribution of plasmid changes throughout the assembly process we cannot analytically quantify the exact amount. This is because in both GP and GPL the polydispersity makes it difficult to categorize each peaks. Therefore without a proper software or algorithm to quantitatively analyze, it is difficult count the exact number of plasmids to see if there are subtle differences between different GP and GPL populations. Furthermore factors such as the uneven labeling of plasmid makes it difficult to precisely quantify the exact number of plasmid within a complex. Although at this stage of the study quantification is not possible, the initial data has already provided

insight into the distribution of plasmids throughout gemini NP assembly. This study is unique compared to other characterization methods since it not only demonstrated the heterogeneity of the external structure but also hinted at differences at the internal structure of the NPs.

6.2.8.3 Current model of gemini NP assembly

To conclude the discussion, a model of the assembly on gemini NP is proposed based on the findings from this study and previous data from the literature. Overall the data from the current and previous studies suggest that formation of gemini NP is a two-step process governed by the addition of the gemini surfactant and the phospholipids. The formation of GP is based on the compaction of the plasmid due to the addition of gemini surfactants to form large particles of approximately 300-500 nm. The FCS and DLS study confirms the GP consists of a collection of large particles/ aggregates whose morphology is governed by the structure of the gemini surfactant. In addition, the lower stability is supported by zeta potential studies that shows that most GPs have a surface charge less +30 mV. In addition, new data from the intensity histograms (Section 6.2.8.2) provides evidence that the initial encapsulation by gemini surfactants is not a simple compaction of a single plasmid, but a collection of multiple plasmids to form larger GP complexes. Based on the new data, it is shown that the aggregates can vary widely and can contain upwards of 20-40 plasmids per complex. Furthermore, due to the low surface charge exhibited by the GP, it would be possible that these finite units of condensed plasmid could collapse to form aggregates or what would appear to be larger particles. The presence of peaks with various intensities suggests the presence of different number of gemini-plasmid units within the larger final GP. While the exact morphology of the GP stage is hard to quantify, a theory is proposed based on existing data. Previous studies have highlighted that gemini/DNA interaction could form "ball-on-a-string" structures [257]. Therefore it could be possible upon addition of gemini surfactants to plasmids, that a fixed number of plasmids could be condensed into finite units with excess gemini surfactant forming micelles. The presence of excess or unbound gemini surfactants could be one explanation of the increased cytotoxicity of GPs compared to GPLs (see appendix 0). This is also supported by other studies have shown that gemini surfactants alone are cytotoxic [186, 189]. The morphology of these units can be determined by the chemical structure of the gemini surfactant. With the 12-s-12 gemini surfactants, the study was shown that the zeta potential and cmc increase with spacer length. At low spacer lengths (s=3-7), the cmc is lower which can promotes the formation of free micelles in solution. This reduces the number of gemini surfactants that can condense the plasmid, resulting in initial gemini-plasmid complexes with lower zeta potential. This results in the smaller gemini-plasmid units aggregating to form the larger GPs that are observed in our study. This can be extended to the 12-7NH-12 which has the

highest cmc of the gemini surfactants screened and also has a higher zeta potential. This could be one factor in the ability of 12-7NH-12 to form smaller and more stable GPs. Although the GPs are more stable, the higher cmc could result in the formation of free monomers of gemini surfactant. This could explain why it stable GPs are as cytotoxic as other GPs. Although the cmc can play a role in governing the morphology of the GPs, other forces are also at work. As the spacer length increases (s=10 and 16) the cmc also increases significantly. This not only allows for more gemini surfactants to be involved in the compaction process resulting in higher zeta potential, the additional hydrophobic interaction, due to the folding spacer, could also aid in the additional stabilization of the gemini-plasmid interaction. Therefore these initial gemini-plasmids units are less prone to aggregations as seen with the smaller particle size of their GPs. This trend can also be applied to the Py-3-12. Although its cmc is the lowest of gemini surfactants screened, it has the highest zeta potential and smallest GPs. This could be due to the ability of the pyrene functional group intercalating with DNA providing additional stabilization [258]. This additional interaction could also limit the formation of free gemini surfactant micelles and explain the observed decrease in cytotoxicity with Py-3-12 GPs compared to GPs (refer to appendix 0). Further evidence of this intercalation is the ability of EtBr to penetrate Py-3-12 based gemini NPs. This is could be due to orientation of the pyrene tail into the DNA molecule which could leave small areas exposed that would allow EtBr to enter as well. This supramolecular aggregate model of GP assemble could also aid in the explanation of the formation of GPL.

Previous studies have demonstrated that addition of the phospholipids to GPL results in a decrease in overall size and formation of stable NPs. This finding is supported by FCS and DLS study and it was shown that the type of phospholipids (DOPE or DD 1:3) had no effect on final morphology. The theory of dispersion effect of the phospholipids is also supported by the raw intensity values. Figure 21 show that the addition of phospholipids not only decrease the intensity of each peak, suggesting there are fewer plasmids, it also increases the frequency of the peaks indicating the presence of more particles in solution. Furthermore, the study also shows that different populations of GPL exist and each contains different amount of plasmids as shown by the small and large peaks. This study has also shown that the number of plasmids within the GPL typically ranges between 10-20 plasmids per complex. Although no study to date has shown the dynamics of the transition between GP and GPL, a theory is proposed based on the data. Since it is believed that the GP is composed of a supramolecular aggregate, the phospholipid may interact with excess gemini to disperse the aggregated GP complexes. The theory is supported by another study has reports that gemini surfactants in fact do interact with the liposomes [259]. This suggests that the addition of the phospholipids acts as a sort of molecular scissor, scavenging free-gemini

surfactants and aiding in the formation of GPL. This would allow the condensed plasmids to disperse forming the final GPL (Figure 39).

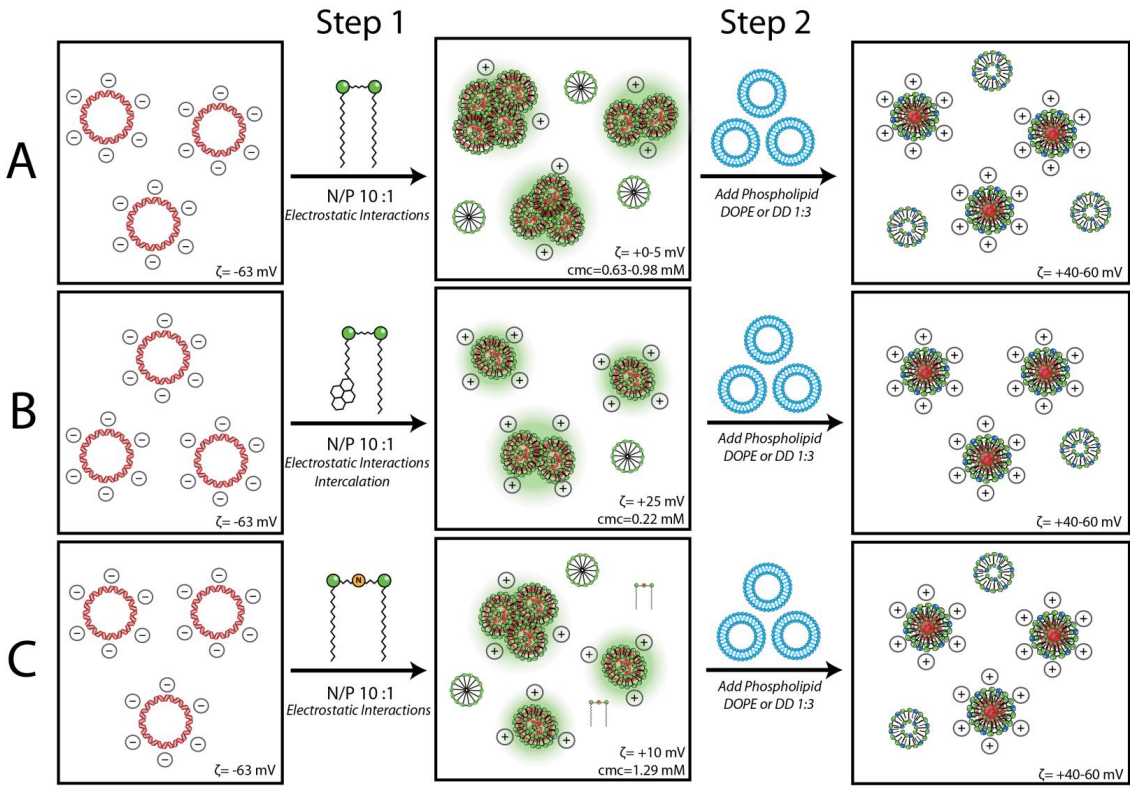

Figure 39: Diagram of the proposed supramolecular aggregate model of gemini NP assembly.

Step 1: Free negatively charged plasmids are initially condensed by the adsorption/binding of cationic gemini surfactant molecules. The initial compaction produces gemini-plasmid units that aggregate due to their lower surface charge and decreased repulsive forces and form the larger supramolecular GPs.

A) In the 12-series of gemini surfactants cmc is relatively high providing sufficient number of monomer surfactants to neutralize the plasmids which results in the decrease in overall charge (low zeta potential values) and aggregation of GPs; gemini surfactants with short spacers especially form GPs with very low zeta potential; for the gemini surfactants with increasing spacer length zeta potential of GPs increases with decreasing cmc and this maybe due to the difference in the interaction with the phosphate groups on the DNA [196]

B) Pyrene gemini surfactants have the lowest cmc but due to possible additional intercalation interactions the resulting GPs are more stable, as shown by smaller particle size and higher zeta potential.

C) The12-7NH-12 gemini surfactant has the highest cmc, with few free micelles and more available monomers to aid in the binding of gemini surfactants to plasmid providing fewer large supramolecular complexes compared to the 12-series of surfactants.

Step 2: The added phospholipids form mixed bilayers and potentially other polymorphic phases (hexagonal and/or cubic [161]) with the gemini surfactants and produce a relatively spherical vesicle-like particles (GPL) with increased overall surface charge which stabilizes the individual GPLs. In addition, some of the phospholipids also form plasmid-free mixed gemini-lipid vesicles.

7.0 Concluding remarks

In this thesis we have described the development and application of a novel method to study gemini NPs using FCS. Monitoring of gemini NP assembly was established using labeled plasmid and optimal conditions for FCS measurement were determined. It was demonstrated that particle size of both the GPs and GPLs could be determined by FCS and was validated by comparing to DLS. In addition to determining particle size, FCS was able to evaluate changes to the plasmid morphology during the various stages based on the mobility in solution. When the FCS raw data was interpreted in an intensity-dependent manner, other values could also be determined such as an approximation of the number of plasmids within GP and GPL complex. By screening various structural changes to both gemini surfactant and lipid gemini NPs it was revealed that FCS was able to reveal even small changes. Overall, FCS provides deeper insight into the mechanism of gemini NP assembly. Based on these finding, a model of gemini NP assembly has been proposed based the formation of GPs composed of "supramolecular aggregates" which are governed by the chemical structure of the excess gemini surfactants followed by dispersion due to the incorporation of the phospholipids to form final GPLs.

8.0 Future directions

This initial study has demonstrated that although FCS is capable of determining the difference between free-DNA, GP and GPL based on shifts in the ACF. Using this existing database, the next phase of the experiments will involve studying the disassembly of NPs in solution. By changing various external factors (e.g. pH, ionic concentration, addition of DNase) shifts in the ACF of GPL can be monitored to see if DNA is released (restoration of free-Cy5-gWiz ACF) or other disassembly phase occurs. Also since the ACF of GPL is established, results can be compared over multiple measurements and over long periods of time to evaluate the stability of various formulations.

One of the technical barriers that need to be overcome to improve the effectiveness of FCS is a more controlled labeling of the targeted molecules. Although this chemical approach (LabelIT kit) was optimized and allows for the simple conjugation of any fluorophore to a plasmid, the labeling was still random allowing for minimal control over the position and degree of labeling. Although it was shown to have little effect on monitoring free plasmids, upon compaction, the higher number of fluorophores resulted in uneven brightness and saturation of the detector that hindered proper ACF analysis. This was particularly evident in the studies with GPs. To overcome this issue, alternatives to the chemical method of fluorophore conjugation must be considered. The field of bio-conjugation chemistry has developed a wide variety of methods to increase the specificity of labeling. Techniques such as triple helix oligonucleotide and sequence-specific methyltransferase-induced labeling (SMILing) have been demonstrated to specifically label plasmid with a variety of labels. Although these methods provide increased specificity they require either the introduction of specific target sequences (triple helix oligonucleotides) or require specialized enzymes and custom labeled nucleotides for SMILing [260] [261]. To further lower the degree of labeling, new dyes are constantly being developed to provide higher quantum yields and offer better brightness for biological applications, for instance the synthesis of new Cy5 that can sequenced into nucleotides [262]. By increasing the specificity of the labeling two objectives can be achieved. The first major step is decreased brightness of the plasmids. This is essential as a majority of the delivery system designs revolves around encapsulation and compaction of DNA which also concentrates the fluorophores. By having more specific reactions one can actually lower the brightness of these molecules so that they can be studied with greater detail by avoiding saturation of the detector. Secondly with a precisely labeled plasmid additional experiments can be performed using FCS. For instance more quantitative studies of particle number or concentration are more accurate since specific concentration can be associated to certain number of fluorophores as shown in previous work by

other groups [237]. Specific regions of the plasmid can also be labeled using specific dye(s) to monitor degradation of DNA (since known cuts of plasmid will have specific diffusion coefficient) or FRET pair can be used to evaluate internal dynamics of compacted plasmids [263-265].

As mentioned in this study, the overall characteristics of gemini NPs is understood better when several techniques are used in tandem to generate a clear image of the vesicles. Although FCS and DLS provide large amounts of particle size data, to gain a deep understanding of the final size, and more importantly shape, additional microscopy images are required. Although previous studies by our group investigated the morphology of a select few GPLs, no in depth screening of various GPL and GP has been performed. Furthermore with the addition of the new phospholipids (DOPE and DD 1:3) showing similar particle sizes additional information could be obtained by studying their morphology using microscopy techniques such as AFM and TEM.

While FCS does provide a new tool in characterization of gemini NP there are limitations. While the changes in the topology of plasmid could be monitored, in multi-component situations such as GPL, one cannot monitor the interactions between the components. Furthermore situations such as the identity of the large peaks in GPL (Figure 21) cannot be determined since the other two components are not labeled. While additional FCS study could be performed with labeled gemini surfactant or lipids, it still would not prove that they are in fact interacting in the gemini NP. To overcome this limitation a derivative of FCS is fluorescence cross correlation spectroscopy (FCCS) can be explored. FCCS, or dual-channel FCS, utilizes two fluorophores that are monitored simultaneously and independent autocorrelation are performed for each channel, and then cross-correlated. These cross-correlation curves generate a new set of information such as binding coefficients, interactions and chemical kinetics [218]. The ability to study the binding or interaction of molecule within a NP can provide even deep insight into the composition of the gemini NP. FCCS could be used to study the interactions of various components of the gemini NP. This would be interesting study to add pieces to the story of the intracellular fate of gemini NPs. Also by understanding the interaction between gemini surfactant and phospholipid could confirm the supramolecular aggregate model to see if fact the phospholipids could scavenge the excess gemini surfactant. A second extension of FCS that also be explored is photon counting histogram (PCH). As shown in Section 6.2.8.2, the intensity of photon can be used to characterize the molecules but that without proper method of analyze the data it becomes difficult to interpret analytically. One method is to use photon counting. Similar to how the FCS utilizes changes in fluorescent fluctuation in time-dependent manner to generate biophysics values, PCH monitors the changes in fluorescent intensity using other mathematical models. PCH would prove to be a more analytically valid method to study the precise

stoichiometry of the gemini NPs. This technique can be applied to our currently experiment to gain a more analytical study of the plasmid number discussed in section 6.2.8.2.

While this study has shown the application of FCS as a complimentary technique to existing methods, there are many other applications of FCS. One of the most exciting is the use FCS for studying the NP in the context of a living cell *in vitro.* Since this study have verified that FCS is capable of collecting information on mobility and particle size, with additional optimization it can be extended to cellular environment. This would provide additional information link in solution characterization to biological function of NPs *in vitro*. One application of *in vitro* FCS is the study of the trafficking of labeled plasmid within the cell. Using a time-lapse experiment, one could monitor the mobility of the plasmid or NP within the cell. By adding other FCS extension such as FCCS, the distribution of NP to different organelles (e.g. using organelle specific dyes and labeled plasmid) can also be monitored. All of this new information will be essential toward the rational design of new generation of non-viral systems to advance nanomedicine.

Appendix

Particle size distribution

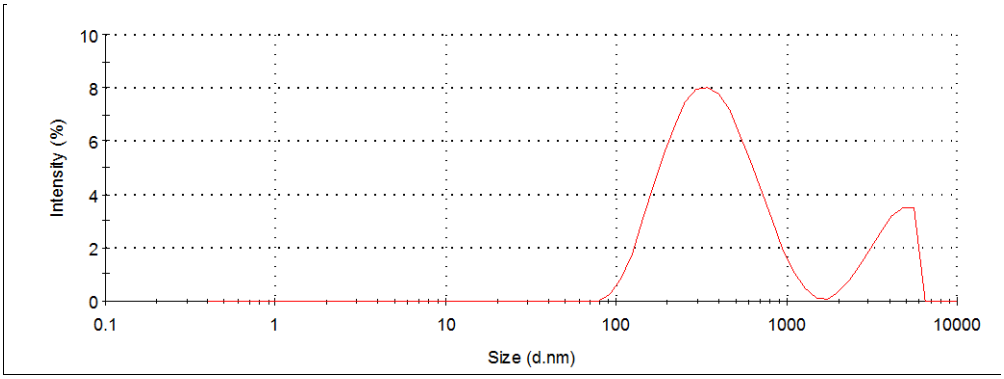

Figure 40: Size distribution by intensity for 12-3-12 GP. Graph was exported from Zetasizer nano software

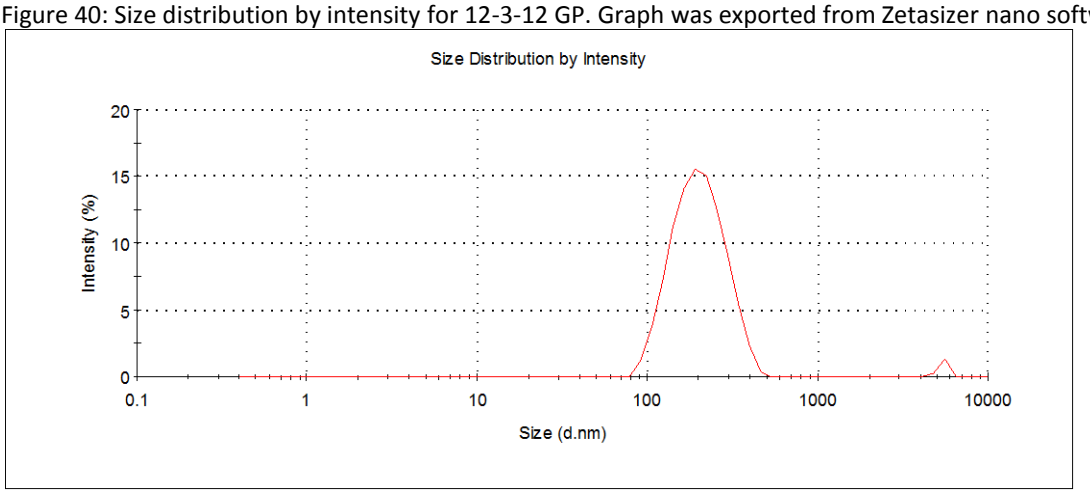

Figure 41: Size distribution by intensity for 12-3-12 GPL prepared with DD 1:3

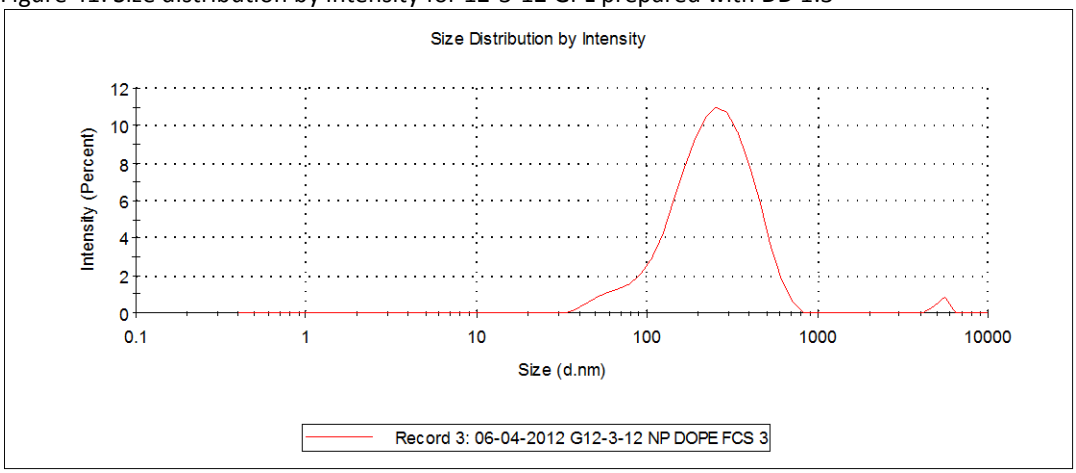

Figure 42 Size distribution by intensity for 12-3-12 GPL prepared with DOPE

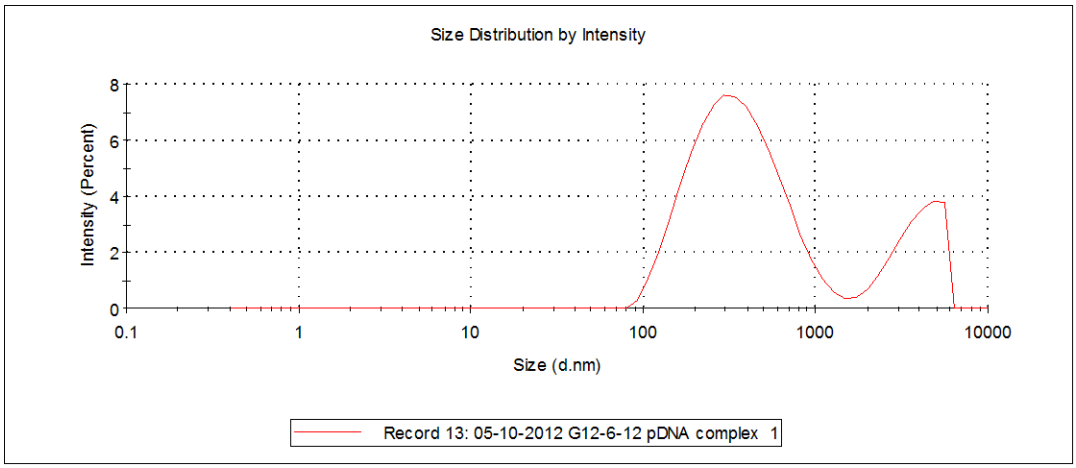

Figure 43: Size distribution by intensity for 12-6-12 GP. Graph was exported from Zetasizer Nano Software

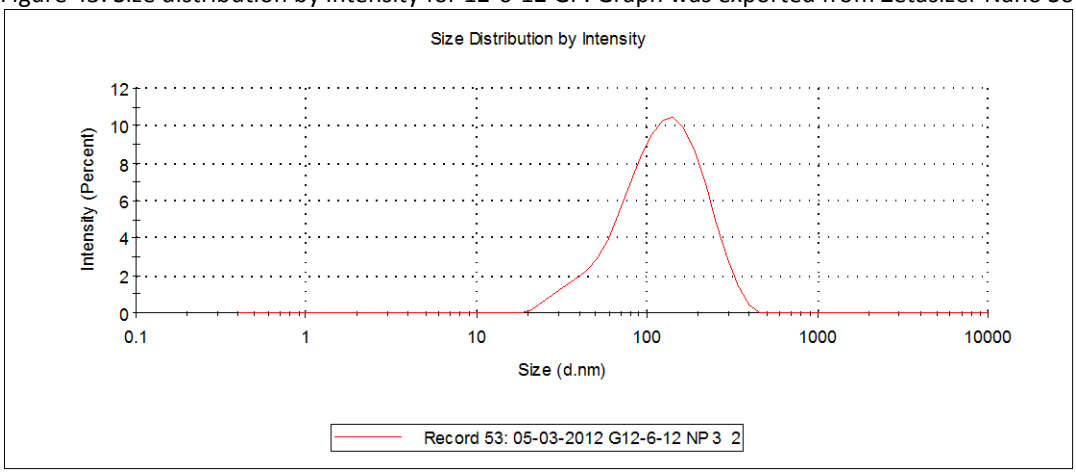

Figure 44: Size distribution by intensity for 12-6-12 GPL prepared with DD 1:3

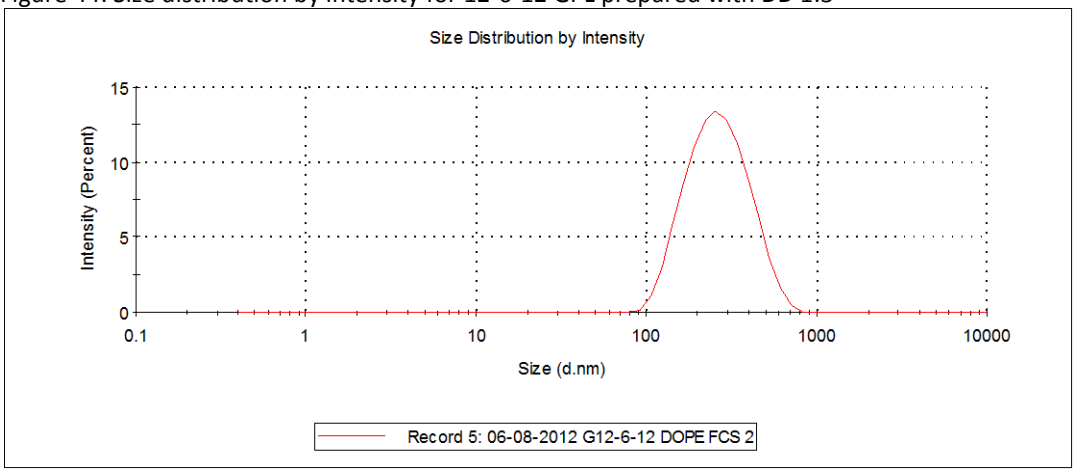

Figure 45:Size distribution by intensity for 12-6-12 GPL prepared with DOPE

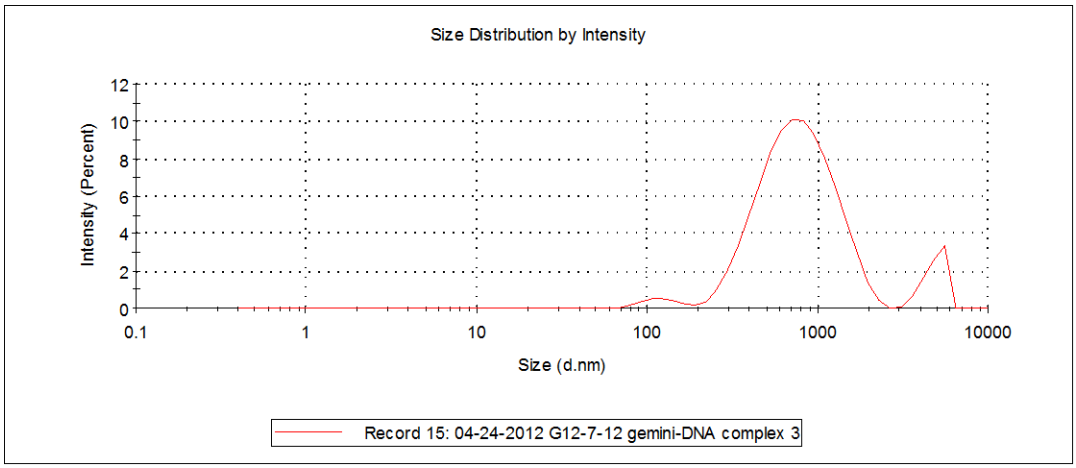

Figure 46: Size distribution by intensity for 12-7-12GP. Graph was exported from Zetasizer Nano Software

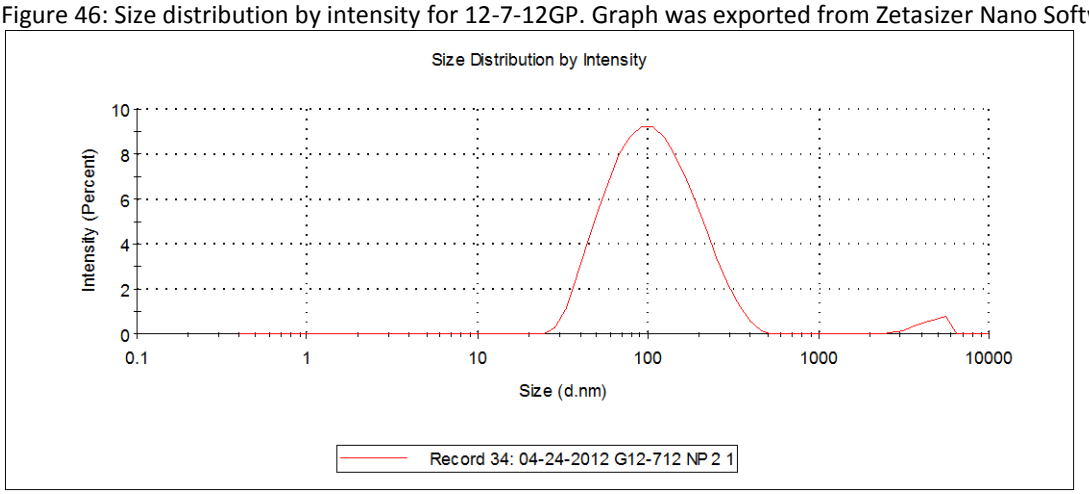

Figure 47: Size distribution by intensity for 12-7-12 GPL prepared with DD 1:3

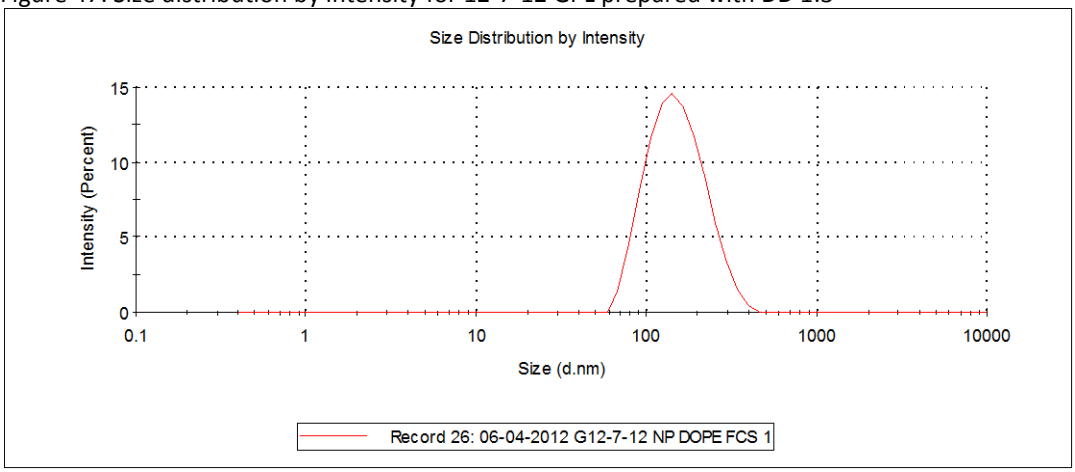

Figure 48: Size distribution by intensity for 12-7-12 GPL prepared with DOPE

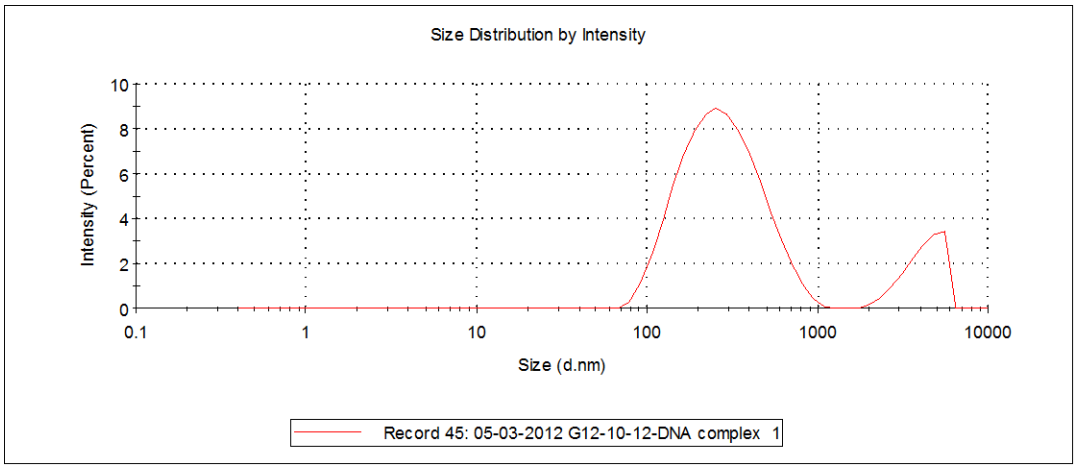

Figure 49: Size distribution by intensity for 12-10-12GP. Graph was exported from Zetasizer Nano Software

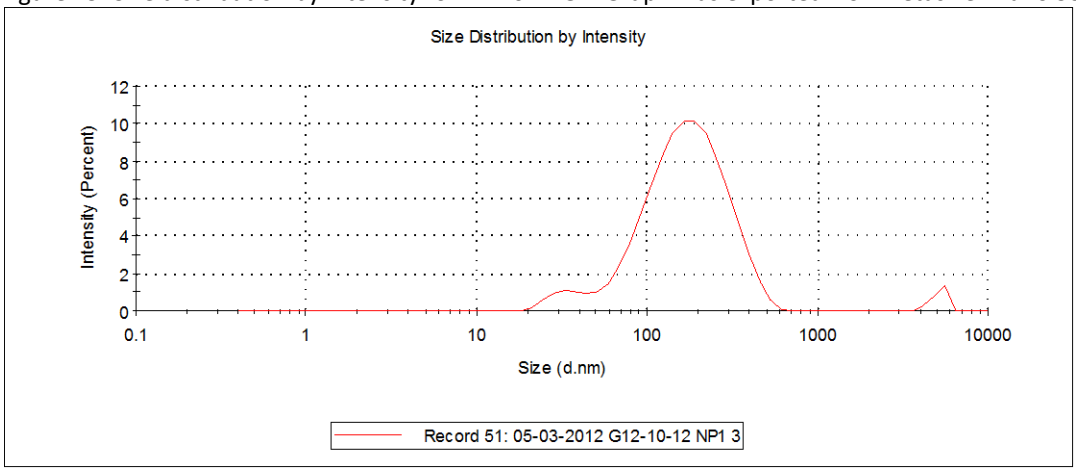

Figure 50 : Size distribution by intensity for 12-10-12 GPL prepared with DD 1:3

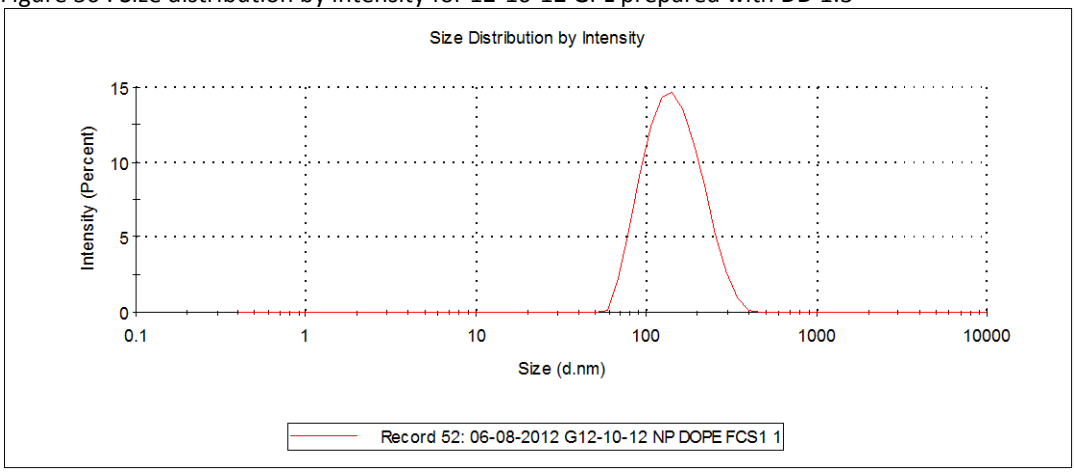

Figure 51: Size distribution by intensity for 12-10-12 GPL prepared with DOPE

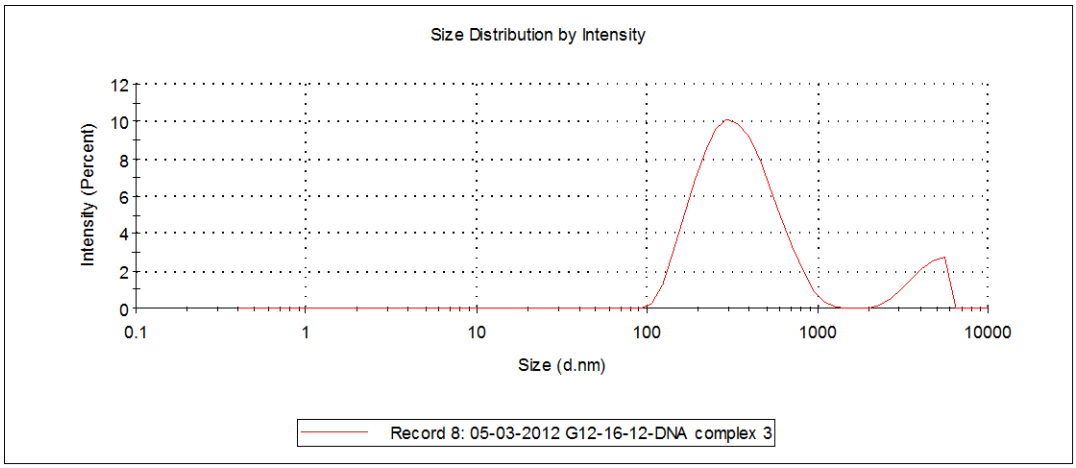

Figure 52 : Size distribution by intensity for 12-16-12GP. Graph was exported from Zetasizer Nano Software

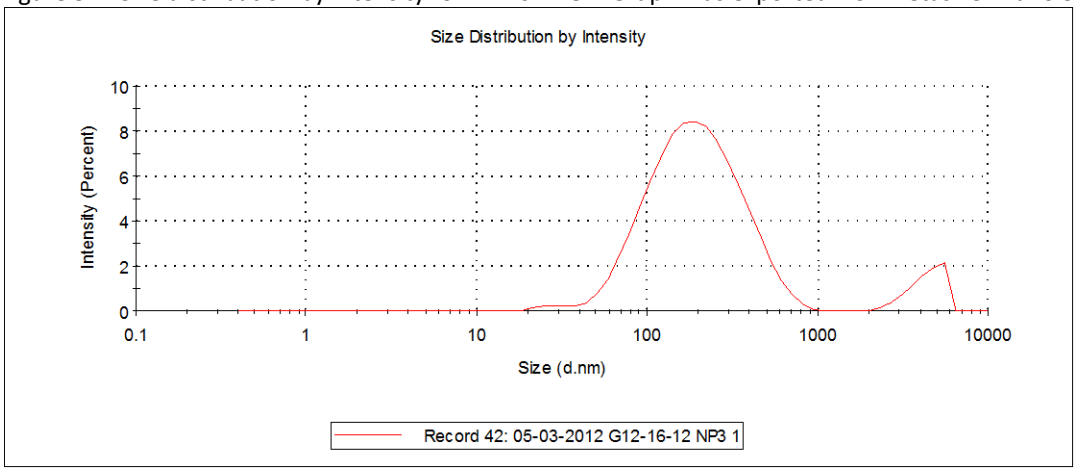

Figure 53 : Size distribution by intensity for 12-16-12 GPL prepared with DD 1:3

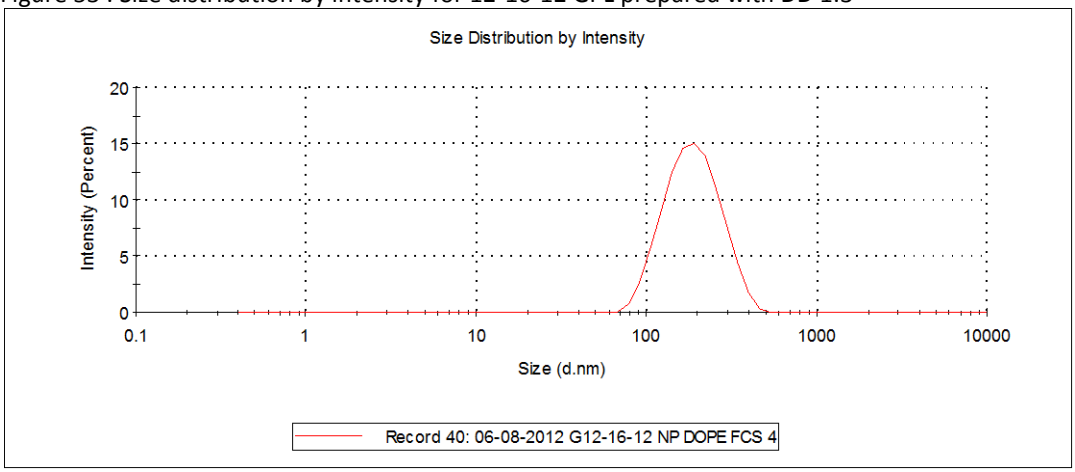

Figure 54: Size distribution by intensity for 12-16-12 GPL prepared with DOPE

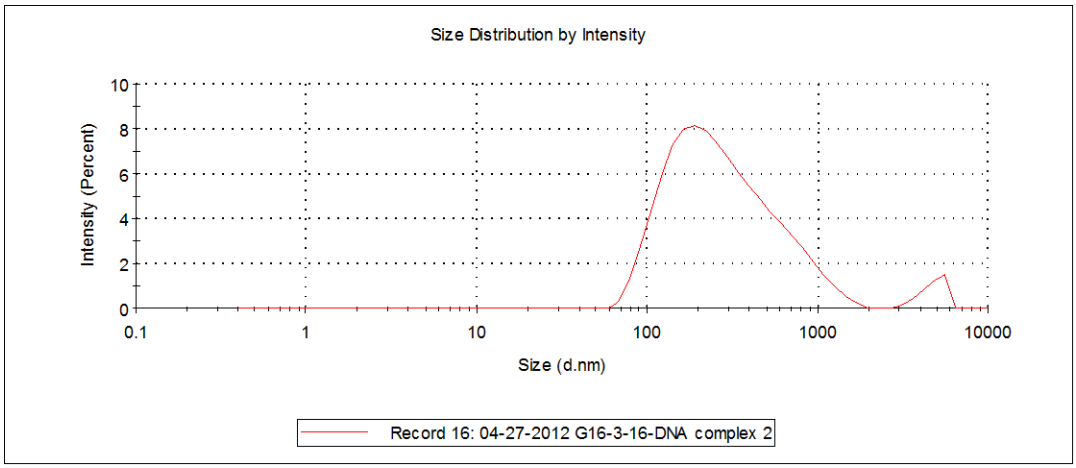

Figure 55: Size distribution by intensity for 16-3-16 GP. Graph was exported from Zetasizer Nano Software

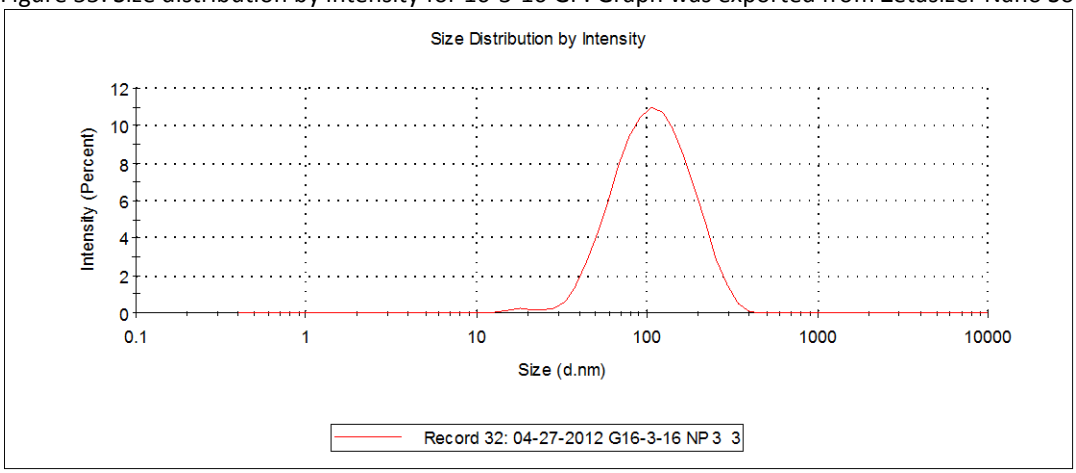

Figure 56: Size distribution by intensity for 16-3-16 GPL prepared with DD 1:3

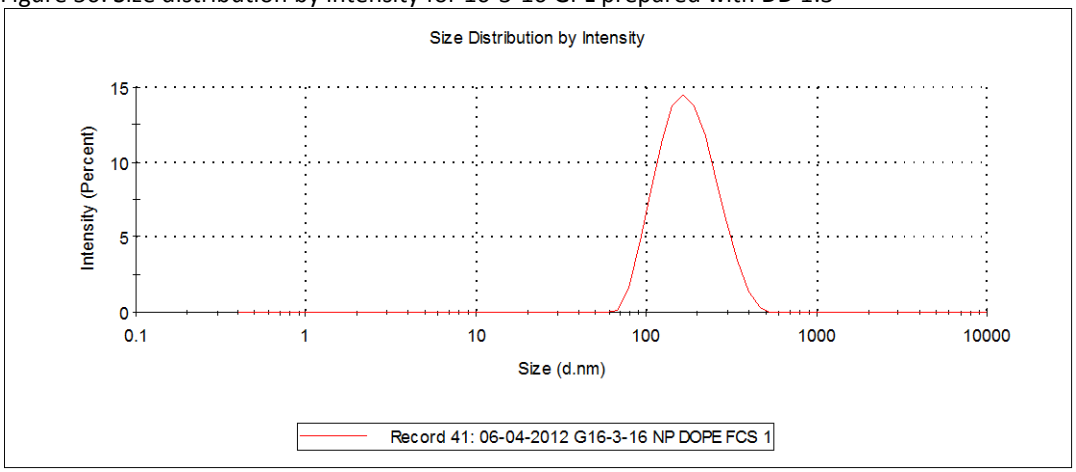

Figure 57: Size distribution by intensity for 16-3-16 GPL prepared with DOPE

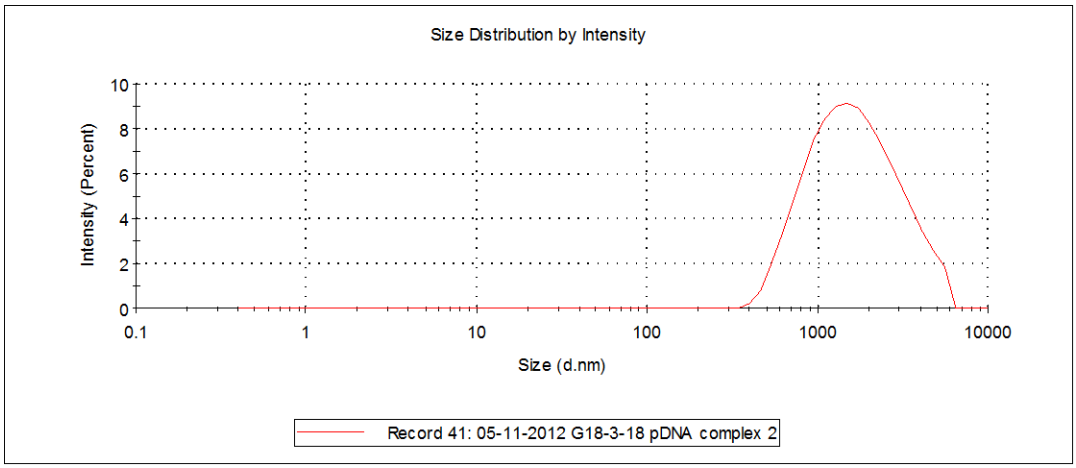

Figure 58: Size distribution by intensity for 18-3-18 GP. Graph was exported from Zetasizer Nano Software

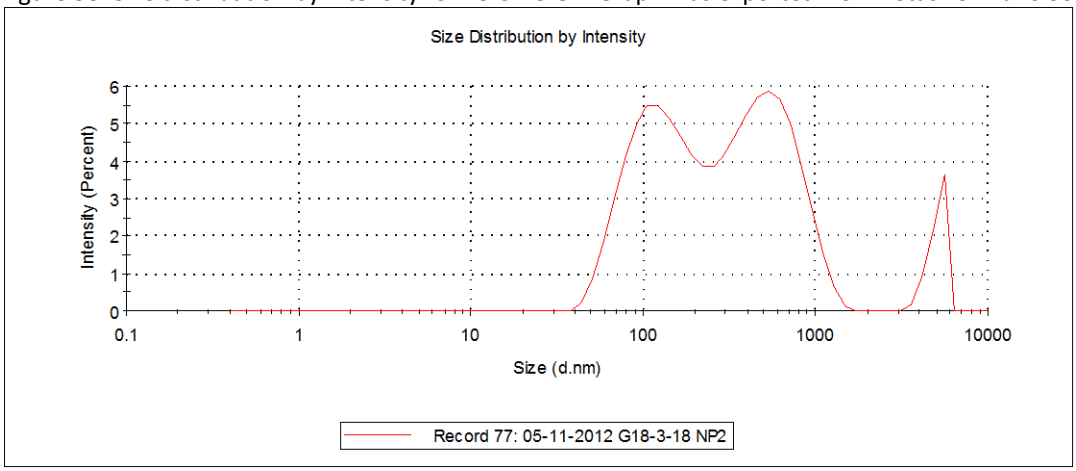

Figure 59: Size distribution by intensity for 18-3-18 GPL prepared with DD 1:3

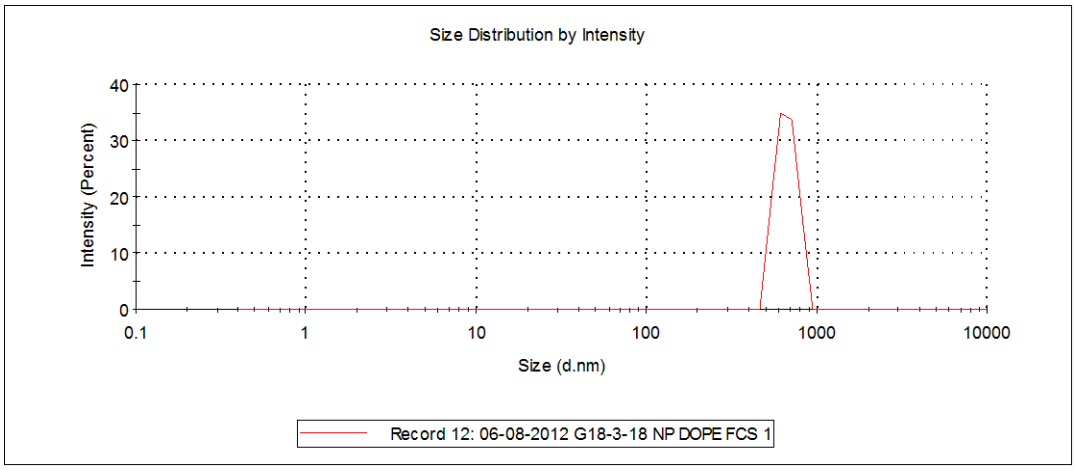

Figure 60: Size distribution by intensity for 18-3-18 GPL prepared with DOPE

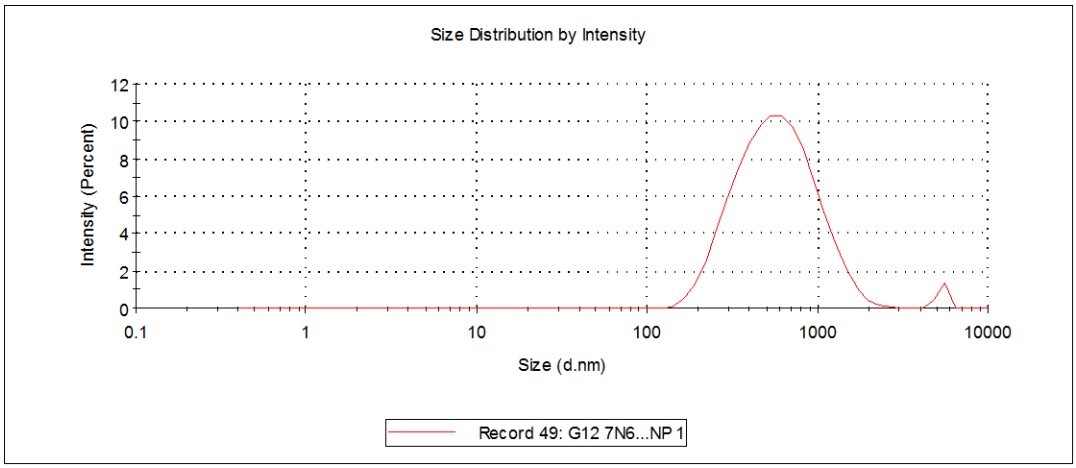

Figure 61: Size distribution by intensity for 12-7NH-12GP. Graph was exported from Zetasizer Nano Software

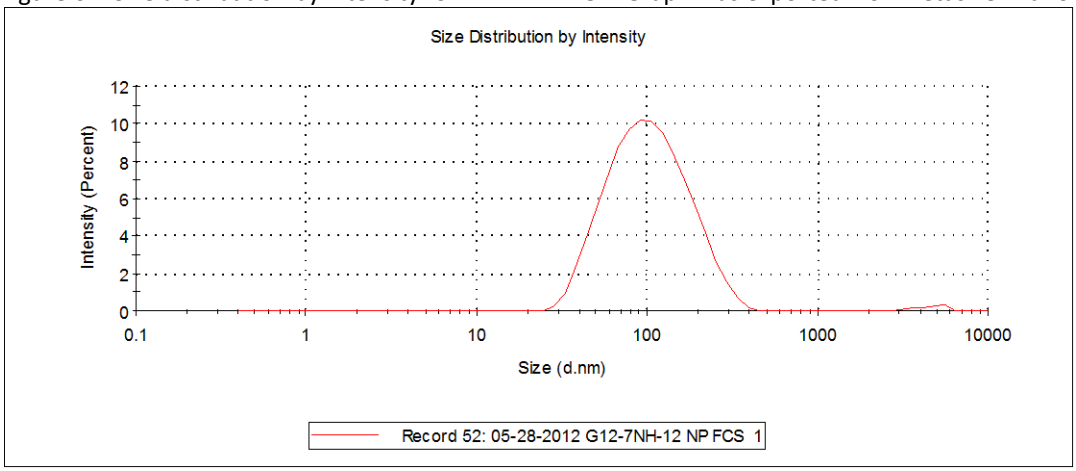

Figure 62: Size distribution by intensity for 12-7NH-12 GPL prepared with DD 1:3

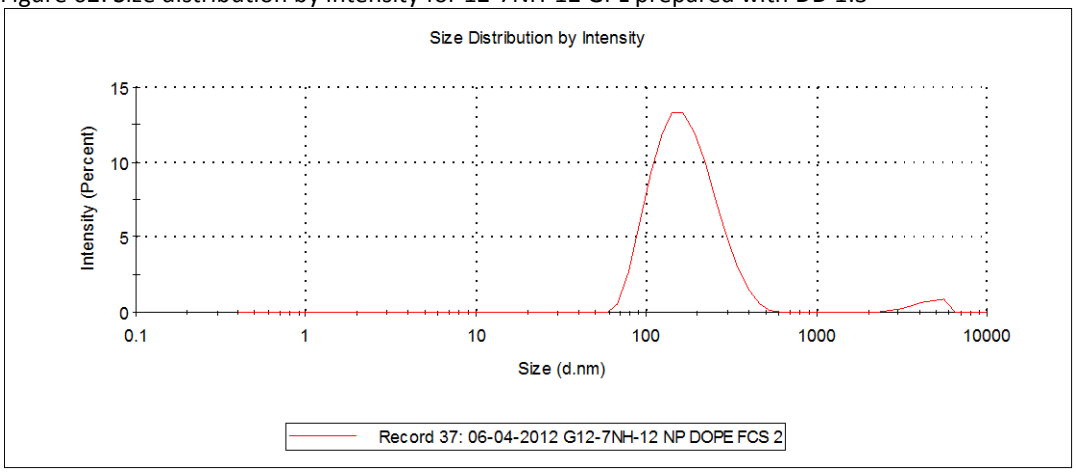

Figure 63: Size distribution by intensity for 12-7NH-12 GPL prepared with DOPE

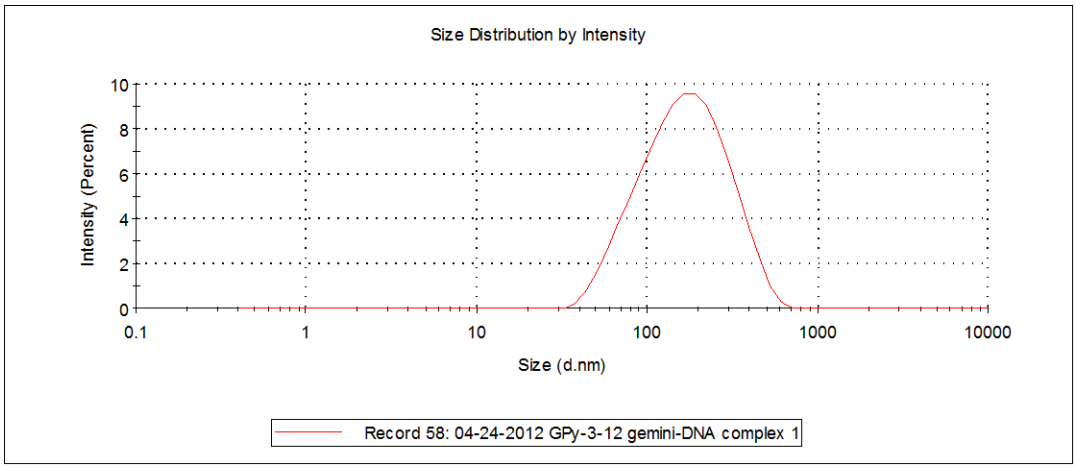

Figure 64: Size distribution by intensity for Py-3-12GP. Graph was exported from Zetasizer Nano Software

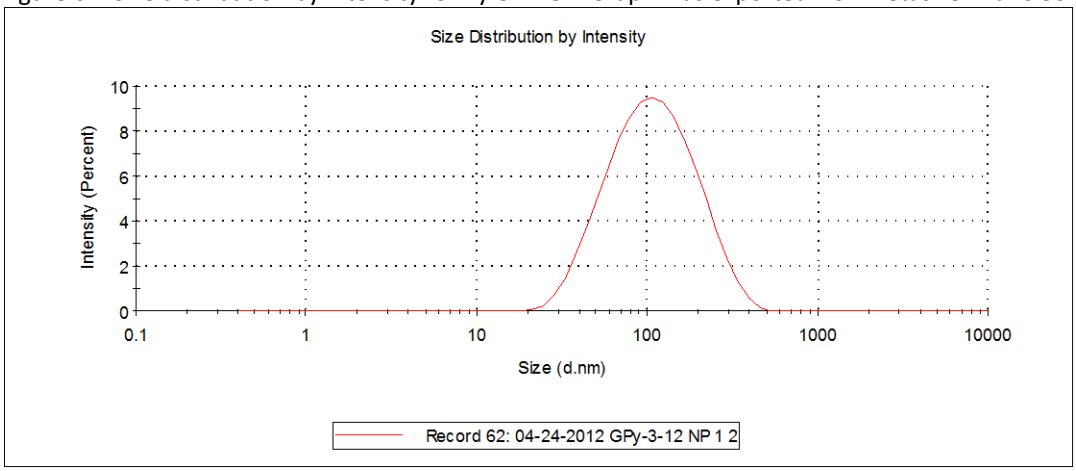

Figure 65: Size distribution by intensity for Py-3-12 GPL prepared with DD 1:3

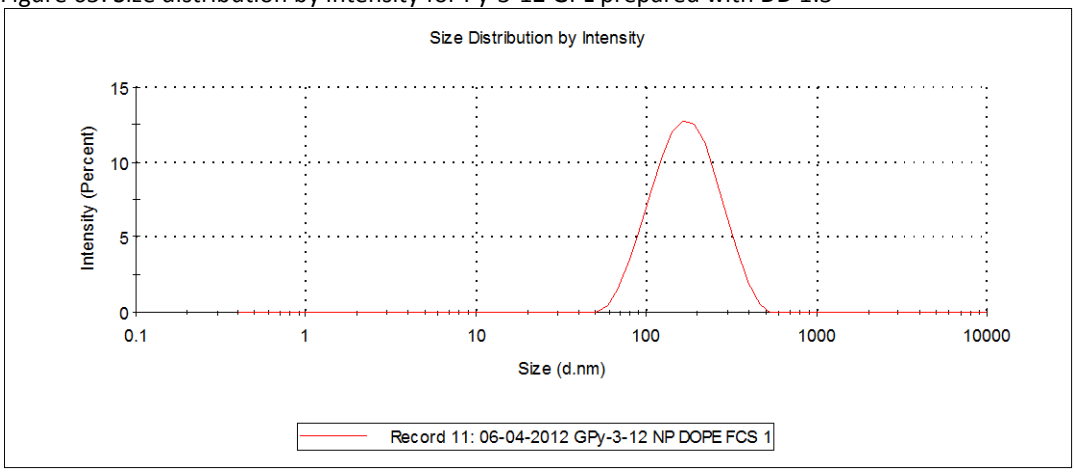

Figure 66: Size distribution by intensity for Py-3-12 GPL prepared with DOPE

In vitro experiments

Cell culture and PrestoBlue® methodology

The origin and characterization of the parental PAM 212 has been described previously [266]. The PAM 212 cell line is a spontaneously malignant transformed cell line derived from neonatal BALB/c keratinocytes *in vitro*, and was provided by Dr. Stuart Yuspa of the National Cancer Institute. The PAM 212 cells were cultures using MEM plus media with 10% FCS and 1% penicillin streptomycin. The cells were routinely cultured at 37°C in a 5% CO_2 and humidified atmosphere until ~70-80% confluency.

PAM 212 were seeded at 20,000 cells per well in a black clear-bottom 96-well plate and incubated for 24 hours. At 80% confluency, cells were washed with MEM and treated with lipofectamine or gemini compounds (GPs and GPLs) in quadruplicate for five hours. Cells were washed and allowed to incubate for 24 hours in supplemented MEM. Cells were washed an incubated in 10 µL of PrestoBlue® (Invitrogen, CA, USA) added to each well with 90 µL of basic MEM for 10 mins at 37°C. PrestoBlue® was excited at 535nm and emission was measured at 615nm using a spectrophotometer (Spectramax M5, Molecular Devices, CA, USA).

Cell viability assays for transfected keratinocytes

To assess the suitability of the gemini NPs for applications for *in vitro* studies, the cytotoxicity of various transfection agents were tested. PrestoBlue® reagent is used to evaluate the viability and proliferation of cells. The resazurin-based reagent used the reducing potential of the intracellular environment as an indicator of cell viability.

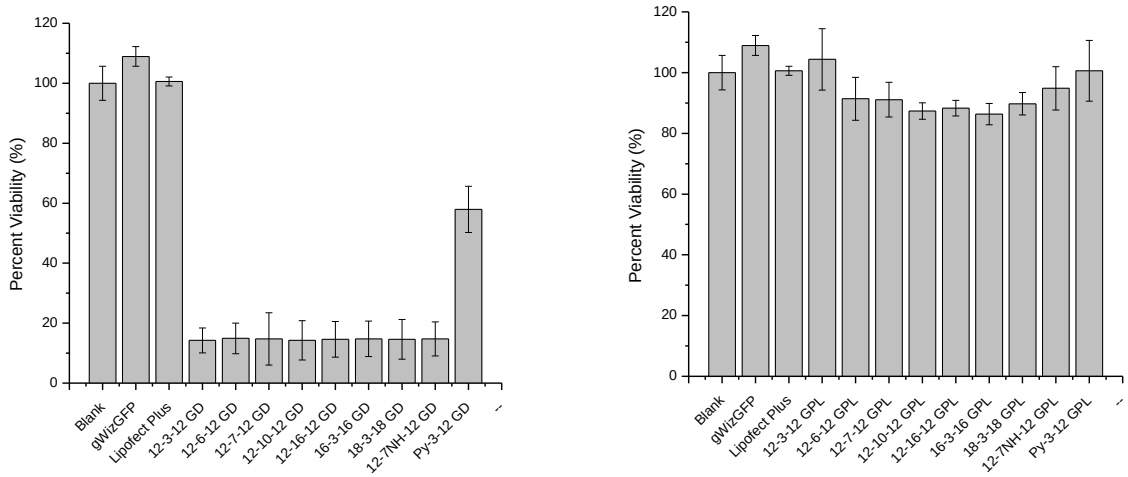

Figure 67: Cell viability assay using Presto Blue reagent in Pam 212 cell line. A) viability assay of various gemini GPs B) viability assay of various GPLs. Measurements expressed as a mean±SD (n=4).

.

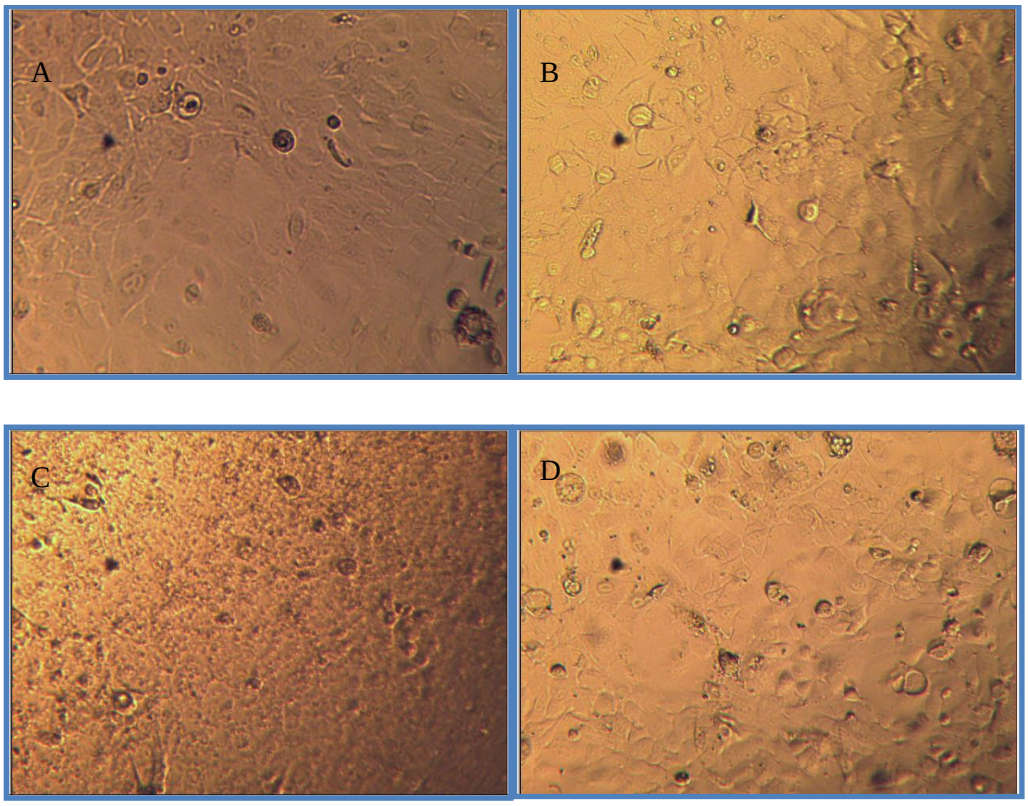

Figure 68 Bright-field microscopy images of Pam 212 cells 24 hour post treatment with various formulations. A) Negative control (MEM medium), B) Lipofectamine C) 12-3-12 GP D) 12-3-12 GPL. Images were taken at 400X magnification.

Figure 67 shows the effects of GPs and GPLs on the viability of the Pam 212 cells. The study showed that both commercial transfection reagent Lipofectamine Plus and GPLs do no significantly affect the health of the Pam 212 cells. This was suggested by the viability measurement of over 95% for both transfection reagents. This was also confirmed by bright field microscopy as shown in Figure 68 to have no rounding or abnormal cell growth (data for other gemini surfactants not shown). All GPs screened in this study were observed to be extremely cytotoxic with viability generally lower than 20%. An exception was with Py-3-12 GP which was significantly less cytotoxic (57±7%). Overall, GPL have no significantly cytotoxicity when evaluated by brightfield and PrestoBlue® assay. Comparison between select DOPE and DD 1:3 NP also demonstrated that there was no significant difference based on lipid composition. Gemini surfactant structure also did not have a significant effect on the viability of the cells. Select DD 1:3 were screened for cytotoxicity due to the absence of transfection in the previous study. In term of GPLs assembly, the additional of the phospholipid is the key factor in regulating cytotoxicty of the GPLs.

References

1. Keeler, C.E., *Gene therapy.* Journal of Heredity, 1947. **38**(10): p. 294-298.

2. Friedmann, T., *A brief history of gene therapy.* Nature Genetics, 1992. **2**(2): p. 93-98.

3. Caplen, N.J., E.W.F.W. Alton, P.G. Middleton, J.R. Dorin, B.J. Stevenson, X. Gao, S.R. Durham, P.K. Jeffery, M.E. Hudson, C. Coutelle, L. Huang, D.J. Porteous, R. Williamson, and D.M. Geddes, *Liposome-mediated CFTR gene transfer to the nasal epithelium of patients with cystic fibrosis.* Nature Medicine, 1995. **1**(1): p. 39-46.

4. Cusack Jr, J.C. and K.K. Tanabe, *Introduction to cancer gene therapy.* Surgical Oncology Clinics of North America, 2002. **11**(3): p. 497-519.

5. Douglas, J.T., *Cancer gene therapy.* Technology in Cancer Research and Treatment, 2003. **2**(1): p. 51-63.

6. Ingolotti, M., O. Kawalekar, D.J. Shedlock, K. Muthumani, and D.B. Weiner, *DNA vaccines for targeting bacterial infections.* Expert Review of Vaccines, 2010. **9**(7): p. 747-763.

7. Leitner, W.W. and J. Thalhamer, *DNA vaccines for non-infectious diseases: New treatments for tumour and allergy.* Expert Opinion on Biological Therapy, 2003. **3**(4): p. 627-638.

8. Resnik, D.B. and P.J. Langer, *Human germline gene therapy reconsidered.* Human Gene Therapy, 2001. **12**(11): p. 1449-1458.

9. Edelstein, M. *Gene Therapy Clinical Trials Worldwide*. The Journal of Gene Medicine 2012 [cited 2012 Oct 25, 2012]; Available from: http://www.wiley.com/legacy/wileychi/genmed/clinical/.

10. Gunter, C., *Genomics: A picture worth 1000 Genomes.* Nature Reviews Genetics, 2010.

11. Wolff, J.A., R.W. Malone, P. Williams, C. Wang, G. Acsadi, A. Jani, and P.L. Felgner, *Direct gene transfer into mouse muscle in vivo.* Science, 1990. **247**(4949 I): p. 1465-1468.

12. Hickman, M.A., R.W. Malone, K. Lehmann-Bruinsma, T.R. Sih, D. Knoell, F.C. Szoka, R. Walzem, D.M. Carlson, and J.S. Powell, *Gene expression following direct injection of DNA into liver.* Human Gene Therapy, 1994. **5**(12): p. 1477-1483.

13. Hengge, U.R., E.F. Chan, R.A. Foster, P.S. Walker, and J.C. Vogel, *Cytokine gene expression in epidermis with biological effects following injection of naked DNA.* Nature Genetics, 1995. **10**(2): p. 161-166.

14. Pachuk, C.J., D.E. McCallus, D.B. Weiner, and C. Satishchandran, *DNA vaccines - Challenges in delivery.* Current Opinion in Molecular Therapeutics, 2000. **2**(2): p. 188-198.

15. Hunt, M.A., M.J. Currie, B.A. Robinson, and G.U. Dachs, *Optimizing transfection of primary human umbilical vein endothelial cells using commercially available chemical transfection reagents.* Journal of Biomolecular Techniques, 2010. **21**(2): p. 66-72.

16. Douglas, K.L., C.A. Piccirillo, and M. Tabrizian, *Cell line-dependent internalization pathways and intracellular trafficking determine transfection efficiency of nanoparticle vectors.* European Journal of Pharmaceutics and Biopharmaceutics, 2008. **68**(3): p. 676-687.

17. von Gersdorff, K., N.N. Sanders, R. Vandenbroucke, S.C. De Smedt, E. Wagner, and M. Ogris, *The Internalization Route Resulting in Successful Gene Expression Depends on both Cell Line and Polyethylenimine Polyplex Type.* Molecular Therapy, 2006. **14**(5): p. 745-753.

18. Mao, H.Q., K. Roy, V.L. Troung-Le, K.A. Janes, K.Y. Lin, Y. Wang, J.T. August, and K.W. Leong, *Chitosan-DNA nanoparticles as gene carriers: Synthesis, characterization and transfection efficiency.* Journal of Controlled Release, 2001. **70**(3): p. 399-421.

19. Rodriguez, R., E.R. Schuur, H.Y. Lim, G.A. Henderson, J.W. Simons, and D.R. Henderson, *Prostate attenuated replication competent adenovirus (ARCA) CN706: A selective cytotoxic for prostate-specific antigen-positive prostate cancer cells.* Cancer Research, 1997. **57**(13): p. 2559-2563.

20. Lu, Y. and P.S. Low, *Folate-mediated delivery of macromolecular anticancer therapeutic agents.* Advanced Drug Delivery Reviews, 2002. **54**(5): p. 675-693.

21. Douglas, J.T., B.E. Rogers, M.E. Rosenfeld, S.I. Michael, M. Feng, and D.T. Curiel, *Targeted gene delivery by tropism-modified adenoviral vectors.* Nature Biotechnology, 1996. **14**(11): p. 1574-1578.

22. Kircheis, R., A. Kichler, G. Wallner, M. Kursa, M. Ogris, T. Felzmann, M. Buchberger, and E. Wagner, *Coupling of cell-binding ligands to polyethylenimine for targeted gene delivery.* Gene Therapy, 1997. **4**(5): p. 409-418.

23. Kawabata, K., Y. Takakura, and M. Hashida, *The fate of plasmid DNA after intravenous injection in mice: Involvement of scavenger receptors in its hepatic uptake.* Pharmaceutical Research, 1995. **12**(6): p. 825-830.

24. Levy, M.Y., L.G. Barron, K.B. Meyer, and F.C. Szoka Jr, *Characterization of plasmid DNA transfer into mouse skeletal muscle: Evaluation of uptake mechanism, expression and secretion of gene products into blood.* Gene Therapy, 1996. **3**(3): p. 201-211.

25. Heller, L.C. and R. Heller, *Electroporation gene therapy preclinical and clinical trials for melanoma.* Current Gene Therapy, 2010. **10**(4): p. 312-317.

26. Gao, X., K.S. Kim, and D. Liu, *Nonviral gene delivery: What we know and what is next.* AAPS Journal, 2007. **9**(1).

27. Aihara, H. and J.I. Miyazaki, *Gene transfer into muscle by electroporation in vivo.* Nature Biotechnology, 1998. **16**(9): p. 867-870.

28. Edelstein, M.L., M.R. Abedi, and J. Wixon, *Gene therapy clinical trials worldwide to 2007 - An update.* Journal of Gene Medicine, 2007. **9**(10): p. 833-842.

29. Rosenberg, S.A., P. Aebersold, K. Cornetta, A. Kasid, R.A. Morgan, R. Moen, E.M. Karson, M.T. Lotze, J.C. Yang, S.L. Topalian, M.J. Merino, K. Culver, A.D. Miller, R.M. Blaese, and

W.F. Anderson, *Gene transfer into humans - Immunotherapy of patients with advanced melanoma, using tumor-infiltrating lymphocytes modified by retroviral gene transduction.* New England Journal of Medicine, 1990. **323**(9): p. 570-578.

30. Cressey, D., *Europe nears first approval for gene therapy*, in *Nature Publishing Group*. 2012, Macmillian Publishers Limited.

31. Thomas, C.E., A. Ehrhardt, and M.A. Kay, *Progress and problems with the use of viral vectors for gene therapy.* Nature Reviews Genetics, 2003. **4**(5): p. 346-358.

32. Waehler, R., S.J. Russell, and D.T. Curiel, *Engineering targeted viral vectors for gene therapy.* Nature Reviews Genetics, 2007. **8**(8): p. 573-587.

33. Brunetti-Pierri, N., D.J. Palmer, A.L. Beaudet, K.D. Carey, M. Finegold, and P. Ng, *Acute Toxicity after High-Dose Systemic Injection of Helper-Dependent Adenoviral Vectors into Nonhuman Primates.* Human Gene Therapy, 2004. **15**(1): p. 35-46.

34. Kagami, H., J.C. Atkinson, S.M. Michalek, B. Handelman, S. Yu, B.J. Baum, and B. O'Connell, *Repetitive adenovirus administration to the parotid gland: Role of immunological barriers and induction of oral tolerance.* Human Gene Therapy, 1998. **9**(3): p. 305-313.

35. Wu, N. and M.M. Ataai, *Production of viral vectors for gene therapy applications.* Current Opinion in Biotechnology, 2000. **11**(2): p. 205-208.

36. *Assessment of adenoviral vector safety and toxicity: Report of the National Institutes of Health recombinant DNA advisory committee.* Human Gene Therapy, 2002. **13**(1): p. 3-13.

37. Hacein-Bey-Abina, S., C. Von Kalle, M. Schmidt, F. Le Deist, N. Wulffraat, E. McIntyre, I. Radford, J.L. Villeval, C.C. Fraser, M. Cavazzana-Calvo, and A. Fischer, *A serious adverse event after successful gene therapy for X-linked severe combined immunodeficiency [1].* New England Journal of Medicine, 2003. **348**(3): p. 255-256.

38. Felgner, P.L., T.R. Gadek, M. Holm, R. Roman, H.W. Chan, M. Wenz, J.P. Northrop, G.M. Ringold, and M. Danielsen, *Lipofection: a highly efficient, lipid-mediated DNA-transfection procedure.* Proceedings of the National Academy of Sciences of the United States of America, 1987. **84**(21): p. 7413-7417.

39. Mintzer, M.A. and E.E. Simanek, *Nonviral Vectors for Gene Delivery.* Chemical Reviews, 2008. **109**(2): p. 259-302.

40. Bloomfield, V.A., *DNA condensation by multivalent cations.* Biopolymers, 1997. **44**(3): p. 269-282.

41. Singh, R., D. Pantarotto, D. McCarthy, O. Chaloin, J. Hoebeke, C.D. Partidos, J.P. Briand, M. Prato, A. Bianco, and K. Kostarelos, *Binding and condensation of plasmid DNA onto functionalized carbon nanotubes: Toward the construction of nanotube-based gene delivery vectors.* Journal of the American Chemical Society, 2005. **127**(12): p. 4388-4396.

42. Bragonzi, A., A. Boletta, A. Biffi, A. Muggia, G. Sersale, S.H. Cheng, C. Bordignon, B.M. Assael, and M. Conese, *Comparison between cationic polymers and lipids in mediating systemic gene delivery to the lungs.* Gene Therapy, 1999. **6**(12): p. 1995-2004.

43. Florea, B.I., P.G.M. Ravenstijn, H.E. Junginger, and G. Borchard, *N-trimethylated oligomeric chitosan (TMO) protects plasmid DNA from DNase I degradation and promotes transfection efficiency in vitro.* S.T.P. Pharma Sciences, 2002. **12**(4): p. 243-249.

44. Godbey, W.T., M.A. Barry, P. Saggau, K.K. Wu, and A.G. Mikos, *Poly(ethylenimine)-mediated transfection: A new paradigm for gene delivery.* Journal of Biomedical Materials Research, 2000. **51**(3): p. 321-328.

45. Moret, I., J. Esteban Peris, V.M. Guillem, M. Benet, F. Revert, F. Dasí, A. Crespo, and S.F. Alio, *Stability of PEI-DNA and DOTAP-DNA complexes: Effect of alkaline pH, heparin and serum.* Journal of Controlled Release, 2001. **76**(1-2): p. 169-181.

46. Song, Y.K., *Characterization of cationic liposome-mediated gene transfer in vivo by intravenous administration.* Human Gene Therapy, 1997. **8**(13): p. 1585-1594.

47. Brown, M.D., A. Schatzlein, A. Brownlie, V. Jack, W. Wang, L. Tetley, A.I. Gray, and I.F. Uchegbu, *Preliminary characterization of novel amino acid based polymeric vesicles as gene and drug delivery agents.* Bioconjugate Chemistry, 2000. **11**(6): p. 880-891.

48. Uchegbu, I.F., A.G. Schätzlein, L. Tetley, A.I. Gray, J. Sludden, S. Siddique, and E. Mosha, *Polymeric chitosan-based vesicles for drug delivery.* Journal of Pharmacy and Pharmacology, 1998. **50**(5): p. 453-458.

49. McPhail, D., L. Tetley, C. Dufes, and I.F. Uchegbu, *Liposomes encapsulating polymeric chitosan based vesicles - A vesicle in vesicle system for drug delivery.* International Journal of Pharmaceutics, 2000. **200**(1): p. 73-86.

50. Whitmore, M., S. Li, and L. Huang, *LPD lipopolyplex initiates a potent cytokine response and inhibits tumor growth.* Gene Therapy, 1999. **6**(11): p. 1867-1875.

51. Ulrich, A.S., *Biophysical aspects of using liposomes as delivery vehicles.* Bioscience Reports, 2002. **22**(2): p. 129-150.

52. Gao, X. and L. Huang, *Cationic liposome-mediated gene transfer.* Gene Therapy, 1995. **2**(10): p. 710-722.

53. Torchilin, V.P., *Recent advances with liposomes as pharmaceutical carriers.* Nature Reviews Drug Discovery, 2005. **4**(2): p. 145-160.

54. Donkuru, M., I. Badea, S. Wettig, R. Verrall, M. Elsabahy, and M. Foldvari, *Advancing nonviral gene delivery: Lipid- and surfactant-based nanoparticle design strategies.* Nanomedicine, 2010. **5**(7): p. 1103-1127.

55. Kreiss, P., B. Cameron, R. Rangara, P. Mailhe, O. Aguerre-Charriol, M. Airiau, D. Scherman, J. Crouzet, and B. Pitard, *Plasmid DNA size does not affect the physicochemical properties of*

lipoplexes but modulates gene transfer efficiency. Nucleic Acids Research, 1999. **27**(19): p. 3792-3798.

56. Yang, J.P. and L. Huang, *Overcoming the inhibitory effect of serum on lipofection by increasing the charge ratio of cationic liposome to DNA.* Gene Therapy, 1997. **4**(9): p. 950-960.

57. Koltover, I., T. Salditt, J.O. Rädler, and C.R. Safinya, *An inverted hexagonal phase of cationic liposome-DNA complexes related to DNA release and delivery.* Science, 1998. **281**(5373): p. 78-81.

58. Crook, K., B.J. Stevenson, M. Dubouchet, and D.J. Porteous, *Inclusion of cholesterol in DOTAP transfection complexes increases the delivery of DNA to cells in vitro in the presence of serum.* Gene Therapy, 1998. **5**(1): p. 137-143.

59. Li, S., W.C. Tseng, D. Beer Stolz, S.P. Wu, S.C. Watkins, and L. Huang, *Dynamic changes in the characteristics of cationic lipidic vectors after exposure to mouse serum: Implications for intravenous lipofection.* Gene Therapy, 1999. **6**(4): p. 585-594.

60. Boussif, O., F. LezoualC'H, M.A. Zanta, M.D. Mergny, D. Scherman, B. Demeneix, and J.P. Behr, *A versatile vector for gene and oligonucleotide transfer into cells in culture and in vivo: Polyethylenimine.* Proceedings of the National Academy of Sciences of the United States of America, 1995. **92**(16): p. 7297-7301.

61. Brown, M.D., A.G. Schätzlein, and I.F. Uchegbu, *Gene delivery with synthetic (non viral) carriers.* International Journal of Pharmaceutics, 2001. **229**(1-2): p. 1-21.

62. Curiel, D.T., S. Agarwal, E. Wagner, and M. Cotten, *Adenovirus enhancement of transferrin-polylysine-mediated gene delivery.* Proceedings of the National Academy of Sciences of the United States of America, 1991. **88**(19): p. 8850-8854.

63. Guang Liu, W. and K. De Yao, *Chitosan and its derivatives - A promising non-viral vector for gene transfection.* Journal of Controlled Release, 2002. **83**(1): p. 1-11.

64. Liu, Y., D. Liggitt, W. Zhong, G. Tu, K. Gaensler, and R. Debs, *Cationic liposome-mediated intravenous gene delivery.* Journal of Biological Chemistry, 1995. **270**(42): p. 24864-24870.

65. Wiethoff, C.M. and C.R. Middaugh, *Barriers to nonviral gene delivery.* Journal of Pharmaceutical Sciences, 2003. **92**(2): p. 203-217.

66. Glover, D.J., H.J. Lipps, and D.A. Jans, *Towards safe, non-viral therapeutic gene expression in humans.* Nature Reviews Genetics, 2005. **6**(4): p. 299-310.

67. Ruponen, M., S. Arkko, A. Urtti, M. Reinisalo, and V.P. Ranta, *Intracellular DNA release and elimination correlate poorly with transgene expression after non-viral transfection.* Journal of Controlled Release, 2009. **136**(3): p. 226-231.

68. Templeton, N.S., D.D. Lasic, P.M. Frederik, H.H. Strey, D.D. Roberts, and G.N. Pavlakis, *Improved DNA: Liposome complexes for increased systemic delivery and gene expression.* Nature Biotechnology, 1997. **15**(7): p. 647-652.

69. Sudimack, J. and R.J. Lee, *Targeted drug delivery via the folate receptor.* Advanced Drug Delivery Reviews, 2000. **41**(2): p. 147-162.

70. Gerasimov, O.V., J.A. Boomer, M.M. Qualls, and D.H. Thompson, *Cytosolic drug delivery using pH- and light-sensitive liposomes.* Advanced Drug Delivery Reviews, 1999. **38**(3): p. 317-338.

71. Farhood, H., N. Serbina, and L. Huang, *The role of dioleoyl phosphatidylethanolamine in cationic liposome mediated gene transfer.* Biochimica et Biophysica Acta - Biomembranes, 1995. **1235**(2): p. 289-295.

72. Reilly, M.J., J.D. Larsen, and M.O. Sullivan, *Polyplexes Traffic through Caveolae to the Golgi and Endoplasmic Reticulum en Route to the Nucleus.* Molecular Pharmaceutics, 2012. **9**(5): p. 1280-1290.

73. Durymanov, M.O., E.A. Beletkaia, A.V. Ulasov, Y.V. Khramtsov, G.A. Trusov, N.S. Rodichenko, T.A. Slastnikova, T.V. Vinogradova, N.Y. Uspenskaya, E.P. Kopantsev, A.A. Rosenkranz, E.D. Sverdlov, and A.S. Sobolev, *Subcellular trafficking and transfection efficacy of polyethylenimine-polyethylene glycol polyplex nanoparticles with a ligand to melanocortin receptor-1.* J Control Release, 2012. **163**(2): p. 211-9.

74. Woodle, M.C. and D.D. Lasic, *Sterically stabilized liposomes.* Biochimica et Biophysica Acta - Reviews on Biomembranes, 1992. **1113**(2): p. 171-199.

75. Oupicky, D., M. Ogris, K.A. Howard, P.R. Dash, K. Ulbrich, and L.W. Seymour, *Importance of lateral and steric stabilization of polyelectrolyte gene delivery vectors for extended systemic circulation.* Molecular Therapy, 2002. **5**(4): p. 463-472.

76. Shim, M.S. and Y.J. Kwon, *Stimuli-responsive polymers and nanomaterials for gene delivery and imaging applications.* Advanced Drug Delivery Reviews, 2012. **64**(11): p. 1046-1059.

77. Preiss, M.R. and G.D. Bothun, *Stimuli-responsive liposome-nanoparticle assemblies.* Expert Opinion on Drug Delivery, 2011. **8**(8): p. 1025-1040.

78. Luo, D., K. Woodrow-Mumford, N. Belcheva, and W.M. Saltzman, *Controlled DNA delivery systems.* Pharmaceutical Research, 1999. **16**(8): p. 1300-1308.

79. Schmidt-Wolf, G.D. and I.G.H. Schmidt-Wolf, *Non-viral and hybrid vectors in human gene therapy: An update.* Trends in Molecular Medicine, 2003. **9**(2): p. 67-72.

80. Morille, M., C. Passirani, A. Vonarbourg, A. Clavreul, and J.P. Benoit, *Progress in developing cationic vectors for non-viral systemic gene therapy against cancer.* Biomaterials, 2008. **29**(24-25): p. 3477-3496.

81. De Laporte, L., J. Cruz Rea, and L.D. Shea, *Design of modular non-viral gene therapy vectors.* Biomaterials, 2006. **27**(7): p. 947-954.

82. Roy, I., T.Y. Ohulchanskyy, D.J. Bharali, H.E. Pudavar, R.A. Mistretta, N. Kaur, and P.N. Prasad, *Optical tracking of organically modified silica nanoparticles as DNA carriers: A nonviral, nanomedicine approach for gene delivery.* Proceedings of the National Academy of Sciences of the United States of America, 2005. **102**(2): p. 279-284.

83. Chithrani, B.D., A.A. Ghazani, and W.C.W. Chan, *Determining the size and shape dependence of gold nanoparticle uptake into mammalian cells.* Nano Letters, 2006. **6**(4): p. 662-668.

84. Breunig, M., U. Lungwitz, R. Liebl, and A. Goepferich, *Fluorescence resonance energy transfer: Evaluation of the intracellular stability of polyplexes.* European Journal of Pharmaceutics and Biopharmaceutics, 2006. **63**(2): p. 156-165.

85. Wattiaux, R., N. Laurent, S. Wattiaux-De Coninck, and M. Jadot, *Endosomes, lysosomes: Their implication in gene transfer.* Advanced Drug Delivery Reviews, 2000. **41**(2): p. 201-208.

86. Hoekstra, D., J. Rejman, L. Wasungu, F. Shi, and I. Zuhorn, *Gene delivery by cationic lipids: in and out of an endosome.* Biochem Soc Trans, 2007. **35**(Pt 1): p. 68-71.

87. Rejman, J., A. Bragonzi, and M. Conese, *Role of clathrin- and caveolae-mediated endocytosis in gene transfer mediated by lipo- and polyplexes.* Mol Ther, 2005. **12**(3): p. 468-74.

88. Rejman, J., V. Oberle, I.S. Zuhorn, and D. Hoekstra, *Size-dependent internalization of particles via the pathways of clathrin- and caveolae-mediated endocytosis.* Biochem J, 2004. **377**(Pt 1): p. 159-69.

89. Vercauteren, D., R.E. Vandenbroucke, A.T. Jones, J. Rejman, J. Demeester, S.C. De Smedt, N.N. Sanders, and K. Braeckmans, *The use of inhibitors to study endocytic pathways of gene carriers: optimization and pitfalls.* Mol Ther, 2010. **18**(3): p. 561-9.

90. Dauty, E. and A.S. Verkman, *Actin cytoskeleton as the principal determinant of size-dependent DNA mobility in cytoplasm: A new barrier for non-viral gene delivery.* Journal of Biological Chemistry, 2005. **280**(9): p. 7823-7828.

91. Huth, S., F. Hoffmann, K. von Gersdorff, A. Laner, D. Reinhardt, J. Rosenecker, and C. Rudolph, *Interaction of polyamine gene vectors with RNA leads to the dissociation of plasmid DNA-carrier complexes.* Journal of Gene Medicine, 2006. **8**(12): p. 1416-1424.

92. Alberts B, J.A., Lewis J, et al. , *Molecular Biology of the Cell*. 4th ed. 2004, New York: Garland Science.

93. Okuda, T., T. Niidome, and H. Aoyagi, *Cytosolic soluble proteins induce DNA release from DNA-gene carrier complexes.* Journal of Controlled Release, 2004. **98**(2): p. 325-332.

94. Iida, T., T. Mori, Y. Katayama, and T. Niidome, *Overall interaction of cytosolic proteins with the PEI/DNA complex.* Journal of Controlled Release, 2007. **118**(3): p. 364-369.

95. McNeil, S.E., A. Vangala, V.W. Bramwell, P.J. Hanson, and Y. Perrie, *Lipoplexes formulation and optimisation: In vitro transfection studies reveal no correlation with in vivo vaccination studies.* Current Drug Delivery, 2010. **7**(2): p. 175-187.

96. Egilmez, N.K., Y. Iwanuma, and R.B. Bankert, *Evaluation and optimization of different cationic liposome formulations for in vivo gene transfer.* Biochemical and Biophysical Research Communications, 1996. **221**(1): p. 169-173.

97. Solodin, I., C.S. Brown, M.S. Bruno, C.Y. Chow, E.H. Jang, R.J. Debs, and T.D. Heath, *A novel series of amphiphilic imidazolinium compounds for in vitro and in vivo gene delivery.* Biochemistry, 1995. **34**(41): p. 13537-13544.

98. Sternberg, B., K. Hong, W. Zheng, and D. Papahadjopoulos, *Ultrastructural characterization of cationic liposome-DNA complexes showing enhanced stability in serum and high transfection activity in vivo.* Biochimica et Biophysica Acta - Biomembranes, 1998. **1375**(1-2): p. 23-35.

99. Freinkel, R.K., Woodley, David., *The biology of the skin*. 2001, New York: Parthenon Pub. Group.

100. Cone, R.A., *Barrier properties of mucus.* Advanced Drug Delivery Reviews, 2009. **61**(2): p. 75-85.

101. Vadlamudi, H.C., Y. Prasanna Raju, B. Rubia Yasmeen, and J. Vulava, *Anatomical, biochemical and physiological considerations of the colon in design and development of novel drug delivery systems.* Current Drug Delivery, 2012. **9**(6): p. 556-565.

102. Sanders, N., C. Rudolph, K. Braeckmans, S.C. De Smedt, and J. Demeester, *Extracellular barriers in respiratory gene therapy.* Advanced Drug Delivery Reviews, 2009. **61**(2): p. 115-127.

103. Kikuchi, Y., K. Tamai, and Y. Kaneda, *Cutaneous gene delivery.* Journal of Dermatological Science, 2008. **50**(2): p. 87-98.

104. Meyer, K.B., M.M. Thompson, M.Y. Levy, L.G. Barron, and F.C. Szoka Jr, *Intratracheal gene delivery to the mouse airway: Characterization of plasmid DNA expression and pharmacokinetics.* Gene Therapy, 1995. **2**(7): p. 450-460.

105. Ensign, L.M., R. Cone, and J. Hanes, *Oral drug delivery with polymeric nanoparticles: The gastrointestinal mucus barriers.* Advanced Drug Delivery Reviews, 2012. **64**(6): p. 557-570.

106. Zelphati, O., L.S. Uyechi, L.G. Barron, and F.C. Szoka Jr, *Effect of serum components on the physico-chemical properties of cationic lipid/oligonucleotide complexes and on their interactions with cells.* Biochimica et Biophysica Acta - Lipids and Lipid Metabolism, 1998. **1390**(2): p. 119-133.

107. Escriou, V., C. Ciolina, F. Lacroix, G. Byk, D. Scherman, and P. Wils, *Cationic lipid-mediated gene transfer: Effect of serum on cellular uptake and intracellular fate of lipopolyamine/DNA complexes.* Biochimica et Biophysica Acta - Biomembranes, 1998. **1368**(2): p. 276-288.

108. Hashida, M., R.I. Mahato, K. Kawabata, T. Miyao, M. Nishikawa, and Y. Takakura, *Pharmacokinetics and targeted delivery of proteins and genes.* Journal of Controlled Release, 1996. **41**(1-2): p. 91-97.

109. Hisazumi, J., N. Kobayashi, M. Nishikawa, and Y. Takakura, *Significant role of liver sinusoidal endothelial cells in hepatic uptake and degradation of naked plasmid DNA after intravenous injection.* Pharmaceutical Research, 2004. **21**(7): p. 1223-1228.

110. Gosse, C., J.B. Le Pecq, P. Defrance, and C. Paoletti, *Initial degradation of deoxyribonucleic acid after injection in mammals.* Cancer Research, 1965. **25**(6): p. 877-883.

111. Wu, T.L. and H.C.J. Ertl, *Immune barriers to successful gene therapy.* Trends in Molecular Medicine, 2009. **15**(1): p. 32-39.

112. Patel, H.M., *Serum opsonins and liposomes: Their interaction and opsonophagocytosis.* Critical Reviews in Therapeutic Drug Carrier Systems, 1992. **9**(1): p. 39-90.

113. Ruponen, M., P. Honkakoski, M. Tammi, and A. Urtti, *Cell-surface glycosaminoglycans inhibit cation-mediated gene transfer.* Journal of Gene Medicine, 2004. **6**(4): p. 405-414.

114. Mounkes, L.C., W. Zhong, G. Cipres-Palacin, T.D. Heath, and R.J. Debs, *Proteoglycans mediate cationic liposome-DNA complex-based gene delivery in vitro and in vivo.* Journal of Biological Chemistry, 1998. **273**(40): p. 26164-26170.

115. Burke, R.S. and S.H. Pun, *Extracellular barriers to in vivo PEI and PEGylated PEI polyplex-mediated gene delivery to the liver.* Bioconjugate Chemistry, 2008. **19**(3): p. 693-704.

116. Singh, J., D. Michel, J.M. Chitanda, R.E. Verrall, and I. Badea, *Evaluation of cellular uptake and intracellular trafficking as determining factors of gene expression for amino acid-substituted gemini surfactant-based DNA nanoparticles.* Journal of Nanobiotechnology, 2012. **10**.

117. Ruponen, M., C.S. Braun, and C.R. Middaugh, *Biophysical characterization of polymeric and liposomal gene delivery systems using empirical phase diagrams.* J Pharm Sci, 2006. **95**(10): p. 2101-14.

118. Choosakoonkriang, S., C.M. Wiethoff, G.S. Koe, J.G. Koe, T.J. Anchordoquy, and C.R. Middaugh, *An infrared spectroscopic study of the effect of hydration on cationic lipid/DNA complexes.* Journal of Pharmaceutical Sciences, 2003. **92**(1): p. 115-130.

119. Staggs, D.R., D.W. Burton, and L.J. Deftos, *Importance of liposome complexing volume in transfection optimization.* BioTechniques, 1996. **21**(5): p. 792-798.

120. Zimmermann, E. and R.H. Müller, *Electrolyte- and pH-stabilities of aqueous solid lipid nanoparticle (SLN™) dispersions in artificial gastrointestinal media.* European Journal of Pharmaceutics and Biopharmaceutics, 2001. **52**(2): p. 203-210.

121. Wettig, S.D., I. Badea, M. Donkuru, R.E. Verrall, and M. Foldvari, *Structural and transfection properties of amine-substituted gemini surfactant-based nanoparticles.* Journal of Gene Medicine, 2007. **9**(8): p. 649-658.

122. Sakurai, F., R. Inoue, Y. Nishino, A. Okuda, O. Matsumoto, T. Taga, F. Yamashita, Y. Takakura, and M. Hashida, *Effect of DNA/liposome mixing ratio on the physicochemical characteristics, cellular uptake and intracellular trafficking of plasmid DNA/cationic liposome complexes and subsequent gene expression.* Journal of Controlled Release, 2000. **66**(2-3): p. 255-269.

123. Crommelin, D.J., *Influence of lipid composition and ionic strength on the physical stability of liposomes.* J Pharm Sci, 1984. **73**(11): p. 1559-63.

124. Rejman, J., V. Oberle, I.S. Zuhorn, and D. Hoekstra, *Size-dependent internalization of particles via the pathways of clathrin-and caveolae-mediated endocytosis.* Biochemical Journal, 2004. **377**(1): p. 159-169.

125. Alexis, F., E. Pridgen, L.K. Molnar, and O.C. Farokhzad, *Factors affecting the clearance and biodistribution of polymeric nanoparticles.* Molecular Pharmaceutics, 2008. **5**(4): p. 505-515.

126. He, C., Y. Hu, L. Yin, C. Tang, and C. Yin, *Effects of particle size and surface charge on cellular uptake and biodistribution of polymeric nanoparticles.* Biomaterials, 2010. **31**(13): p. 3657-3666.

127. Crommelin, D.J.A. and G. Storm, *Liposomes: From the bench to the bed.* Journal of Liposome Research, 2003. **13**(1): p. 33-36.

128. Xu, X., M.A. Khan, and D.J. Burgess, *A quality by design (QbD) case study on liposomes containing hydrophilic API: I. Formulation, processing design and risk assessment.* International Journal of Pharmaceutics, 2011. **419**(1-2): p. 52-59.

129. Boeckle, S., K. von Gersdorff, S. van der Piepen, C. Culmsee, E. Wagner, and M. Ogris, *Purification of polyethylenimine polyplexes highlights the role of free polycations in gene transfer.* Journal of Gene Medicine, 2004. **6**(10): p. 1102-1111.

130. Xu, Y., S.W. Hui, P. Frederik, and F.C. Szoka Jr, *Physicochemical characterization and purification of cationic lipoplexes.* Biophysical Journal, 1999. **77**(1): p. 341-353.

131. Lv, H., S. Zhang, B. Wang, S. Cui, and J. Yan, *Toxicity of cationic lipids and cationic polymers in gene delivery.* Journal of Controlled Release, 2006. **114**(1): p. 100-109.

132. Köping-Höggård, M., Y.S. Mel'nikova, K.M. Vårum, B. Lindman, and P. Artursson, *Relationship between the physical shape and the efficiency of oligomeric chitosan as a gene delivery system in vitro and in vivo.* Journal of Gene Medicine, 2003. **5**(2): p. 130-141.

133. Jiang, X., W. Qu, D. Pan, Y. Ren, J.M. Williford, H. Cui, E. Luijten, and H.Q. Mao, *Plasmid-templated shape control of condensed DNA-block copolymer nanoparticles.* Advanced Materials, 2013. **25**(2): p. 227-232.

134. Hud, N.V. and I.D. Vilfan, *Toroidal DNA condensates: Unraveling the fine structure and the role of nucleation in determining size*. 2005. p. 295-318.

135. Erbacher, P., S. Zou, T. Bettinger, A.M. Steffan, and J.S. Remy, *Chitosan-based vector/DNA complexes for gene delivery: Biophysical characteristics and transfection ability.* Pharmaceutical Research, 1998. **15**(9): p. 1332-1339.

136. Safinya, C.R., *Structures of lipid-DNA complexes: Supramolecular assembly and gene delivery.* Current Opinion in Structural Biology, 2001. **11**(4): p. 440-448.

137. Rehman, Z.U., I.S. Zuhorn, and D. Hoekstra, *How cationic lipids transfer nucleic acids into cells and across cellular membranes: Recent advances.* Journal of Controlled Release, 2013. **166**(1): p. 46-56.

138. Lin, A.J., N.L. Slack, A. Ahmad, C.X. George, C.E. Samuel, and C.R. Safinya, *Three-dimensional imaging of lipid gene-carriers: Membrane charge density controls universal transfection behavior in lamellar cationic liposome-DNA complexes.* Biophysical Journal, 2003. **84**(5): p. 3307-3316.

139. Foldvari, M., I. Badea, S. Wettig, R. Verrall, and M. Bagonluri, *Structural characterization of novel gemini non-viral DNA delivery systems for cutaneous gene therapy.* Journal of Experimental Nanoscience, 2006. **1**(2): p. 165-176.

140. Gaumet, M., A. Vargas, R. Gurny, and F. Delie, *Nanoparticles for drug delivery: The need for precision in reporting particle size parameters.* European Journal of Pharmaceutics and Biopharmaceutics, 2008. **69**(1): p. 1-9.

141. Davidson, M.W. and M. Abramowit, *Optical Microscopy.* 2002: p. 1-40.

142. Almgren, M., K. Edwards, and G. Karlsson, *Cryo transmission electron microscopy of liposomes and related structures.* Colloids and Surfaces A: Physicochemical and Engineering Aspects, 2000. **174**(1-2): p. 3-21.

143. Huebner, S., B.J. Battersby, R. Grimm, and G. Cevc, *Lipid-DNA complex formation: Reorganization and rupture of lipid vesicles in the presence of DNA as observed by cryoelectron microscopy.* Biophysical Journal, 1999. **76**(6): p. 3158-3166.

144. Ruozi, B., G. Tosi, E. Leo, and M.A. Vandelli, *Application of atomic force microscopy to characterize liposomes as drug and gene carriers.* Talanta, 2007. **73**(1): p. 12-22.

145. Spyratou, E., E.A. Mourelatou, M. Makropoulou, and C. Demetzos, *Atomic force microscopy: A tool to study the structure, dynamics and stability of liposomal drug delivery systems.* Expert Opinion on Drug Delivery, 2009. **6**(3): p. 305-317.

146. Tang, M.X. and F.C. Szoka, *The influence of polymer structure on the interactions of cationic polymers with DNA and morphology of the resulting complexes.* Gene Therapy, 1997. **4**(8): p. 823-832.

147. Petersen, H., K. Kunath, A.L. Martin, S. Stolnik, C.J. Roberts, M.C. Davies, and T. Kissel, *Star-shaped poly(ethylene glycol)-block-polyethlenimine copolymers enhance DNA condensation of low molecular weight polyethylenimines.* Biomacromolecules, 2002. **3**(5): p. 926-936.

148. Merdan, T., K. Kunath, H. Petersen, U. Bakowsky, K.H. Voigt, J. Kopecek, and T. Kissel, *PEGylation of poly(ethylene imine) affects stability of complexes with plasmid DNA under in vivo conditions in a dose-dependent manner after intravenous injection into mice.* Bioconjugate Chemistry, 2005. **16**(4): p. 785-792.

149. Lim, Y.B., Y.H. Choi, and J.S. Park, *A self-destroying polycationic polymer: Biodegradable poly(4-hydroxy-L- proline ester).* Journal of the American Chemical Society, 1999. **121**(24): p. 5633-5639.

150. Choi, J.S., K. Nam, J.Y. Park, J.B. Kim, J.K. Lee, and J.S. Park, *Enhanced transfection efficiency of PAMAM dendrimer by surface modification with l-arginine.* Journal of Controlled Release, 2004. **99**(3): p. 445-456.

151. Carr, R., Hole, P. and Malloy,A. *Sizing of nanoparticles by visualising and simultaneously tracking the Brownian motion of nanoparticles separately within a suspension*. in *th International Congress on Optical Particle Characterisation*. 2007. Karl-Franzens University Graz, Austria.

152. Pease Iii, L.F., D.I. Lipin, D.H. Tsai, M.R. Zachariah, L.H.L. Lua, M.J. Tarlov, and A.P.J. Middelberg, *Quantitative characterization of virus-like particles by asymmetrical flow field flow fractionation, electrospray differential mobility analysis, and transmission electron microscopy.* Biotechnology and Bioengineering, 2009. **102**(3): p. 845-855.

153. Ma, P.L., M.D. Buschmann, and F.M. Winnik, *One-step analysis of DNA/chitosan complexes by field-flow fractionation reveals particle size and free chitosan content.* Biomacromolecules, 2010. **11**(3): p. 549-554.

154. Fraunhofer, W., G. Winter, and C. Coester, *Asymmetrical Flow Field-Flow Fractionation and Multiangle Light Scattering for Analysis of Gelatin Nanoparticle Drug Carrier Systems.* Analytical Chemistry, 2004. **76**(7): p. 1909-1920.

155. Chuan, Y.P., Y.Y. Fan, L. Lua, and A.P.J. Middelberg, *Quantitative analysis of virus-like particle size and distribution by field-flow fractionation.* Biotechnology and Bioengineering, 2008. **99**(6): p. 1425-1433.

156. Yohannes, G., M. Jussila, K. Hartonen, and M.L. Riekkola, *Asymmetrical flow field-flow fractionation technique for separation and characterization of biopolymers and bioparticles.* Journal of Chromatography A, 2011. **1218**(27): p. 4104-4116.

157. Mehnert, W. and K. Mäder, *Solid lipid nanoparticles: Production, characterization and applications.* Advanced Drug Delivery Reviews, 2001. **47**(2-3): p. 165-196.

158. Safinya, C.R., K.K. Ewert, and C. Leal, *Cationic liposome-nucleic acid complexes: Liquid crystal phases with applications in gene therapy.* Liquid Crystals, 2011. **38**(11-12): p. 1715-1723.

159. Caracciolo, G., R. Caminiti, F. Natali, and A.C. Castellano, *A new approach for the study of cationic lipid-DNA complexes by energy dispersive X-ray diffraction.* Chemical Physics Letters, 2002. **366**(3-4): p. 200-204.

160. Zidovska, A., H.M. Evans, K.K. Ewert, J. Quispe, B. Carragher, C.S. Potter, and C.R. Safinya, *Liquid crystalline phases of dendritic lipid-DNA self-assemblies: Lamellar, hexagonal, and DNA bundles.* Journal of Physical Chemistry B, 2009. **113**(12): p. 3694-3703.

161. Foldvari, M., S. Wettig, I. Badea, R. Verrall, and M. Bagonluri. *Dicationic gemini surfactant gene delivery complexes contain cubic-lamellar mixed polymorphic phase*. 2006. Boston, MA.

162. Badea, I., S. Wettig, R. Verrall, and M. Foldvari, *Topical non-invasive gene delivery using gemini nanoparticles in interferon-γ-deficient mice.* European Journal of Pharmaceutics and Biopharmaceutics, 2007. **65**(3): p. 414-422.

163. Matulis, D., I. Rouzina, and V.A. Bloomfield, *Thermodynamics of cationic lipid binding to DNA and DNA condensation: Roles of electrostatics and hydrophobicity.* Journal of the American Chemical Society, 2002. **124**(25): p. 7331-7342.

164. Lobo, B.A., A. Davis, G. Koe, J.G. Smith, and C.R. Middaugh, *Isothermal titration calorimetric analysis of the interaction between cationic lipids and plasmid DNA.* Archives of Biochemistry and Biophysics, 2001. **386**(1): p. 95-105.

165. Wettig, S.D., P. Nowak, and R.E. Verrall, *Thermodynamic and aggregation properties of gemini surfactants with hydroxyl substituted spacers in aqueous solution.* Langmuir, 2002. **18**(14): p. 5354-5359.

166. Lobo, B.A., S.A. Rogers, S. Choosakoonkriang, J.G. Smith, G. Koe, and C.R. Middaugh, *Differential scanning calorimetric studies of the thermal stability of plasmid DNA complexed with cationic lipids and polymers.* Journal of Pharmaceutical Sciences, 2002. **91**(2): p. 454-466.

167. Yamano, S., J. Dai, and A.M. Moursi, *Comparison of transfection efficiency of nonviral gene transfer reagents.* Molecular Biotechnology, 2010. **46**(3): p. 287-300.

168. Sonawane, N.D., F.C. Szoka Jr, and A.S. Verkman, *Chloride Accumulation and Swelling in Endosomes Enhances DNA Transfer by Polyamine-DNA Polyplexes.* Journal of Biological Chemistry, 2003. **278**(45): p. 44826-44831.

169. Lukacs, G.L., P. Haggie, O. Seksek, D. Lechardeur, N. Freedman, and A.S. Verkman, *Size-dependent DNA mobility in cytoplasm and nucleus.* Journal of Biological Chemistry, 2000. **275**(3): p. 1625-1629.

170. Meyvis, T.K.L., S.C. De Smedt, P. Van Oostveldt, and J. Demeester, *Fluorescence recovery after photobleaching: A versatile tool for mobility and interaction measurements in pharmaceutical research.* Pharmaceutical Research, 1999. **16**(8): p. 1153-1162.

171. Braun, C.S., J.A. Vetro, D.A. Tomalia, G.S. Koe, J.G. Koe, and C.R. Middaugh, *Structure/function relationships of polyamidoamine/DNA dendrimers as gene delivery vehicles.* Journal of Pharmaceutical Sciences, 2005. **94**(2): p. 423-436.

172. Braun, C.S., L.A. Kueltzo, and C. Russell Middaugh, *Ultraviolet absorption and circular dichroism spectroscopy of nonviral gene delivery complexes.* Methods Mol Med, 2001. **65**: p. 253-84.

173. Choosakoonkriang, S., C.M. Wiethoff, T.J. Anchordoquy, G.S. Koe, J.G. Smith, and C.R. Middaugh, *Infrared Spectroscopic Characterization of the Interaction of Cationic Lipids with Plasmid DNA.* Journal of Biological Chemistry, 2001. **276**(11): p. 8037-8043.

174. Menger, F.M. and J.S. Keiper, *Gemini surfactants.* Angewandte Chemie - International Edition, 2000. **39**(11): p. 1906-1920.

175. Menger, F.M. and C.A. Littau, *Gemini surfactants: A new class of self-assembling molecules.* Journal of the American Chemical Society, 1993. **115**(22): p. 10083-10090.

176. Hait, S.K. and S.P. Moulik, *Gemini surfactants: A distinct class of self-assembling molecules.* Current Science, 2002. **82**(9): p. 1101-1111.

177. Zana, R., M. Benrraou, and R. Rueff, *Alkanediyl-α,ω-bis(dimethylalkylammonium bromide) surfactants. 1. Effect of the spacer chain length on the critical micelle concentration and micelle ionization degree.* Langmuir, 1991. **7**(6): p. 1072-1075.

178. Zana, R., *Dimeric (gemini) surfactants: Effect of the spacer group on the association behavior in aqueous solution.* Journal of Colloid and Interface Science, 2002. **248**(2): p. 203-220.

179. Elsner, M., Weuthen, M., Raths, H. , *Mixtures of gemini surfactants and fatty alcohol alkoxylates in rinse agents*. 2002, Cognis Deutschland GmbH & Co. KG: United States.

180. Xu, J., X. Han, H. Liu, and Y. Hu, *Synthesis of monodisperse gold nanoparticles stabilized by gemini surfactant in reverse micelles.* Journal of Dispersion Science and Technology, 2005. **26**(4): p. 473-476.

181. Ma, Q.Y., R.F. Guan, and G.Z. Li, *Synthesis of gold nanostructures using Langmuir monolayers of ionic liquid-type Gemini imidazolium surfactants.* Micro and Nano Letters, 2011. **6**(6): p. 454-458.

182. Ling, Z., J. Tifeng, and L. Minghua, *A facile method to the synthesis of gold nanoprisms using a series of gemini amphiphiles.* Journal of Nanoscience and Nanotechnology, 2009. **9**(4): p. 2726-2730.

183. Esumi, K., J. Hara, N. Aihara, K. Usui, and K. Torigoe, *Preparation of anisotropic gold particles using a gemini surfactant template.* Journal of Colloid and Interface Science, 1998. **208**(2): p. 578-581.

184. Guerrero-Martinez, A., J. Perez-Juste, E. Carbo-Argibay, G. Tardajos, and L.M. Liz-Marzan, *Gemini-surfactant-directed self-assembly of monodisperse gold nanorods into standing superlattices.* Angew Chem Int Ed Engl, 2009. **48**(50): p. 9484-8.

185. Massi, L., F. Guittard, R. Levy, Y. Duccini, and S. Géribaldi, *Preparation and antimicrobial behaviour of gemini fluorosurfactants.* European Journal of Medicinal Chemistry, 2003. **38**(5): p. 519-523.

186. Laatiris, A., M. El Achouri, M. Rosa Infante, and Y. Bensouda, *Antibacterial activity, structure and CMC relationships of alkanediyl α,ω-bis(dimethylammonium bromide) surfactants.* Microbiological Research, 2008. **163**(6): p. 645-650.

187. Hoque, J., P. Akkapeddi, V. Yarlagadda, D.S.S.M. Uppu, P. Kumar, and J. Haldar, *Cleavable cationic antibacterial amphiphiles: Synthesis, mechanism of action, and cytotoxicities.* Langmuir, 2012. **28**(33): p. 12225-12234.

188. Colomer, A., A. Pinazo, M.A. Manresa, M.P. Vinardell, M. Mitjans, M.R. Infante, and L. Pérez, *Cationic surfactants derived from lysine: Effects of their structure and charge type on antimicrobial and hemolytic activities.* Journal of Medicinal Chemistry, 2011. **54**(4): p. 989-1002.

189. Caillier, L., E. Taffin de Givenchy, R. Levy, Y. Vandenberghe, S. Geribaldi, and F. Guittard, *Polymerizable semi-fluorinated gemini surfactants designed for antimicrobial materials.* Journal of Colloid and Interface Science, 2009. **332**(1): p. 201-207.

190. Chen, X. and F. Huang, *Research progress of temperature-resistant and salt-tolerant surfactants for enhanced oil recovery.* Shiyou Huagong/Petrochemical Technology, 2010. **39**(12): p. 1306-1312.

191. Wei, H., W. Liu, G. Wei, F. Yin, and J. Liu. *Molecular design and fractal applications in enhancing oil recovery from low-permeability oil reservoirs by gemini surfactant flooding*. 2010. Port of Spain.

192. Xiao, J., J. Cai, and X. Guo, *Reverse micellar extraction of bovine serum albumin - A comparison between the effects of gemini surfactant and its corresponding monomeric surfactant.* Food Chemistry, 2012. **136**(2): p. 1063-1069.

193. Mo, Z., Y. Zhang, F. Zhao, F. Xiao, G. Guo, and B. Zeng, *Sensitive voltammetric determination of Sudan I in food samples by using gemini surfactant-ionic liquid-multiwalled carbon nanotube composite film modified glassy carbon electrodes.* Food Chemistry, 2010. **121**(1): p. 233-237.

194. Karlsson, L., M.C.P. Van Eijk, and O. Söderman, *Compaction of DNA by gemini surfactants: Effects of surfactant architecture.* Journal of Colloid and Interface Science, 2002. **252**(2): p. 290-296.

195. Badea, I., R. Verrall, M. Baca-Estrada, S. Tikoo, A. Rosenberg, P. Kumar, and M. Foldvari, *In vivo cutaneous interferon-γ gene delivery using novel dicationic (gemini) surfactant-plasmid complexes.* Journal of Gene Medicine, 2005. **7**(9): p. 1200-1214.

196. Donkuru, M., S.D. Wettig, R.E. Verrall, I. Badea, and M. Foldvari, *Designing pH-sensitive gemini nanoparticles for non-viral gene delivery into keratinocytes.* Journal of Materials Chemistry, 2012. **22**(13): p. 6232-6244.

197. Singh, J., P. Yang, D. Michel, R.E. Verrall, M. Foldvari, and I. Badea, *Amino acid-substituted gemini surfactant-based nanoparticles as safe and versatile gene delivery agents.* Current Drug Delivery, 2011. **8**(3): p. 299-306.

198. Dalby, B., S. Cates, A. Harris, E.C. Ohki, M.L. Tilkins, P.J. Price, and V.C. Ciccarone, *Advanced transfection with Lipofectamine 2000 reagent: Primary neurons, siRNA, and high-throughput applications.* Methods, 2004. **33**(2): p. 95-103.

199. Jacobsen, L.B., S.A. Calvin, K.E. Colvin, and M. Wright, *FuGENE 6 Transfection Reagent: The gentle power.* Methods, 2004. **33**(2): p. 104-112.

200. Wei, Y., L. Wang, and X. Wu, *Study of the optimized transfection condition of a novel nanoscopic vector, Superfect™.* Medical Journal of Wuhan University, 2006. **27**(6): p. 703-706.

201. Arnold, A.S., V. Laporte, S. Dumont, A. Appert-Collin, P. Erbacher, G. Coupin, R. Levy, P. Poindron, and J.P. Gies, *Comparing reagents for efficient transfection of human primary myoblasts: FuGENE 6, Effectene and ExGen 500.* Fundamental and Clinical Pharmacology, 2006. **20**(1): p. 81-89.

202. Pollard, H., J.S. Remy, G. Loussouarn, S. Demolombe, J.P. Behr, and D. Escande, *Polyethylenimine but not cationic lipids promotes transgene delivery to the nucleus in mammalian cells.* Journal of Biological Chemistry, 1998. **273**(13): p. 7507-7511.

203. Kay, M.A., *State-of-the-art gene-based therapies: The road ahead.* Nature Reviews Genetics, 2011. **12**(5): p. 316-328.

204. Li, S.D. and L. Huang, *Gene therapy progress and prospects: Non-viral gene therapy by systemic delivery.* Gene Therapy, 2006. **13**(18): p. 1313-1319.

205. Hama, S., H. Akita, R. Ito, H. Mizuguchi, T. Hayakawa, and H. Harashima, *Quantitative comparison of intracellular trafficking and nuclear transcription between adenoviral and lipoplex systems.* Molecular Therapy, 2006. **13**(4): p. 786-794.

206. Philipp Seib, F., A.T. Jones, and R. Duncan, *Establishment of subcellular fractionation techniques to monitor the intracellular fate of polymer therapeutics I. Differential centrifugation fractionation B16F10 cells and use to study the intracellular fate of HPMA copolymer-doxorubicin.* Journal of Drug Targeting, 2006. **14**(6): p. 375-390.

207. De Smedt, S.C., K. Remaut, B. Lucas, K. Braeckmans, N.N. Sanders, and J. Demeester, *Studying biophysical barriers to DNA delivery by advanced light microscopy.* Advanced Drug Delivery Reviews, 2005. **57**(1 SPEC. ISS): p. 191-210.

208. Braeckmans, K., K. Buyens, B. Naeye, D. Vercauteren, H. Deschout, K. Raemdonck, K. Remaut, N.N. Sanders, J. Demeester, and S.C. De Smedt, *Advanced fluorescence microscopy methods illuminate the transfection pathway of nucleic acid nanoparticles.* Journal of Controlled Release, 2010. **148**(1): p. 69-74.

209. Gordon, S.P., S. Berezhna, D. Scherfeld, N. Kahya, and P. Schwille, *Characterization of interaction between cationic lipid-oligonucleotide complexes and cellular membrane lipids using confocal imaging and fluorescence correlation spectroscopy.* Biophysical Journal, 2005. **88**(1): p. 305-316.

210. Seiffert, S. and W. Oppermann, *Systematic evaluation of FRAP experiments performed in a confocal laser scanning microscope.* Journal of Microscopy, 2005. **220**(1): p. 20-30.

211. Olmsted, S.S., J.L. Padgett, A.I. Yudin, K.J. Whaley, T.R. Moench, and R.A. Cone, *Diffusion of macromolecules and virus-like particles in human cervical mucus.* Biophysical Journal, 2001. **81**(4): p. 1930-1937.

212. Braeckmans, K., L. Peeters, N.N. Sanders, S.C. De Smedt, and J. Demeester, *Three-dimensional fluorescence recovery after photobleaching with the confocal scanning laser microscope.* Biophysical Journal, 2003. **85**(4): p. 2240-2252.

213. Piston, D.W. and G.J. Kremers, *Fluorescent protein FRET: the good, the bad and the ugly.* Trends in Biochemical Sciences, 2007. **32**(9): p. 407-414.

214. Elson, E.L. and D. Magde, *Fluorescence correlation spectroscopy. I. Conceptual basis and theory.* Biopolymers, 1974. **13**(1): p. 1-27.

215. Magde, D., E. Elson, and W.W. Webb, *Thermodynamic Fluctuations in a Reacting System—Measurement by Fluorescence Correlation Spectroscopy.* Physical Review Letters, 1972. **29**(11): p. 705.

216. Magde, D., E.L. Elson, and W.W. Webb, *Fluorescence correlation spectroscopy. II. An experimental realization.* Biopolymers, 1974. **13**(1): p. 29-61.

217. Bacia, K. and P. Schwille, *Fluorescence Correlation Spectroscopy*, in *Lipid Rafts*, T.J. McIntosh, Editor. 2007, Humana Press Inc.: Totowa. p. 73-84.

218. Bacia, K., S.A. Kim, and P. Schwille, *Fluorescence cross-correlation spectroscopy in living cells.* Nature Methods, 2006. **3**(2): p. 83-89.

219. Schwille, P., *Fluorescence correlation spectroscopy and its potential for intracellular applications.* Cell Biochemistry and Biophysics, 2001. **34**(3): p. 383-408.

220. Rigler, R., U. Mets, J. Widengren, and P. Kask, *Fluorescence correlation spectroscopy with high count rate and low background: Analysis of translational diffusion.* European Biophysics Journal, 1993. **22**(3): p. 169-175.

221. Lakowicz, J.R., *Principles of Fluorescence Spectroscopy*. 3rd ed. 2006, New York: Springer Science+Business media, LLC. 954.

222. Lakowicz, J.R., *Principles of fluorescence spectroscopy*. 3rd ed. 2009: Springer.

223. Remy, J.S., B. Abdallah, M.A. Zanta, O. Boussif, J.P. Behr, and B. Demeneix, *Gene transfer with lipospermines and polyethylenimines.* Advanced Drug Delivery Reviews, 1998. **30**(1-3): p. 85-95.

224. Kral, T., M. Hof, and M. Langner, *The effect of spermine on plasmid condensation and dye release observed by fluorescence correlation spectroscopy.* Biological Chemistry, 2002. **383**(2): p. 331-335.

225. Yoshida, N., M. Kinjo, and M. Tamura, *Microenvironment of endosomal aqueous phase investigated by the mobility of microparticles using fluorescence correlation spectroscopy.* Biochemical and Biophysical Research Communications, 2001. **280**(1): p. 312-318.

226. Wang, C., S.D. Wettig, M. Foldvari, and R.E. Verrall, *Synthesis, characterization, and use of asymmetric pyrenyl-gemini surfactants as emissive components in DNA-lipoplex systems.* Langmuir, 2007. **23**(17): p. 8995-9001.

227. Bonasera, V., S. Alberti, and A. Sacchetti, *Protocol for high-sensitivity/long linear-range spectrofluorimetric DNA quantification using ethidium bromide.* BioTechniques, 2007. **43**(2): p. 173-176.

228. Van Rompaey, E., Y. Engelborghs, N. Sanders, S.C. De Smedt, and J. Demeester, *Interactions between oligonucleotides and cationic polymers investigated by fluorescence correlation spectroscopy.* Pharmaceutical Research, 2001. **18**(7): p. 928-936.

229. Binks, B.P., *Modern Aspects of Emulsion Science*, B.P. Binks, Editor. 1998, Royal Society of Chemistry.

230. Hafez, I.M. and P.R. Cullis, *Roles of lipid polymorphism in intracellular delivery.* Advanced Drug Delivery Reviews, 2001. **47**(2–3): p. 139-148.

231. Gibson, N., O. Shenderova, T.J.M. Luo, S. Moseenkov, V. Bondar, A. Puzyr, K. Purtov, Z. Fitzgerald, and D.W. Brenner, *Colloidal stability of modified nanodiamond particles.* Diamond and Related Materials, 2009. **18**(4): p. 620-626.

232. Olmsted Iii, J. and D.R. Kearns, *Mechanism of ethidium bromide fluorescence enhancement on binding to nucleic acids.* Biochemistry, 1977. **16**(16): p. 3647-3654.

233. Wiethoff, C.M., M.L. Gill, G.S. Koe, J.G. Koe, and C.R. Middaugh, *A fluorescence study of the structure and accessibility of plasmid DNA condensed with cationic gene delivery vehicles.* Journal of Pharmaceutical Sciences, 2003. **92**(6): p. 1272-1285.

234. Margineanu, A., S. De Feyter, S. Melnikov, D. Marchand, A. van Aerschot, P. Herdewijn, S. Habuchi, F.C. De Schryver, and J. Hofkens, *Complexation of lipofectamine and cholesterol-modified DNA sequences studied by single-molecule fluorescence techniques.* Biomacromolecules, 2007. **8**(11): p. 3382-3392.

235. Remaut, K., B. Lucas, K. Braeckmans, N.N. Sanders, S.C. De Smedt, and J. Demeester, *FRET-FCS as a tool to evaluate the stability of oligonucleotide drugs after intracellular delivery.* Journal of Controlled Release, 2005. **103**(1): p. 259-271.

236. Remaut, K., B. Lucas, K. Braeckmans, N.N. Sanders, J. Demeester, and S.C. De Smedt, *Protection of oligonucleotides against nucleases by pegylated and non-pegylated liposomes as studied by fluorescence correlation spectroscopy.* Journal of Controlled Release, 2005. **110**(1): p. 212-226.

237. Merkle, D., S.P. Lees-Miller, and D.T. Cramb, *Structure and dynamics of lipoplex formation examined using two-photon fluorescence cross-correlation spectroscopy.* Biochemistry, 2004. **43**(23): p. 7263-7272.

238. Lucas, B., K. Remaut, N.N. Sanders, K. Braeckmans, S.C. De Smedt, and J. Demeester, *Towards a better understanding of the dissociation behavior of liposome-oligonucleotide complexes in the cytosol of cells.* Journal of Controlled Release, 2005. **103**(2): p. 435-450.

239. Mustapa, M.F.M., P.C. Bell, C.A. Hurley, A. Nicol, E. Guénin, S. Sarkar, M.J. Writer, S.E. Barker, J.B. Wong, M.A. Pilkington-Miksa, B. Papahadjopoulos-Sternberg, P.A. Shamlou, H.C. Hailes, S.L. Hart, D. Zicha, and A.B. Tabor, *Biophysical characterization of an integrin-targeted lipopolyplex gene delivery vector.* Biochemistry, 2007. **46**(45): p. 12930-12944.

240. Levy, M.S., P. Lotfian, R. O'Kennedy, M.Y. Lo-Yim, and P.A. Shamlou, *Quantitation of supercoiled circular content in plasmid DNA solutions using a fluorescence-based method.* Nucleic Acids Research, 2000. **28**(12).

241. Kalkbrenner, T., A. Arnold, and S.J. Tans, *Internal dynamics of supercoiled DNA molecules.* Biophysical Journal, 2009. **96**(12): p. 4951-4955.

242. Bacia, K. and P. Schwille, *Practical guidelines for dual-color fluorescence cross-correlation spectroscopy.* Nature Protocols, 2007. **2**(11): p. 2842-2856.

243. Prabha, S., W.Z. Zhou, J. Panyam, and V. Labhasetwar, *Size-dependency of nanoparticle-mediated gene transfection: Studies with fractionated nanoparticles.* International Journal of Pharmaceutics, 2002. **244**(1-2): p. 105-115.

244. Sternberg, B., *New structures in complex formation between DNA and cationic liposomes visualized by freeze-fracture electron microscopy.* FEBS Letters, 1994. **356**(2-3): p. 361-366.

245. Gonçalves, E., R.J. Debs, and T.D. Heath, *The Effect of Liposome Size on the Final Lipid/DNA Ratio of Cationic Lipoplexes.* Biophysical Journal, 2004. **86**(3): p. 1554-1563.

246. Hsieh, A.T.H., N. Hori, R. Massoudi, P.J.H. Pan, H. Sasaki, Y.A. Lin, and A.P. Lee, *Nonviral gene vector formation in monodispersed picolitre incubator for consistent gene delivery*. Lab on a Chip - Miniaturisation for Chemistry and Biology, 2009. **9**(18): p. 2638-2643.

247. Rakhmanova, V.A., E.V. Pozharski, and R.C. MacDonald, *Mechanisms of lipoplex formation: Dependence of the biological properties of transfection complexes on formulation procedures.* Journal of Membrane Biology, 2004. **200**(1): p. 35-45.

248. Chen, G., F. Song, X. Wang, S. Sun, J. Fan, and X. Peng, *Bright and stable Cy3-encapsulated fluorescent silica nanoparticles with a large Stokes shift.* Dyes and Pigments, 2012. **93**(1-3): p. 1532-1537.

249. Wettig, S.D. and R.E. Verrall, *Thermodynamic studies of aqueous m-s-m gemini surfactant systems.* Journal of Colloid and Interface Science, 2001. **235**(2): p. 310-316.

250. Menger, F.M., J.S. Keiper, B.N.A. Mbadugha, K.L. Caran, and L.S. Romsted, *Interfacial composition of gemini surfactant micelles determined by chemical trapping.* Langmuir, 2000. **16**(23): p. 9095-9098.

251. Chen, X., J. Wang, N. Shen, Y. Luo, L. Li, M. Liu, and R.K. Thomas, *Gemini surfactant/DNA complex monolayers at the air-water interface: Effect of surfactant structure on the assembly, stability, and topography of monolayers.* Langmuir, 2002. **18**(16): p. 6222-6228.

252. Clamme, J.P., J. Azoulay, and Y. Mély, *Monitoring of the formation and dissociation of polyethylenimine/DNA complexes by two photon fluorescence correlation spectroscopy.* Biophysical Journal, 2003. **84**(3): p. 1960-1968.

253. Domingos, R.F., M.A. Baalousha, Y. Ju-Nam, M.M. Reid, N. Tufenkji, J.R. Lead, G.G. Leppard, and K.J. Wilkinson, *Characterizing manufactured nanoparticles in the environment: Multimethod determination of particle sizes.* Environmental Science and Technology, 2009. **43**(19): p. 7277-7284.

254. Provder, T., *Challenges in particle size distribution measurement past, present and for the 21st century.* Progress in Organic Coatings, 1997. **32**(1-4): p. 143-153.

255. Mazouchi, A., B. Liu, A. Bahram, and C.C. Gradinaru, *On the performance of bioanalytical fluorescence correlation spectroscopy measurements in a multiparameter photon-counting microscope.* Analytica Chimica Acta, 2011. **688**(1): p. 61-69.

256. Liu, B., S. Fletcher, M. Avadisian, P.T. Gunning, and C.C. Gradinaru, *A photostable, pH-invariant fluorescein derivative for Single-molecule microscopy.* Journal of Fluorescence, 2009. **19**(5): p. 915-920.

257. Wang, X.L., X.H. Zhang, M. Cao, H.Z. Zheng, B. Xiao, Y. Wang, and M. Li, *Gemini surfactant-induced DNA condensation into a beadlike structure.* Journal of Physical Chemistry B, 2009. **113**(8): p. 2328-2332.

258. Wolfe, A., G.H. Shimer Jr, and T. Meehan, *Polycyclic aromatic hydrocarbons physically intercalate into duplex regions of denatured DNA.* Biochemistry, 1987. **26**(20): p. 6392-6396.

259. Almeida, J.A.S., E.F. Marques, A.S. Jurado, and A.A.C.C. Pais, *The effect of cationic gemini surfactants upon lipid membranes. An experimental and molecular dynamics simulation study.* Physical Chemistry Chemical Physics, 2010. **12**(43): p. 14462-14476.

260. Schmidt, F.H.G., M. Hüben, B. Gider, F. Renault, M.P. Teulade-Fichou, and E. Weinhold, *Sequence-specific Methyltransferase-Induced Labelling (SMILing) of plasmid DNA for studying cell transfection.* Bioorganic and Medicinal Chemistry, 2008. **16**(1): p. 40-48.

261. Chiou, C.C., S.W. Chen, J.D. Luo, and Y.T. Chien, *Monitoring triplex DNA formation with fluorescence resonance energy transfer between a fluorophore-labeled probe and intercalating dyes.* Analytical Biochemistry, 2011. **416**(1): p. 1-7.

262. Hall, L.M., M. Gerowska, and T. Brown, *A highly fluorescent DNA toolkit: Synthesis and properties of oligonucleotides containing new Cy3, Cy5 and Cy3B monomers.* Nucleic Acids Research, 2012. **40**(14).

263. Shusterman, R., T. Gavrinyov, and O. Krichevsky, *Internal dynamics of superhelical DNA.* Physical Review Letters, 2008. **100**(9).

264. Ehrlich, N., K. Anhalt, C. Hübner, and S. Brakmann, *Exonuclease III action on microarrays: Observation of DNA degradation by fluorescence correlation spectroscopy.* Analytical Biochemistry, 2010. **399**(2): p. 251-256.

265. Sasaki, A. and M. Kinjo, *Monitoring intracellular degradation of exogenous DNA using diffusion properties.* J Control Release, 2010. **143**(1): p. 104-11.

266. Yuspa, S.H., P. Hawley-Nelson, B. Koehler, and J.R. Stanley, *A survey of transformation markers in differentiating epidermal cell lines in culture.* Cancer Research, 1980. **40**(12): p. 4694-4703.